21 cm Cosmology and HI experiments

Saleem Zaroubi
The Open Univ., IL
Univ. of Groningen, NL

Literature

1. Excellent review article: Cosmology at Low Frequencies: The 21 cm Transition and the High-Redshift Universe, by: Furlanetto, Oh & Briggs, 2006, Physics Reports
2. The First Galaxies: Theoretical Predictions and Observational Clues, Wilkind, Mobasher & Bromm (Editors), Springer, 2013
    1. The Epoch of Reionization, S. Zaroubi
3. Interferometry and Synthesis in Radio Astronomy, Thomson, Moran & Swenson, Springer Open, 2017.

21 cm Cosmology & HI experiments

Lecture 1	Lecture 2	Lecture 3
Physics of the 21cm probe	**The Cosmic history of HI**	**Interferometers and current results.**
• Basic Formulae (Field 1958) • Excitation mechanisms (Ly-α, collisions,..) • Global evolution of the spin temp. • Patchy evolution • Simulation results	• The History of the spin temperature • Dark Ages, Cosmic Dawn & EoR • Current & future experiments. • Total intensity experiments and the Edges results.	• Key parameters in experiments. • Observational issues: uv coverage, foregrounds, ionosphere, instrument, noise. • Extraction issues. • Calibration. • Polarization. • The current status of the results • The Future

Credit: Science magazine

The History

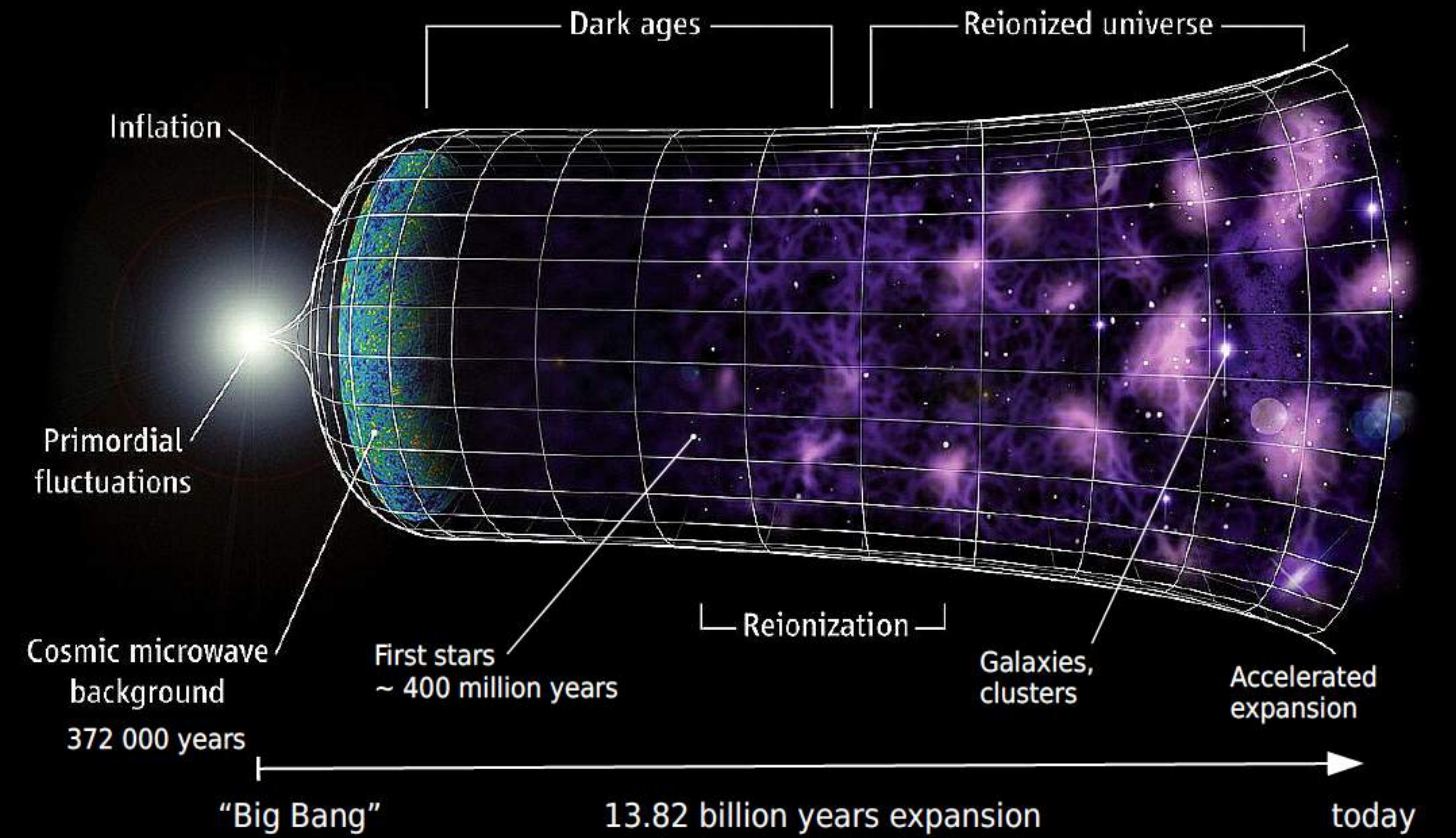

Key Probes of Reionization

- CMB (integral constraint)
- Redshifted 21 cm emission (absorption)
- 21 cm forest at high z
- Gamma ray bursts: How many we should have to constrain reionization?
- Luminosity function of first objects, e.g., Galaxies: Recent HST results.
- Background detections: IR, soft x-ray.
- Lyman-α absorption system: ionization, metallicity, thermal history, UV background, proximity effect.
- Lyman alpha emitters
- Metals at high redshift.
- Using the local volume to study reionization.

Talk by: Xiaohui Fan

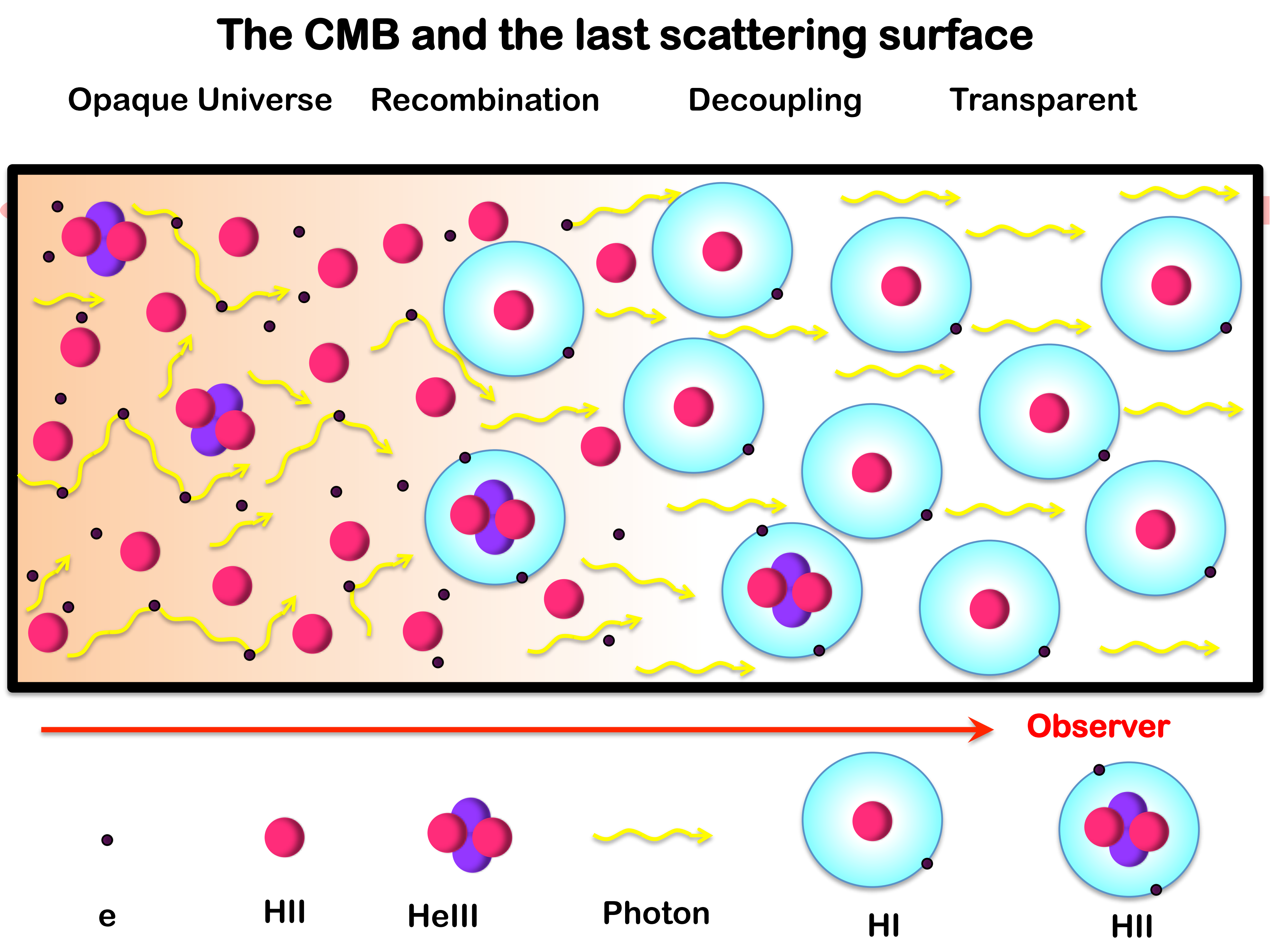

The CMB and the last scattering surface
Opaque Universe
Recombination
Decoupling
Transparent
Observer
e
HII
HeIII
Photon
HI
HII

CMB photons Thomson scatter off free electrons

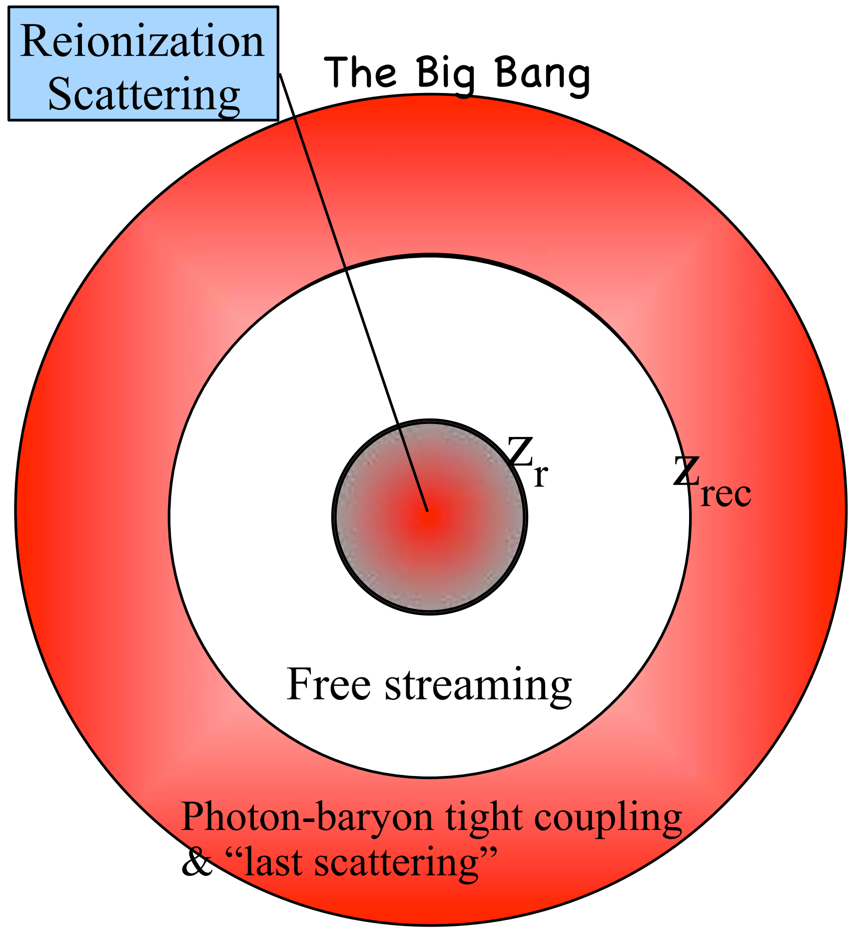

Reionization & CMB Temperature

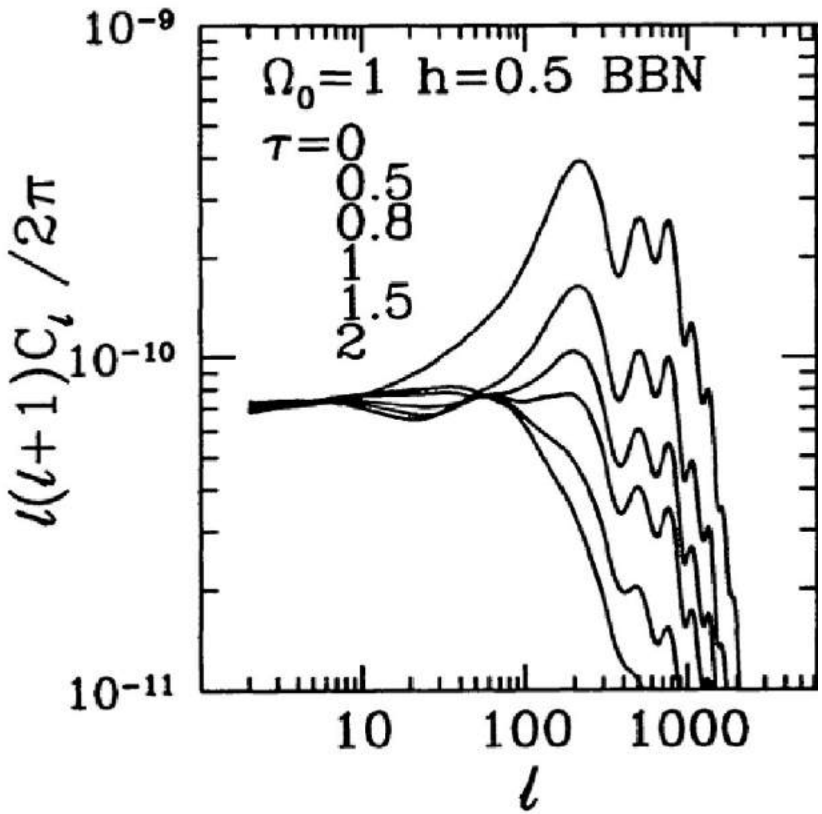

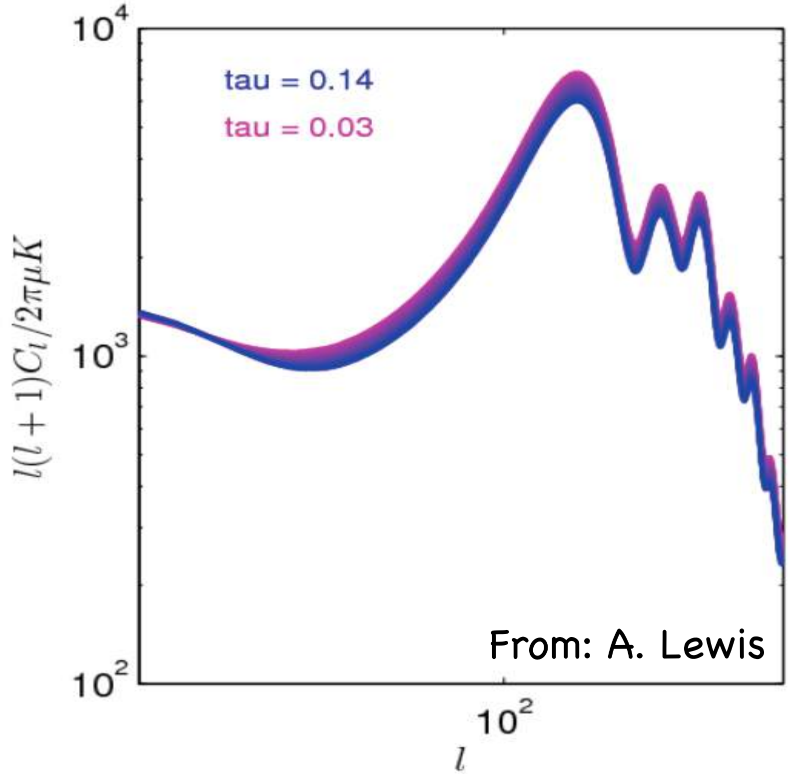

The influence of reionization on the CMB temperature angular power spectrum. (from Sugiyama 1995)

CMB and Reionization: Polarization

Q

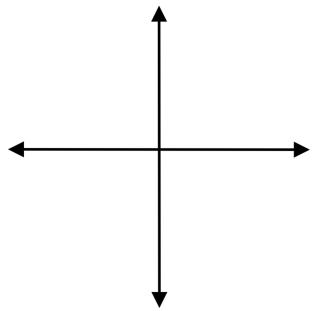

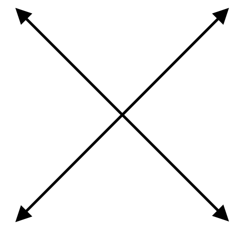

U

Polarization: Stokes parameters

Q $\rightarrow$ -Q, U $\rightarrow$ -U under 90 degree rotation
Q $\rightarrow$ U, U $\rightarrow$ -Q under 45 degree rotation

$$P = \sqrt{Q^2 + U^2} \quad \text{and} \quad \alpha = \frac{1}{2}\arctan(U/Q).$$

amplitude angle

E and B polarization modes

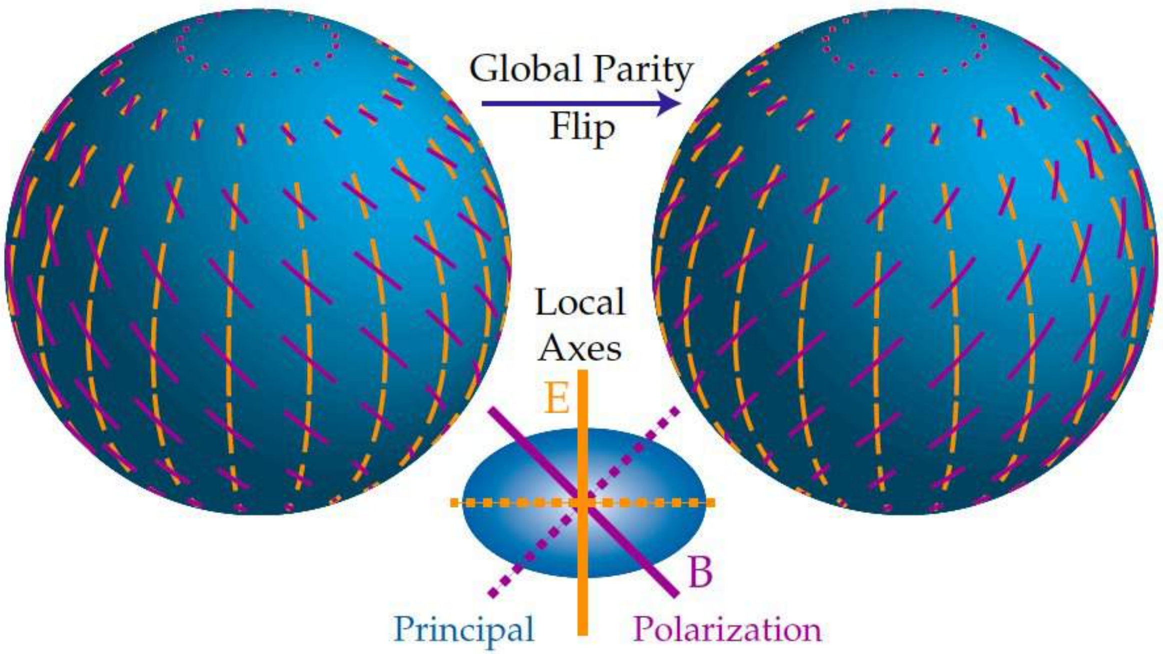

E-mode has $(-1)^l$ parity whereas B-mode $(-1)^{l+1}$

The WMAP cosntraint

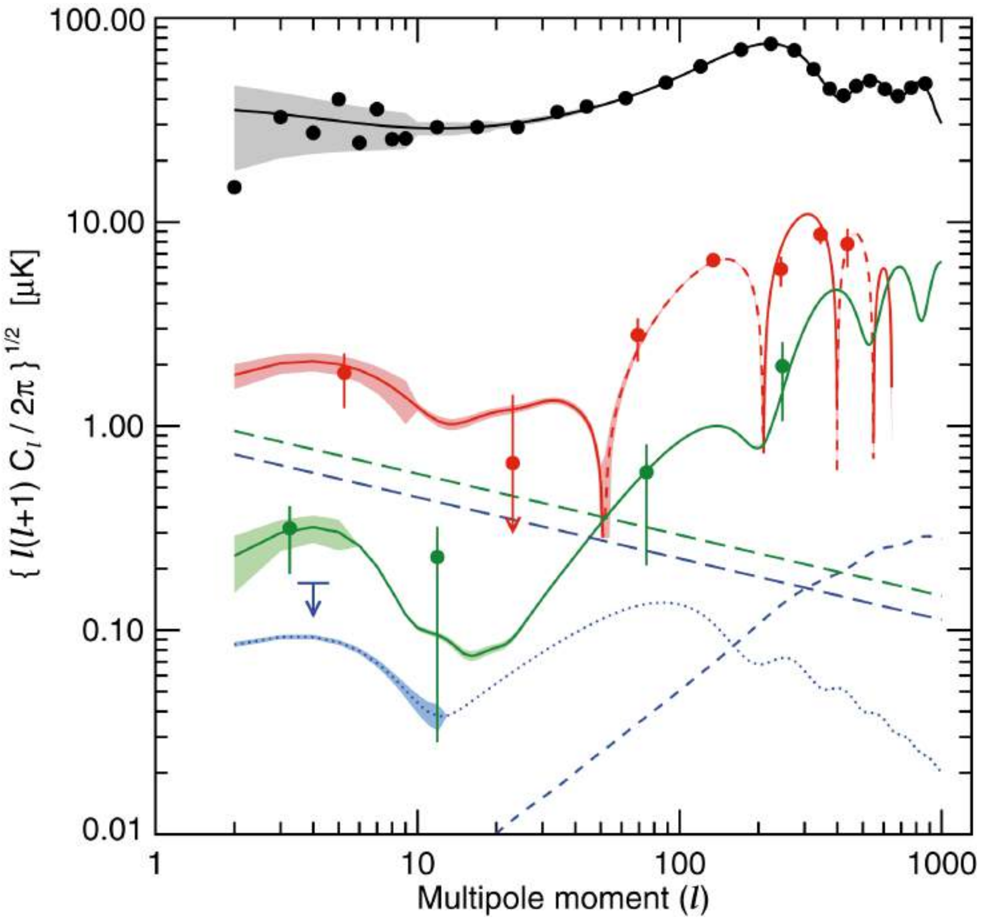

$\tau \sim 0.088$

- The WMAP polarization measurement tells us only about the optical depth not about exact ionization redshift. For that one needs a reionization history model. However, reasonable reionization models suggest that ionization has happened at about z~10.

Thomson Scattering

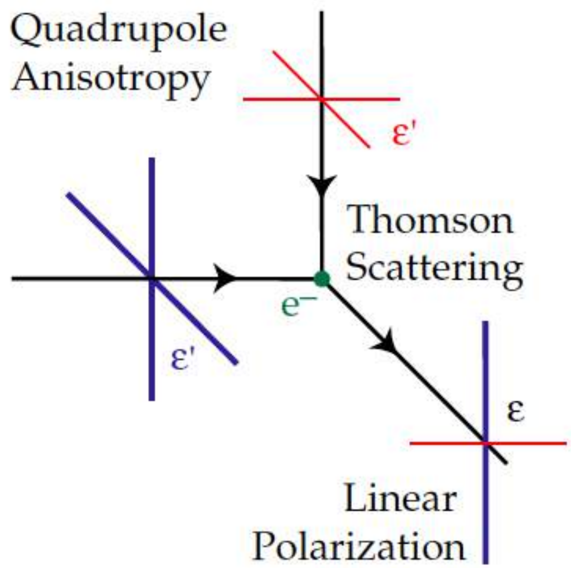

Q and U are generated by Thomson scattering of unpolarized light. Notice no V (circular polarization) is generated.

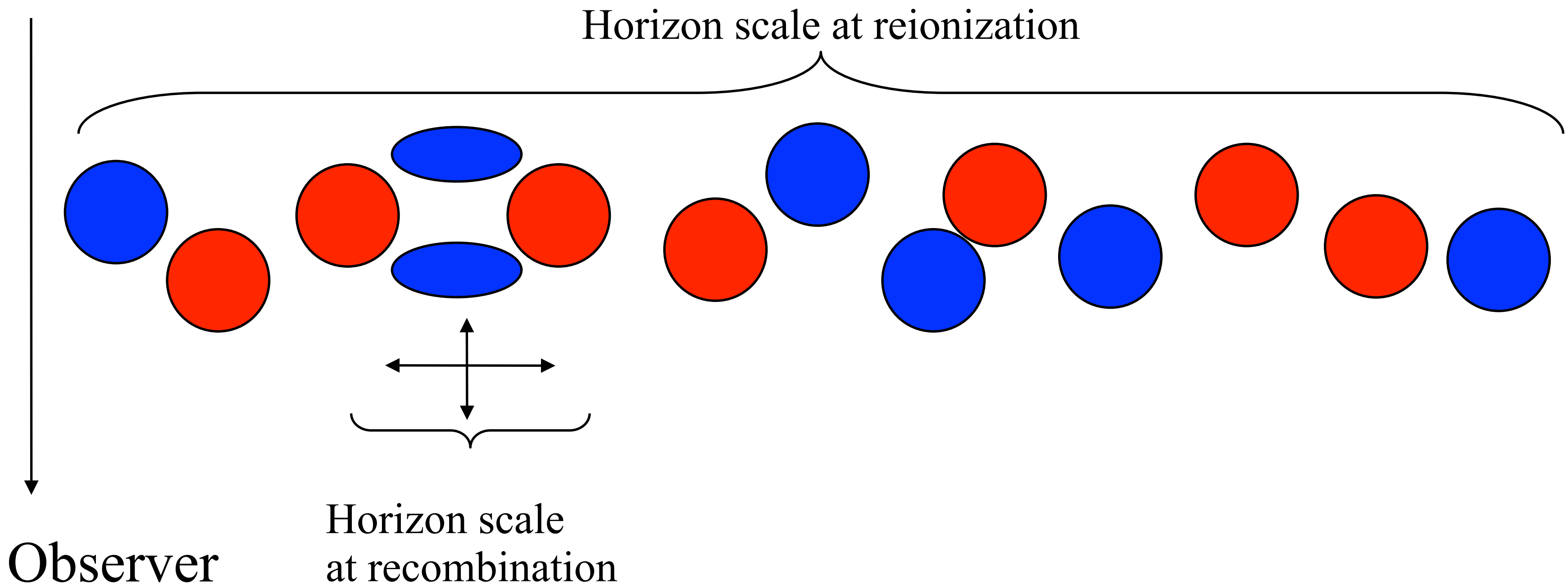

Given the geometry of linear polarization the amplitude of the signal at any scale depends on the local quadrupole that scatters the photons. However, at scales larger than horizon scales (either at recombination or during reionization) there is no coherence and the signal decays.

The Planck constraint

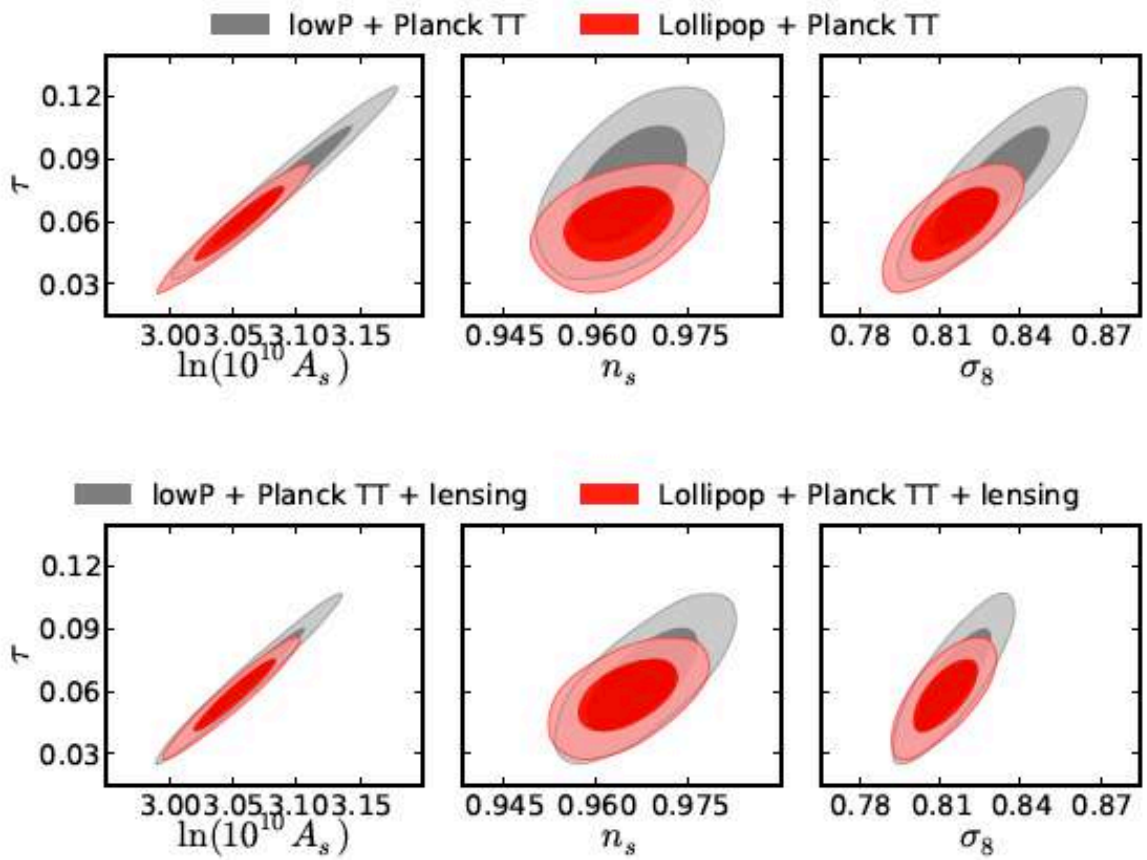

$$\tau = 0.053^{+0.014}_{-0.016}, \qquad \texttt{lollipop}^{5};$$

$$\tau = 0.058^{+0.012}_{-0.012}, \qquad \texttt{lollipop}\text{+PlanckTT};$$

$$\tau = 0.058^{+0.011}_{-0.012}, \qquad \texttt{lollipop}\text{+PlanckTT+lensing};$$

$$\tau = 0.054^{+0.012}_{-0.013}, \qquad \texttt{lollipop}\text{+PlanckTT+VHL}.$$

Physics of the 21cm line probe

- Historic overview
- Basic Formulae (Field 1958)
- Excitation mechanisms (Ly-α, collisions,..)
- Global evolution of the spin temp.
- Patchy evolution
- Simulation results

Historic overview

- H.C. van de Hulst (inspired by J. Oort) showed the potential of the 21 cm transition in astronomy - 1945
- The first astronomical observation of the 21 cm: H.I. Ewen & E.M. Purcell (1951, Nat. 168, 356) C.A. Muller & J.H. Oort (1951, Nat. 168, 357-8)
- Excitation mechanism Wouthuysen (1952). Field (1958, 1959) gave the proper framework.
- Importance for cosmology was inspired by Zel'dovich's top down scenario.

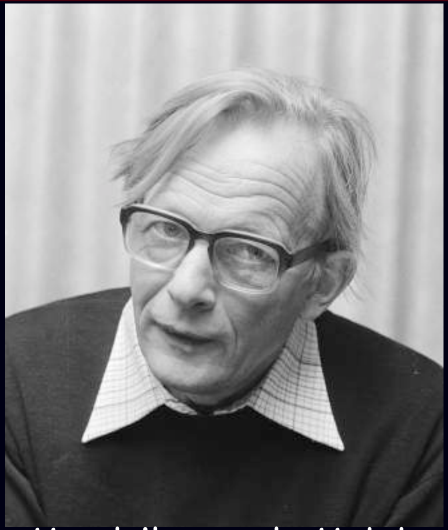

Hendrik van de Hulst

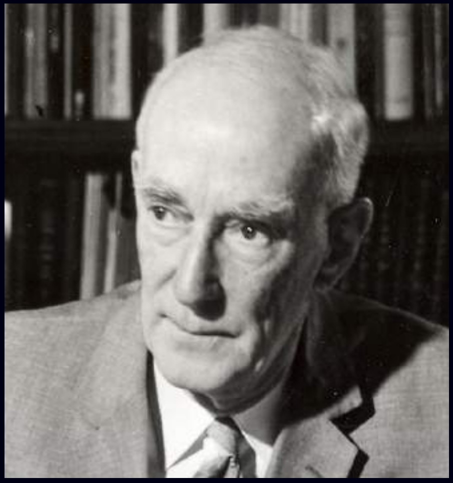

Jaan Oort

Historic overview

- Scott & Rees (1992) pointed out that a signal could detected from high z 21 cm.
- Madau, Meiksin & Rees (1997) were the first to consider the interplay between the first sources and the 21 cm transition.
- Over the years many observational attempts failed. Shaver et al. 1999 argued that we can observe high redshift 21 cm radiation.
- Many telescopes targeting the high redshift Universe have been build or in the process of being built.

Martin Rees

21-cm Physics

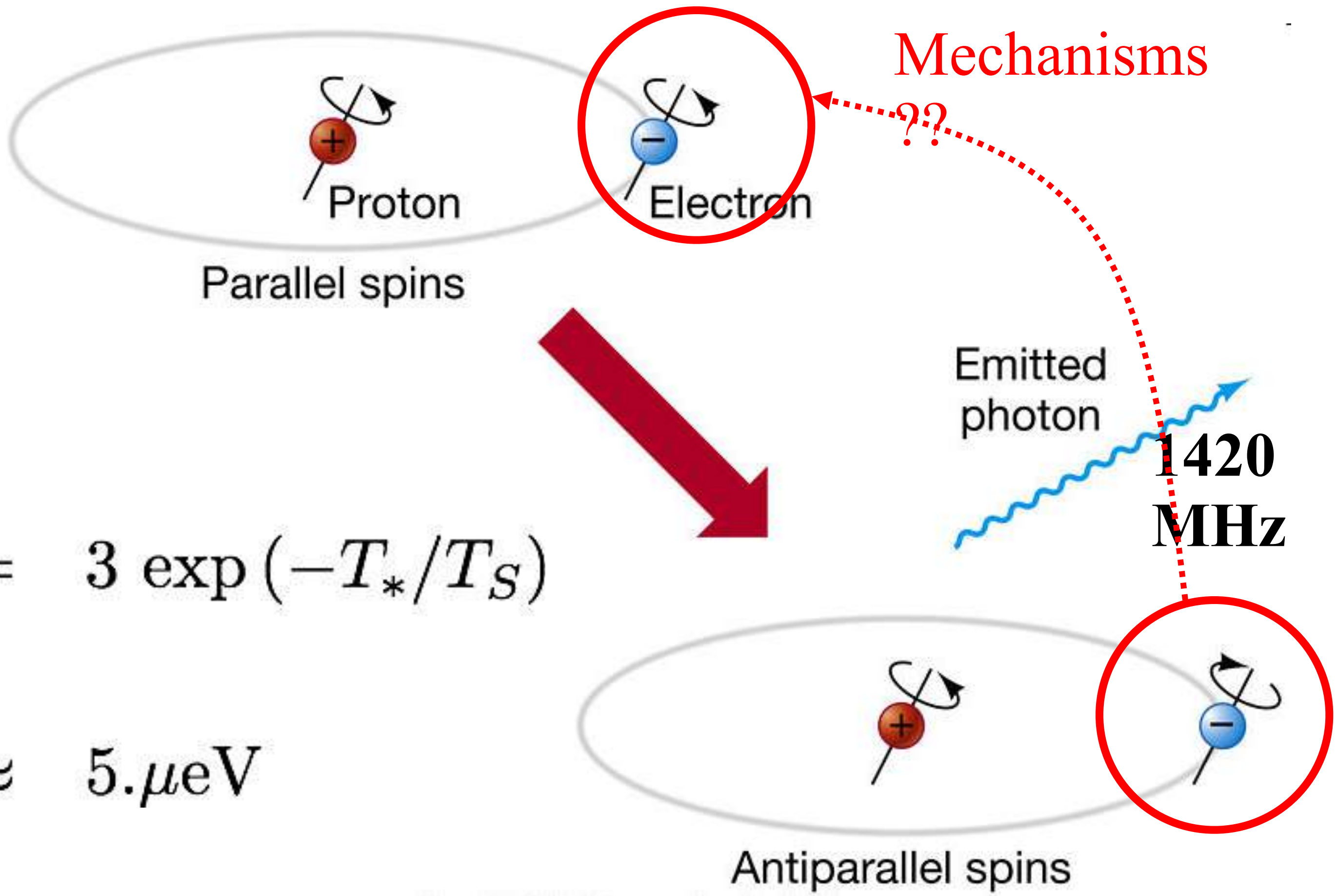

$$\frac{n_1}{n_0} = 3 \exp\left(-T_*/T_S\right)$$

$$T_* \approx 5.\mu\mathrm{eV}$$

Lifetime of ~10 Myrs

The 21 cm transition

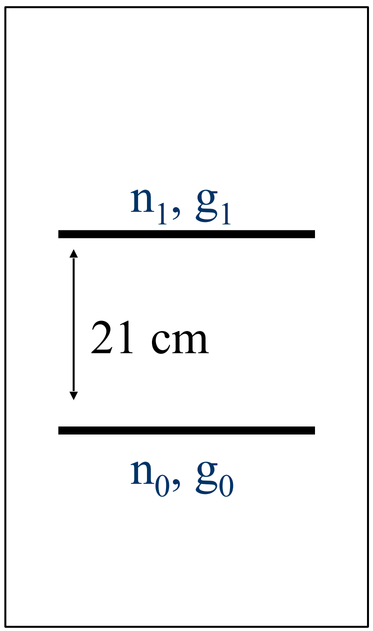

- The value of the T_s is given by:

$$T_s^{-1} = \frac{T_{CMB}^{-1} + x_c T_k^{-1} + x_\alpha T_k^{-1}}{1 + x_c + x_\alpha}$$

Field 1958
Madau et al 98
Ciardi & Madau 2003
Furlanetto et al. 2006

Lyman-α Coupling

- The Wouthuysen-Fiel effect, also known as Lyman-alpha pumping.

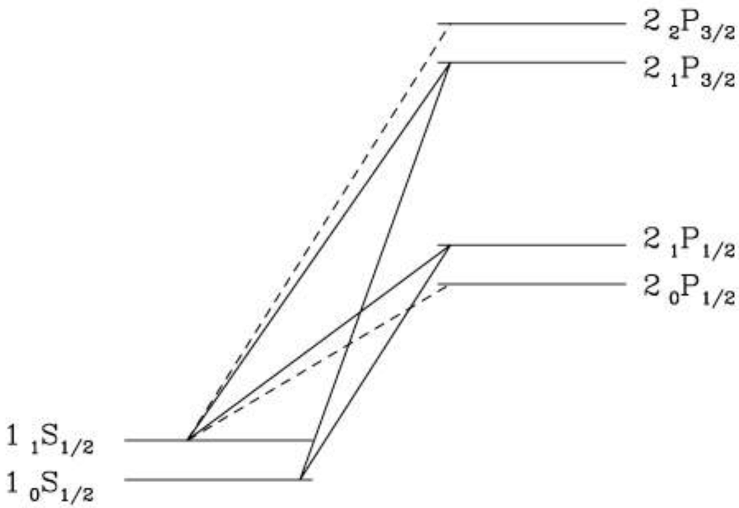

Dominant in both in the case of stars and Black-holes, due to photo and collisional excitations, respectively.

Wouthuysen 1952
Field 1958

of the larger component. Because of the slight depth of eclipse and the trouble with comparison stars, the above results by themselves cannot be considered as anything more than suggestive. However, E. F. Carpenter's observations taken in the blue, yellow, and ultra-violet on this night and the preceding one, show this effect very clearly and leave little doubt of its reality.

It should further be noted that if the present fragmentary results prove to be a fair sample, the system is free from those erratic light changes which add such complexities to the interpretation of other systems of this sort.

Flower and Cook Observatories,
University of Pennsylvania.

Woolard, Edgar W. A comparison of Brown's Lunar Tables with the theory from which they were constructed.

For 60 dates at half-day intervals, from 1948 April 24.0 to May 24.0 UT, the longitude and latitude of the moon to two decimals of a second of arc and the parallax to three decimals were taken from Brown's tables and compared with values that had been computed to 5 decimals directly from Brown's theoretical expressions by the Selective Sequence Electronic Computer of International Business Machines Corporation.

Significant differences between the SSEC and the tabular values were evident in the longitude and in the latitude. The discrepancy in the longitude is very small but is systematic, the principal part apparently having a period of about a month, with an amplitude of the order of $0\overset{''}{.}1$; the discrepancy in the latitude is strongly periodic, with an amplitude about $0\overset{''}{.}15$ and a period about a month.

An analysis of these differences to determine their source appeared advisable. The SSEC computations were therefore compared in detail with the tabular computations for the longitude on 14 selected dates, and for the latitude on 12 of these dates. The differences are for the most part satisfactorily accounted for by approximations and expedients adopted by Brown and Hedrick in the construction of the tables to facilitate their practical use, and are within the standards of accuracy that were set for the tables. The large discrepancy in the latitude, however, is principally due to an oversight in the tables; in constructing the tables, the effect of the long period variations of the lunar inclination upon several of the large terms in the latitude was inadvertently included twice.

The resulting error in the tabular latitude is large enough to be detected in observations; it has been found in a comparison of the tabular latitude with the observed latitude obtained with the 6-inch transit circle at the U. S. Naval Observatory during 1929–1949.

U. S. Naval Observatory,
Washington, D. C.

Wouthuysen, S. A. On the excitation mechanism of the 21-cm (radio-frequency) interstellar hydrogen emission line.

The mechanism proposed here is a radiative one: as a consequence of absorption and re-emission of Lyman-α resonance radiation, a redistribution over the two hyperfine-structure components of the ground level will take place. Under the assumption—here certainly permitted—that induced emissions can be negelcted, it can easily be shown that the relative distribution of the two levels in question, under stationary conditions, will depend solely on the shape of the radiation spectrum in the Lα region, and not on the absolute intensity.

The shape of the spectrum of resonance radiation, quasi-imprisoned in a large gas cloud, could only be determined by a careful study of the "scattering" process (absorption and re-emission) in a cloud of definite shape and dimensions. The spectrum will turn out to depend upon the localization in the cloud.

Some features can be inferred from more general considerations. Take a gas in a large container, with perfectly reflecting walls. Let the gas be in equilibrium at temperature T, together with Planck radiation of that same temperature. The scattering processes will not affect the radiation spectrum. One can infer from this fact that the photons, after an infinite number of scattering processes on gas atoms with kinetic temperature T, will obtain a statistical distribution over the spectrum proportional to the Planck-radiation spectrum of temperature T. After a finite but large number of scattering processes the Planck shape will be produced in a region around the initial frequency.

Photons reaching a point far inside an interstellar gas cloud, with a frequency near the Lα resonance frequency, will have suffered on the average a tremendous number of collisions. Hence in that region, which is wider the larger the optical depth of the cloud is for the Lyman radiation, the Planck spectrum corresponding to the gas-kinetic temperature will be established

as far as the shape is concerned. Because, however, the relative occupation of the two hyperfine-structure components of the ground state depends only upon the shape of the spectrum near the Lα frequency, this occupation will be the one corresponding to equilibrium at the gas temperature.

The conclusion is that the resonance radiation provides a long-range interaction between gas atoms, which forces the internal (spin-)degree of freedom into thermal equilibrium with the thermal motion of the atoms.

Institute for Theoretical
Physics of the City University,
Amsterdam.

Zechiel, Leon N. and Geoffrey Keller. A survey of eclipsing binary systems showing apsidal motion.

Thirty eclipsing binary systems of known or suspected apsidal motion were analyzed to determine whether a correlation could be made between the mass distribution within the stars and the spectral type. A set of combined photometric and spectroscopic elements for each system was assembled. Some systems have not been observed spectroscopically, and the values of the eccentricity and the apsidal period had to be estimated from photometric data alone in these cases. The data has been tabulated for all systems which have been adequately observed. Fourteen cases in which apsidal motion has been indicated, but for which the data are insufficient to support detailed analysis, were rejected.

The final sets of elements for each system were analyzed by the method of Sterne, yielding the apsidal coefficients, k_2, which are a measure of the degree of central condensation of the mass of the stars. Values of the effective polytropic index of each star were obtained from the quantities k_2 in the usual manner. The absolute dimensions of the systems were derived from the elements by various methods suited to the data available in each case.

The final results were embodied in a table, and a plot of the effective polytropic index versus the spectral type was made. A similar plot was constructed from the analysis by Russell in 1939. A comparison shows considerable change in the plot due to the reclassification of the spectra of several of the stars and to the inclusion of new data. There appears to be a limitation of n_{eff} to values between 2.9 and 4.1, with the lower values tending to be associated with earlier spectral types. The ratio of central density to mean density is 54 for a polytrope of index 3.0 and 614 for a polytrope of index 4.0. While the stars in this survey were not assumed to be polytropes these two cases represent models having values of k_2 corresponding roughly to the observed range. The spectral types represented in the survey ranged from O8.5 to F2.

Perkins Observatory,
Delaware, Ohio.

TITLES OF ADDITIONAL PAPERS PRESENTED AT THE MEETING IN CLEVELAND, OHIO

Anderson, J. Pamelia. The position of the moon at the time of the 1948 eclipse.
Bidelman, W. P. and W. W. Morgan. A remarkable O-type star.
Binnendijk, L. The space distribution of interstellar material in the Milky Way.
Bok, Bart J. and Margaret Olmsted. Magnitude standards for the southern hemisphere.
Cook, Allan F. II. Radiative equilibrium in a hydrogen atmosphere.
Eckert, W. J., Rebecca B. Jones and H. K. Clark. A precise lunar ephemeris.
Genatt, Sol H. Note on a graphical method for the prediction of occultations.
Goldberg, Leo, R. R. McMath, O. C. Mohler and A. K. Pierce. Identification of *CO* in the solar atmosphere.
Harwood, Margaret. The nova-like variable CM Aquilae.
Henriksen, S. W. Note on the kinematics of the moon's motion.
Johnson, Harold L. Magnitude systems.
McKellar, Andrew, G. J. Odgers and L. H. Aller. The chromospheric K-line during the recent eclipse of 31 Cygni.
Mears, D. D. Field techniques for occultation observation.
Millis, John. The genesis of Saturn and its rings.
Neyman, J. and C. D. Shane. A model of spatial distribution of galaxies. Preliminary report.
O'Keefe, John A. and J. Pamelia Anderson. Calculation of the earth's radius from occultation data.
Osterbrock, Donald A. The time of relaxation for stars in a fluctuating density field.
Panay, T. N. and John A. O'keefe. Progress on the measurements of darkening at the sun's limb from the results of the 1948 eclipse.
Scott, Elizabeth R. Theoretical counterparts of certain observable distributions relating to galaxies.
Swope, Henrietta H. Photographic magnitudes and colors in the globular cluster NGC 6397.
Thomsen, Warren J. The path and orbit of the detonating meteor of August 29, 1951.
White, Marvin S. Note on the accuracy of Hayn's charts as measured by photoelectric observation.
Wrubel, Marshal H. On the decay of a primeval stellar magnetic field.
Wylie, C. C. The path and orbit of the detonating meteor of July 28, 1951.

Collisional Coupling

- H-H collisions that excite the 21 cm transition. This interaction proceeds through electron exchange.

- H-e collisions. Especially important around primordial X-ray sources (mini-quasars).
  - This effect might also excite Lyman-alpha transition which adds to the T_s- T_{CMB} decoupling efficiency.

δT_b, The Brightness Temperature

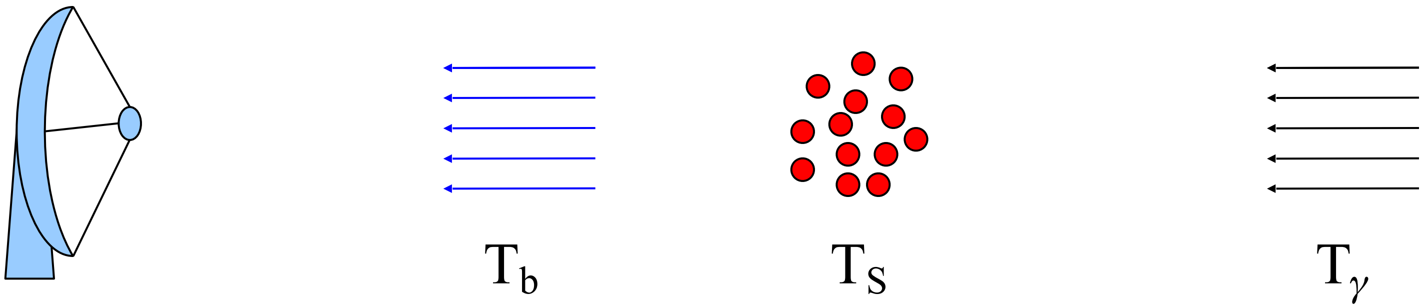

$$T_b(\nu) = T_S\left(1 - e^{-\tau_\nu}\right) + T_\gamma(\nu) e^{-\tau_\nu}$$

$$\delta T_b(\nu) \equiv T_b - T_\gamma = (T_S - T_\gamma)\left(1 - e^{-\tau_\nu}\right)$$

Where the optical depth is given by:

$$\tau_\nu = \int \mathrm{d}s\, \sigma_{01}\left(1 - e^{-E_{10}/k_B T_S}\right)\phi(\nu)\, n_0$$

$$\tau_\nu \approx \sigma_{01} \left(\frac{h\nu}{k_B T_s} \right) \left(\frac{N_{HI}}{4} \right) \phi(\nu)$$

$$\sigma_{01} \equiv \frac{3c^2 A_{10}}{8\pi\nu^2}$$

- $A_{10} = 2.85 \times 10^{-15}\ s^{-1}$ is the spontaneous emission coefficient. It corresponds to a lifetime of the triplet state of 1.1×10^7 years.
- N_{HI} is the column density of HI, defined as $\int n_0 ds$
- 1/4 accounts for the fraction of HI atoms in the singlet state
- $\phi(\nu)$ is the line profile. Generally, the this profile is broadened by four effects: Natural, thermal, turbulent and pressure, here through the bulk motion which leads to broadening of the line is the main effect. Remember

$$\int \phi(\nu)\mathrm{d}\nu$$

The change in velocity ΔV is roughly $\Delta s\, H(z)$, therefore,

$$\phi(\nu) \propto c/\Delta s H(z)\nu$$

We also substitute $$N_{HI} = x_{HI} n_H \Delta s$$

An accurate calculation of the optical depth at a given redshift, which takes into account line profile broadening due to Hubble expansion and casts the relation in terms of number density, yields:

$$\begin{aligned} \tau_{\nu_0} &= \frac{3}{32\pi} \frac{hc^3 A_{10}}{k_B T_S \nu_0^2} \frac{\mathrm{x}_{HI} n_H}{(1+z)\left(\mathrm{d}v_{\|}/\mathrm{d}r_{\|}\right)} \\ &\approx 0.0092\,(1+\delta)\,(1+z)^{3/2} \frac{\mathrm{x}_{H\,I}}{T_S} \left[\frac{H(z)/(1+z)}{\mathrm{d}v_{\|}/\mathrm{d}r_{\|}}\right] \end{aligned}$$

δT_b: Brightness temperature

$$\delta T_b \approx 28\mathrm{mK}\,(1+\delta)\,x_{HI}\,\frac{T_s - T_{CMB}}{T_s}\,\frac{\Omega_b h^2}{0.02}\left[\frac{0.24}{\Omega_m}\left(\frac{1+z}{10}\right)\right]^{\frac{1}{2}}\left[\frac{H(z)/(1+z)}{dv_{\parallel}/dr_{\parallel}}\right]$$

Astrophysics

Cosmology

- The Interpretation might be very complicated
- Notice that the signal in absorption can be much smaller

The Global evolution of the Spin Temperature

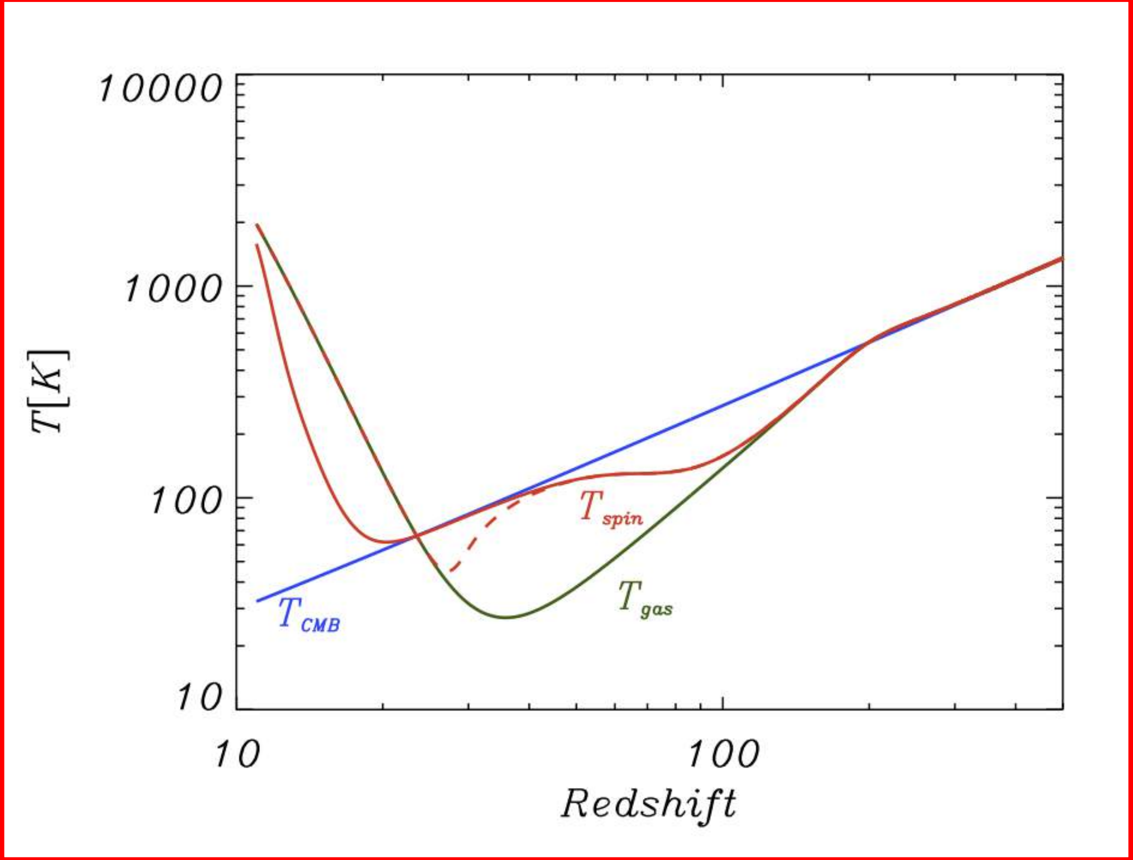

At z~20 T_s is tightly coupled to T_{CMB}. In order to observe the 21 cm radiation decoupling must occur.

Heating much above the CMB temp. and decoupling do not necessarily occur together.

Loeb & Zaldarriaga 2004,Pritchard & Loeb 2008, Baek et al. 2010, Thomas & Zaroubi 2010

The Global evolution of T_s

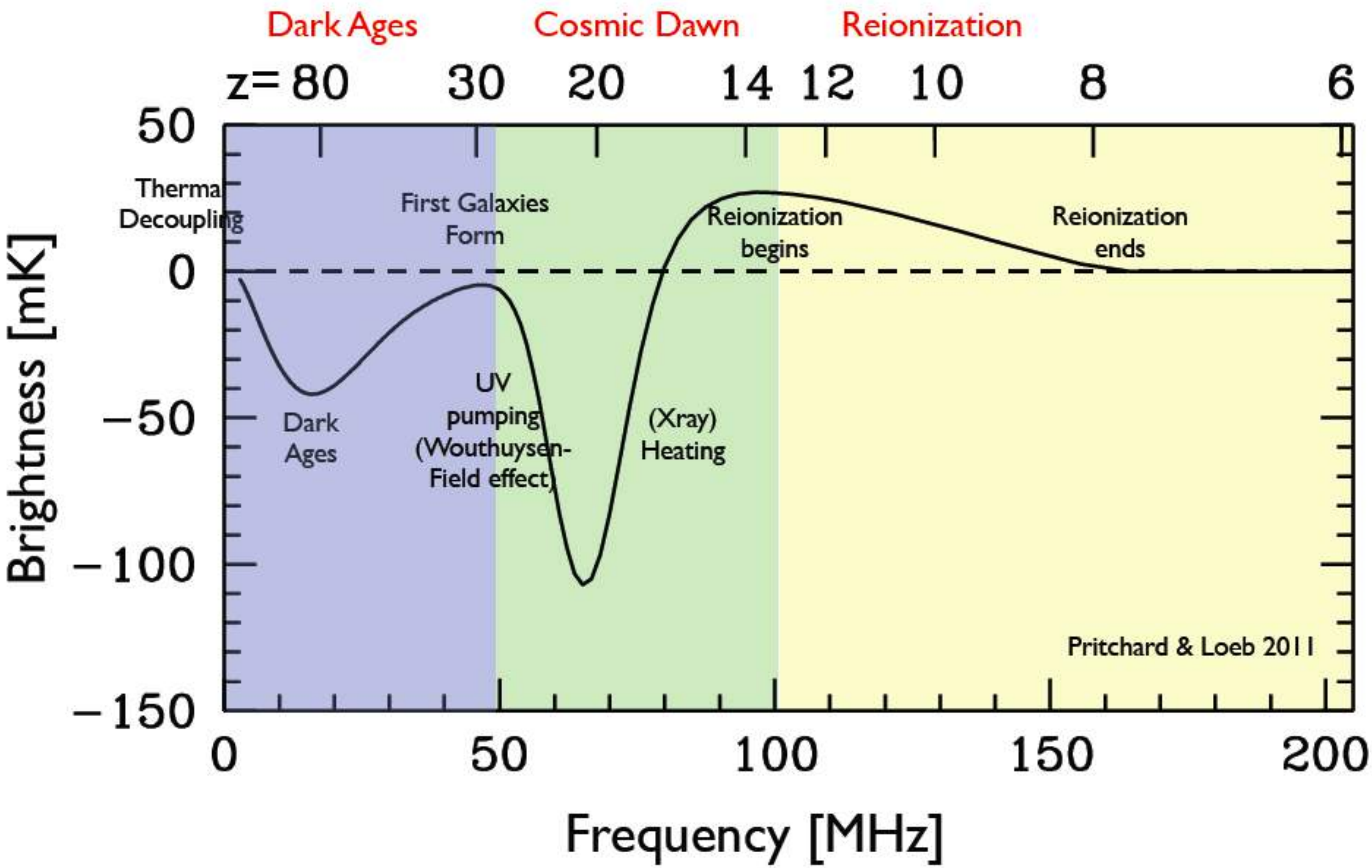

$T_{CMB} \propto 1+z$ $T_k \propto (1+z)^2$

Compton heating rate $\epsilon_{comp} \approx \frac{n_e k_B (T_{CMB} - T_k)}{t_{comp}}$

Compton cooling time

$$t_{comp} = \frac{3 m_e c}{8 \sigma_T u_\gamma}$$

$$u_\gamma \propto T_{CMB}^4$$

This drives the Compton heating rate to almost zero

The redshift of thermal decoupling is about 200

(proper calculation could be done with the publicly available code RECFAST)

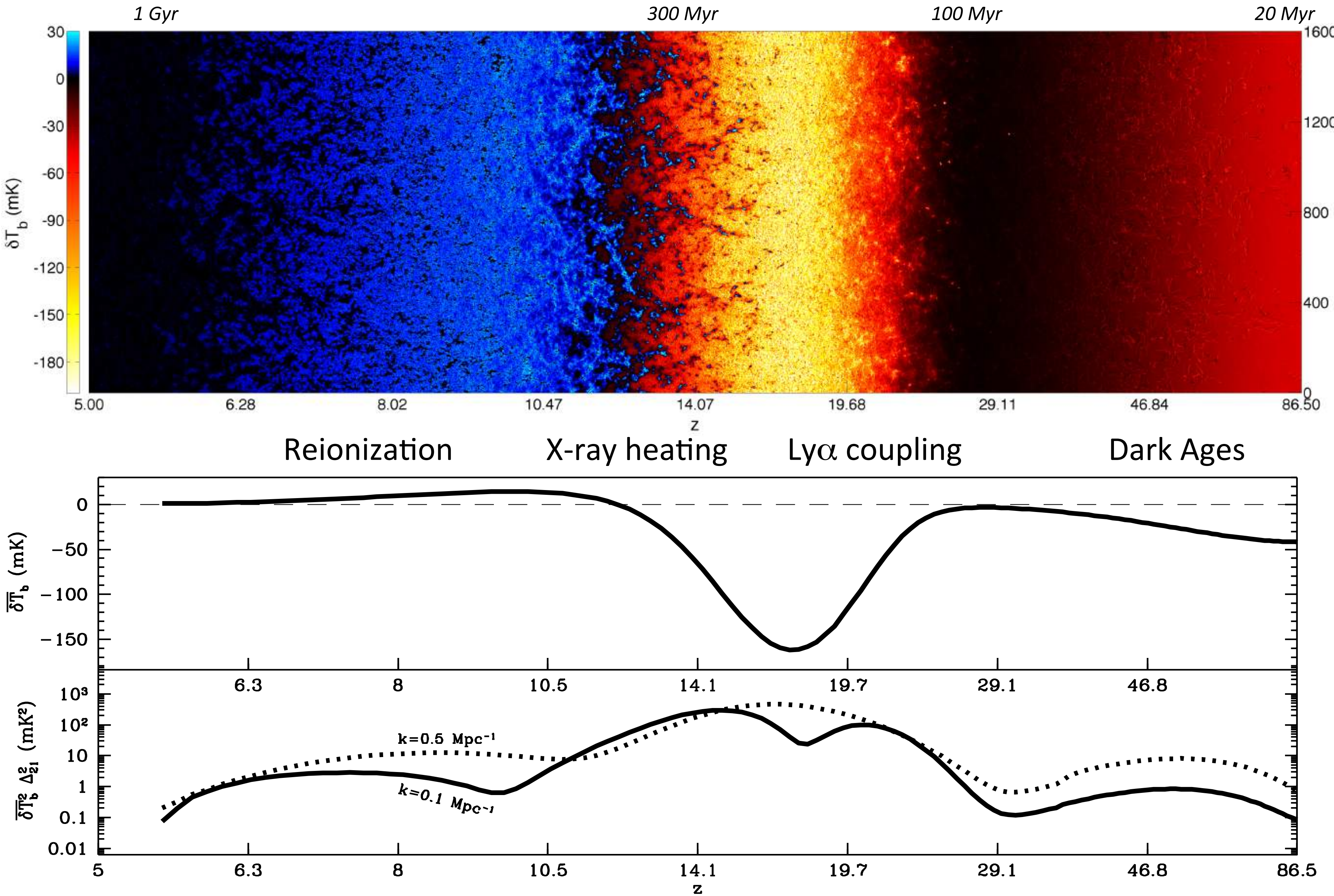

Mesinger et al. 2016, Koopmans et. al 2019

The Dark Ages

Only feasible from the Moon

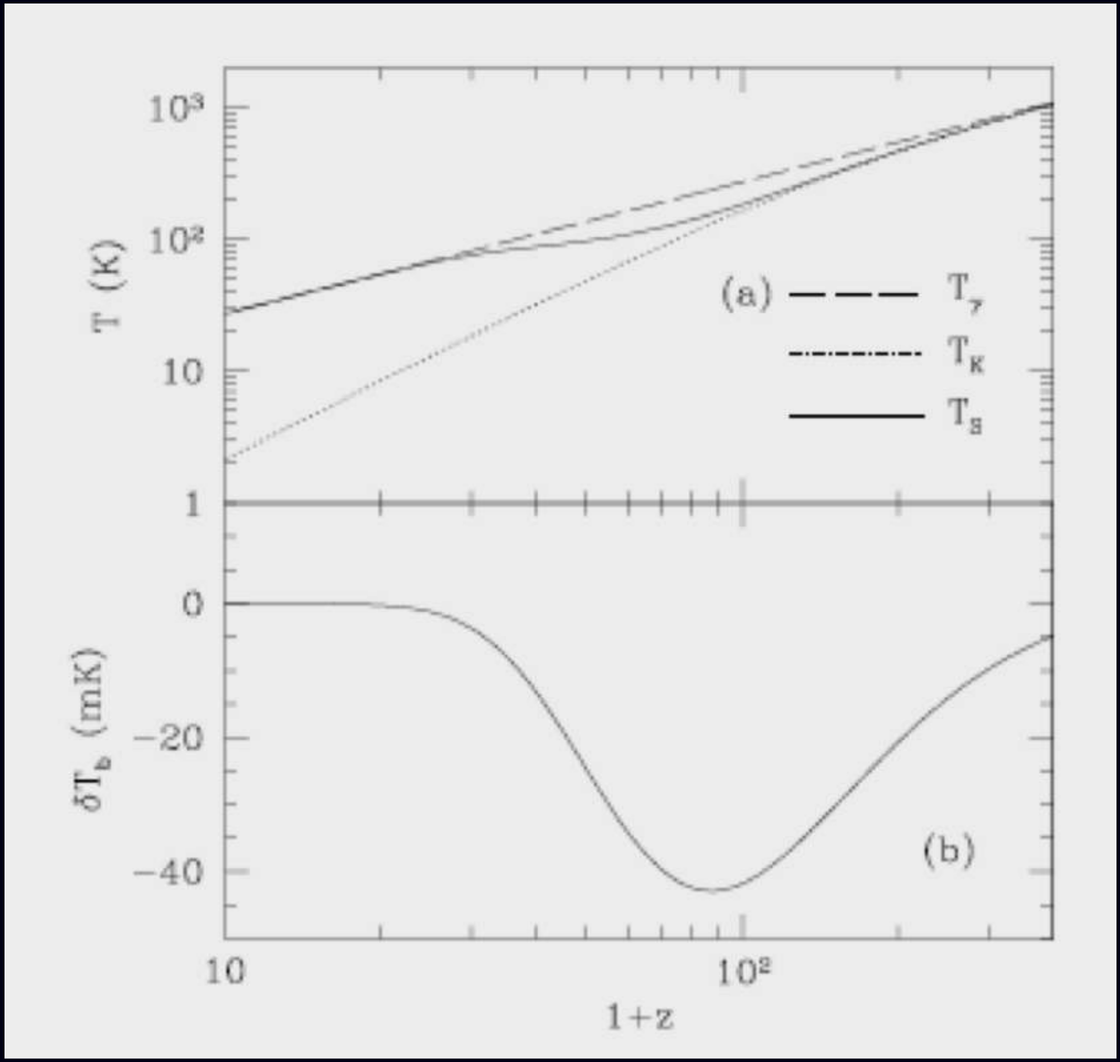

Loeb & Zaldarriaga 04

Ionization sources

Mean free path

$$\langle l_E \rangle \approx \frac{1}{n_H \sigma_H(E)}$$

Bound-free
Cross section

$$\sigma_H(E) = \sigma_0 \left(E_0/E\right)^3$$

$n_H = 2.2 \times 10^{-7}\ \mathrm{cm}^{-3}\ (1+z)^3$
$\sigma_0 = 6 \times 10^{-18}\ \mathrm{cm}^2$
$E_0 = 13.6\ eV$

At $z = 9$: For $E = E_0$ $\langle l_E \rangle \approx 2$ kpc comoving
For $E = 1$ keV $\langle l_E \rangle \approx 1$ Mpc comoving

UV photons

Large cross section but ejected electron has low energy

X-ray photons

Low cross section but ejected electron has high energy

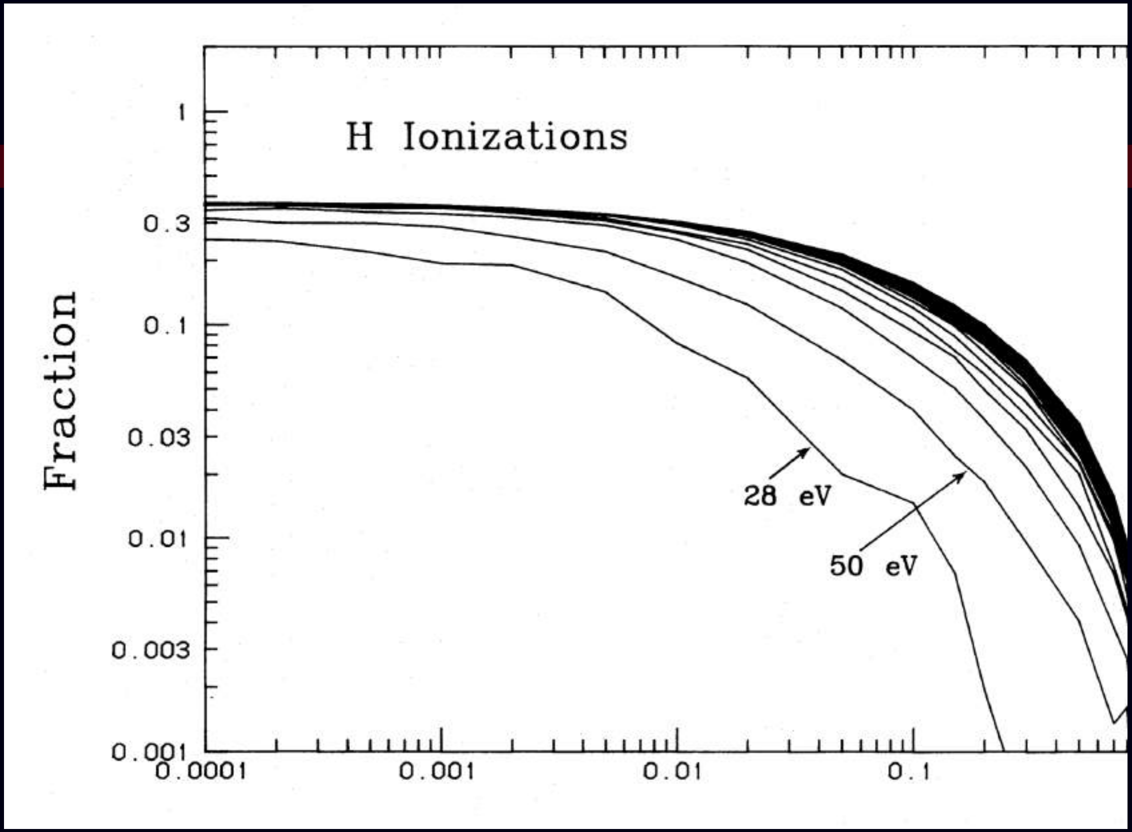

The fraction of photon energy that goes to reionization, heating and excitation is roughly 1:1:1 as calculated with Monte-Carlo radiative transfer code by Shull & van Steenberg (1986) and Valdes et al. 2009.

The signal: Stars vs. Miniqsos

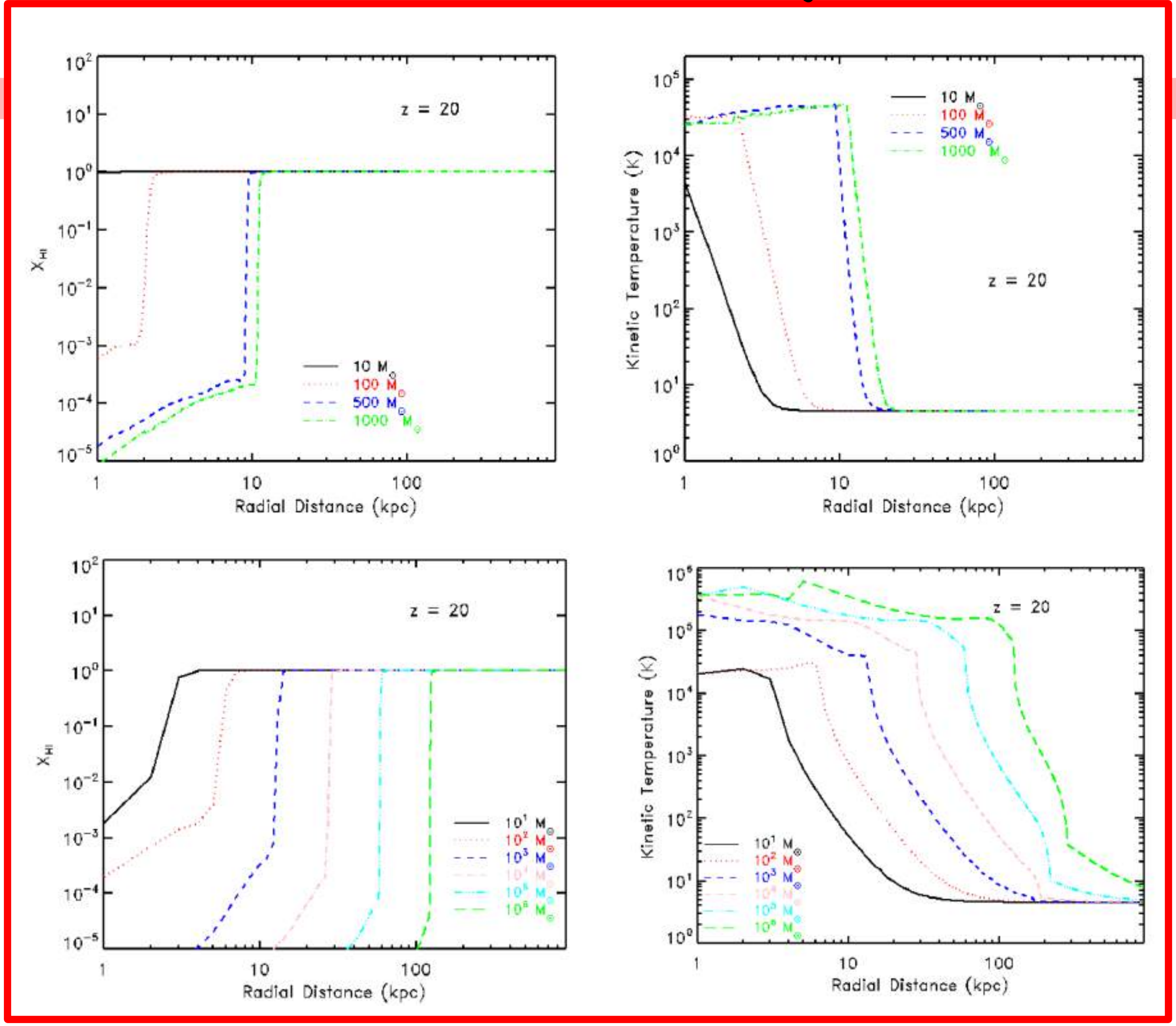

Thomas & Zaroubi 2008

What happens around a high Redshift x-ray source

Kinetic temperature is greatly heated just beyond the HII region,
but further out it has been adiabatically cooled.

21cm absorption strongly dominates over the inner emission core

$M_{BH}=10^4\ M_{sun}$

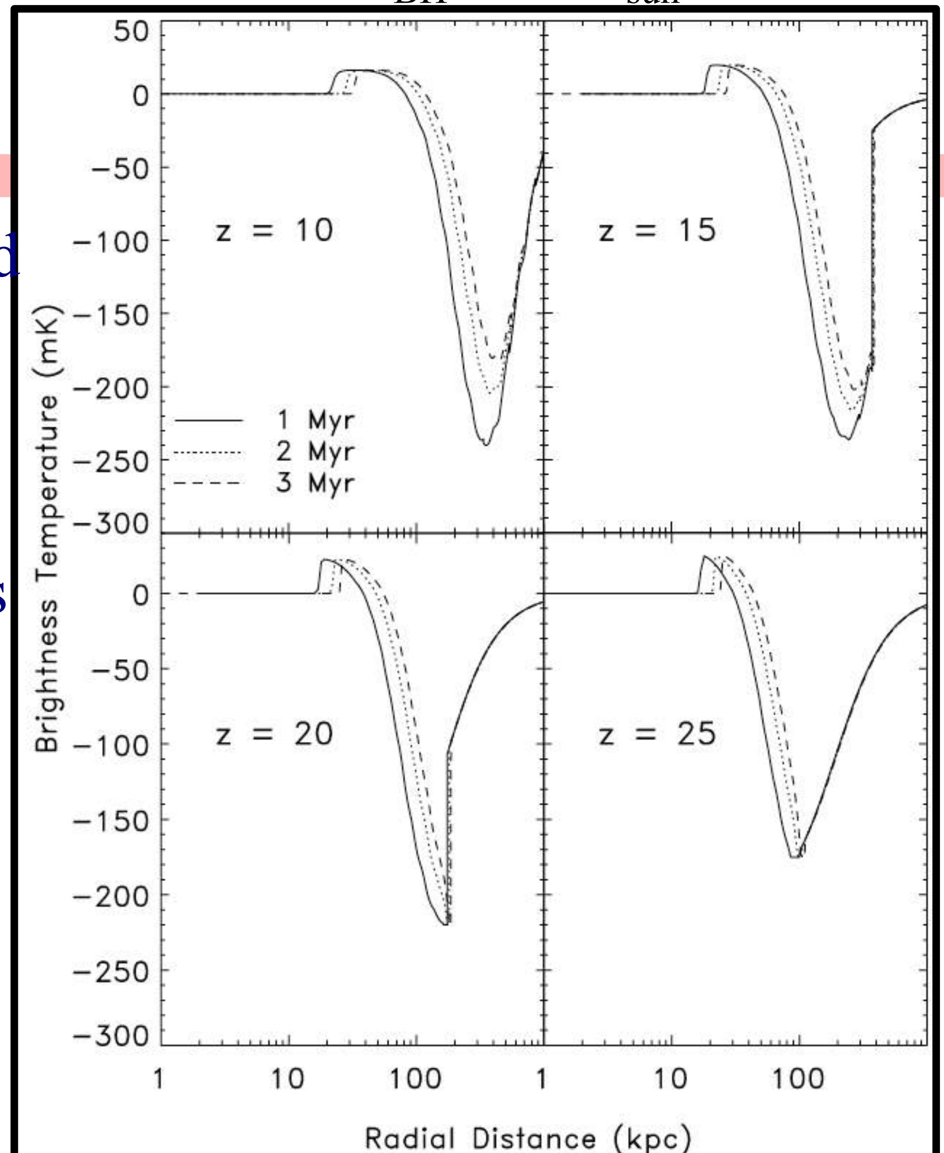

Thomas & Zaroubi 2008

Simulations of the EoR

- Cosmological Hydro simulations:
  - 1- High enough resolution to resolve halos in which ionization sources form.
  - 2- Spans Large Scales as well as small scales, especially since designed arrays have small 1' res.
  - 3- In certain cases DM only simulations are sufficient.
- Out of equilibrium Radiative Transfer:
  - 1- Source and their flux.
  - 2- Ionization of H and He (not always done).
  - 3- Heating due to the radiative processes.
  - 4- Spin temp decoupling (Lyα RT).
- It is very difficult to account for all the physical aspects of the problem and approximations are normally made.

Credit: Marcelo Alvarez

Different Scenarios in high res. sim.

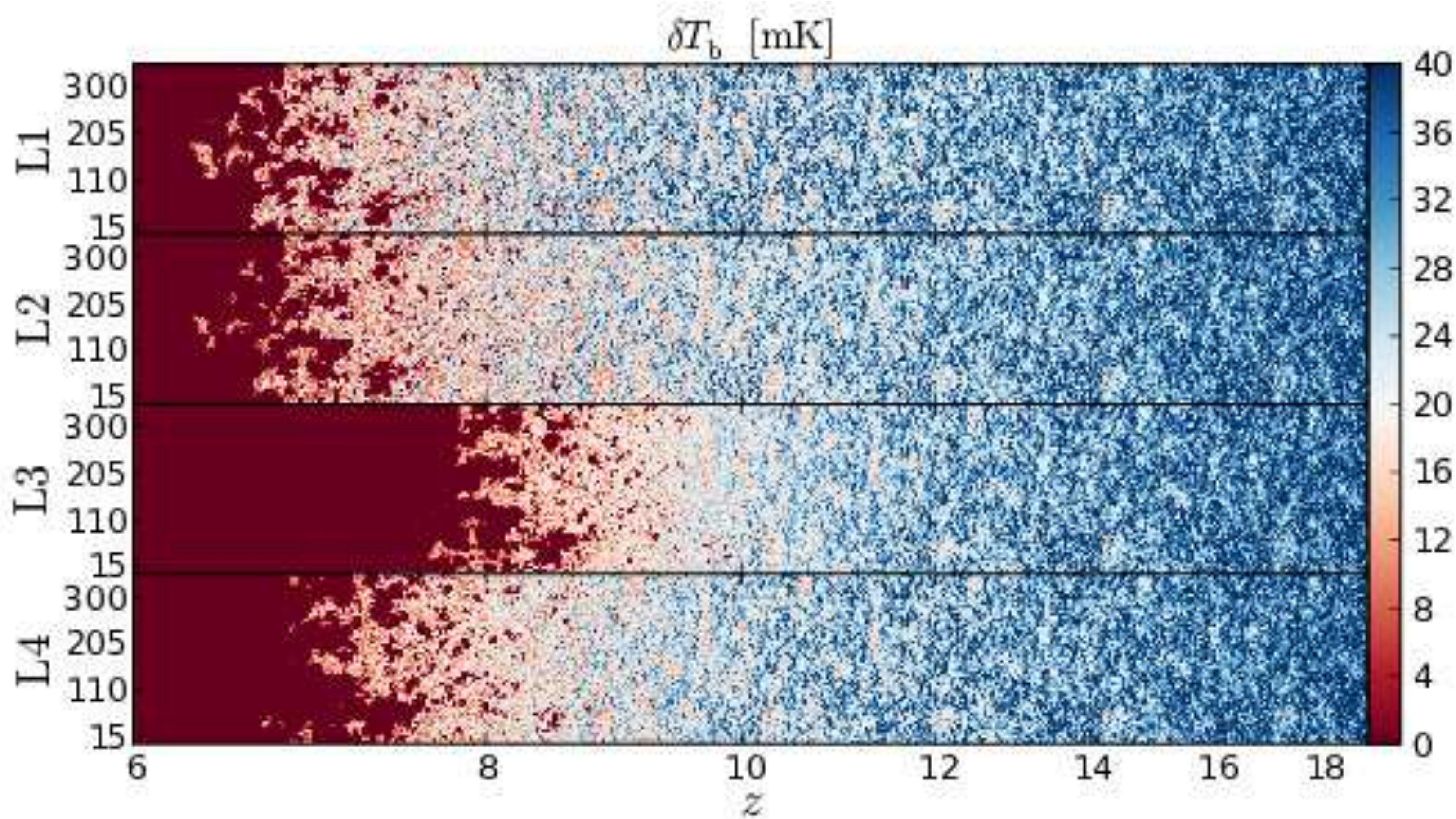

Dixon et al. 2015

Approximate Numerical Methods:

There are a number of approximate methods. The most developed of them is 21cmFast developed by A. Mesinger & co.

It relates the emission rate of ionising photons per baryon $\dot{n}_{ion}/b$ to the collapse factor of the IGM using Press-Schechter like formalism.

$$\dot{n}_{\rm ion/b} = \frac{d}{dt}\left[\bar{\rho}_m^{-1}\int_{M_{\rm min}}^{\infty} dM_h \frac{dn}{d\ln M_h} f_{\rm b} f_* N_{\gamma/b} f_{\rm esc}\right]$$

where f_b is the baryon fraction of a halo, f_* is the fraction of halo baryons ending up as stars, N_γ/b the number of ionizing photons per stellar baryon and f_{esc} is the escape fraction into the IGM.
This could rewritten in terms of collapse fraction as follows:

$$\dot{n}_{\rm ion/b} = \zeta \frac{df_{\rm coll}(> M_{\rm min}, z)}{dt}$$

(Mesinger & Furlanetto 2007; Mesinger et al. 2011).

21cmFast light cone

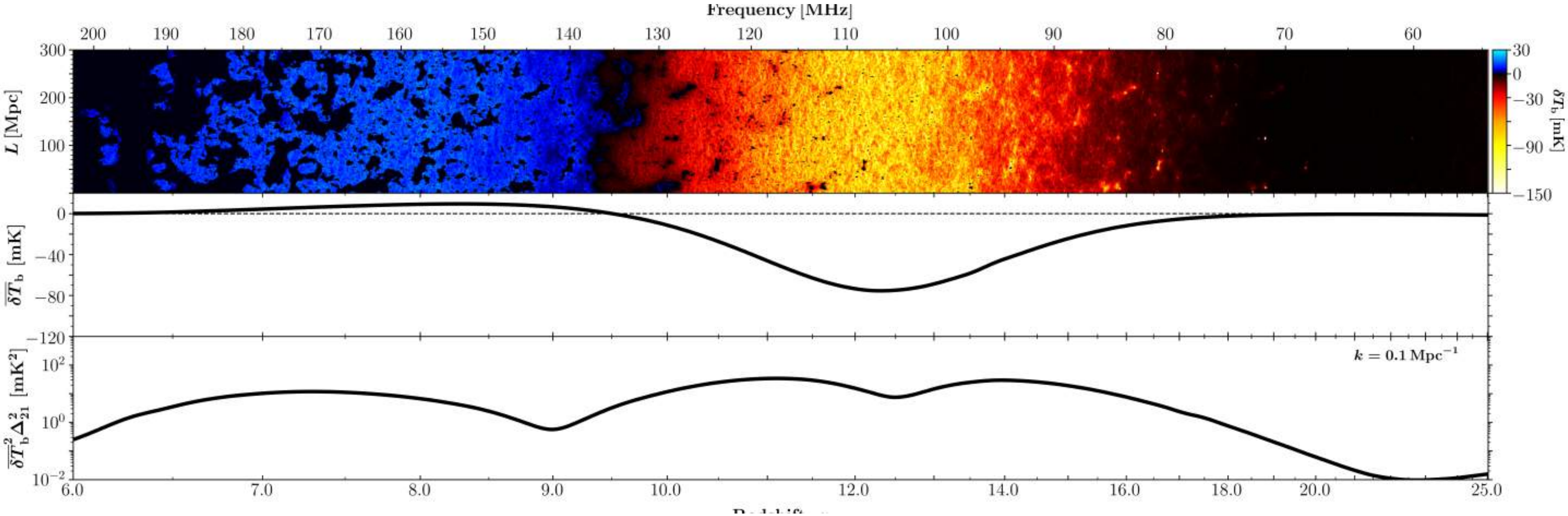

A similar approach was developed by Santos et al. 2010 SimFast21.

Spherically symmetric 1D RT

This approach is in between full simulations and 21cmFast.

- It needs an N-body simulation and identifications of the haloes as a function of redshift.
- It assumes a spherical symmetry of ionising bubbles around the sources and calculates in detail the ionization and heating profile around each source.
-It deals with bubble overlap in an efficient way.

(Thomas+ 2008,2009,2011, Krause+ 2018)

The method was adopted by Ghara who called it GRIZZLY

(Ghara+ 2015, 2017, 2019)

Results from BEARS & GRIZLEY

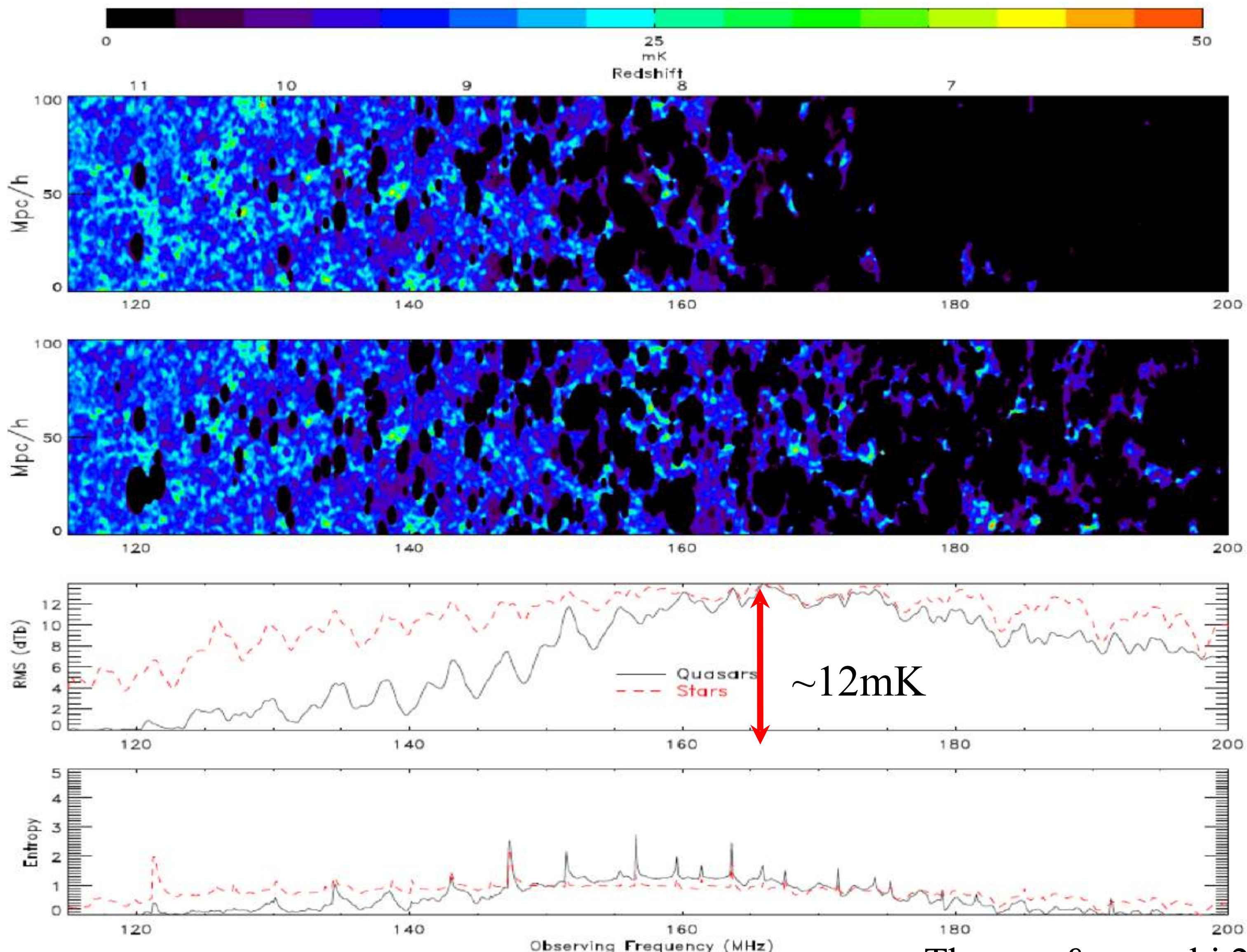

Thomas & zaroubi 2008

Full vs. approximate simulations

- Full 3D RT simulations are more accurate but computationally expensive. They provide crucial insight about the physical processes (especially on small scales).
- Approximate methods are less accurate but easier to produce and allow for an exploration of the parameters space. This is especially important for interpretation of the data

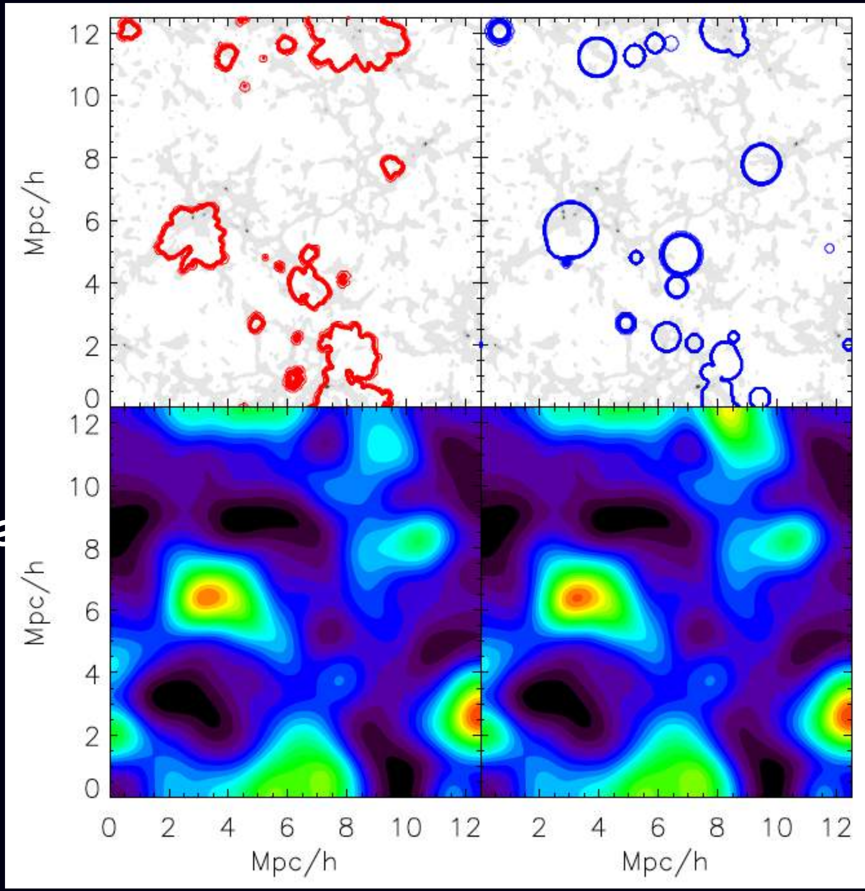

Thomas et al 2009

Spin Temperature issues

In case the spin temp. is of the order the CMB temp. or smaller an absorption signature is expected at high redshifts.

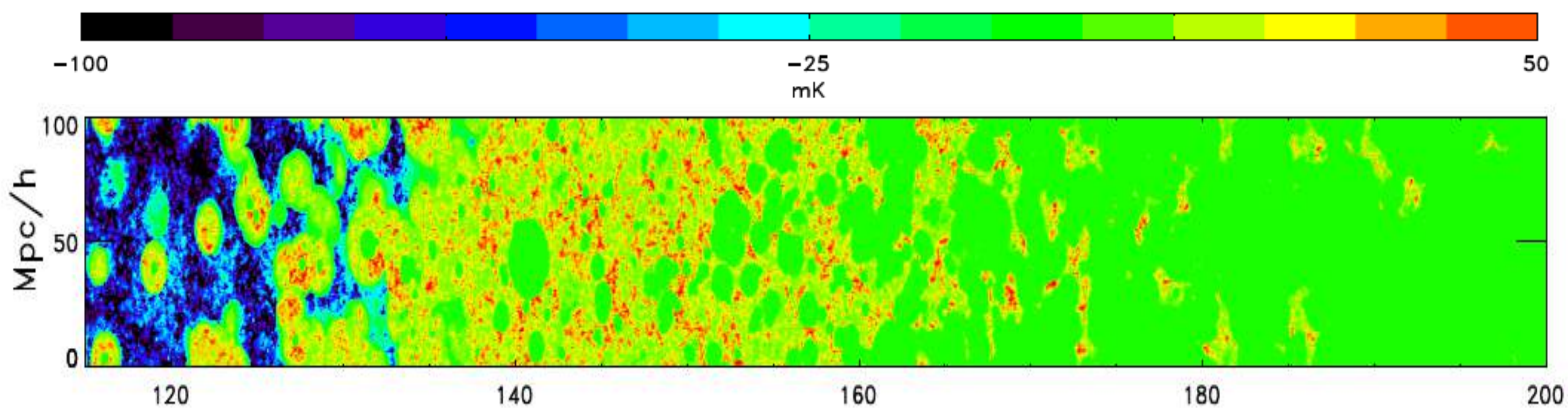

$$\delta T_b \approx 28\mathrm{mK}\,(1+\delta)x_{HI}\frac{T_s - T_{CMB}}{T_s}\frac{\Omega_b h^2}{0.02}\left[\frac{0.24}{\Omega_m}\left(\frac{1+z}{10}\right)\right]^{\frac{1}{2}}$$

Thomas & Zaroubi 2010
See also Baek et al. 2010

The 21 cm forest

The equivalent of the Ly-alpha forest. Requires high z

(Carilli et al. 2005 2007)

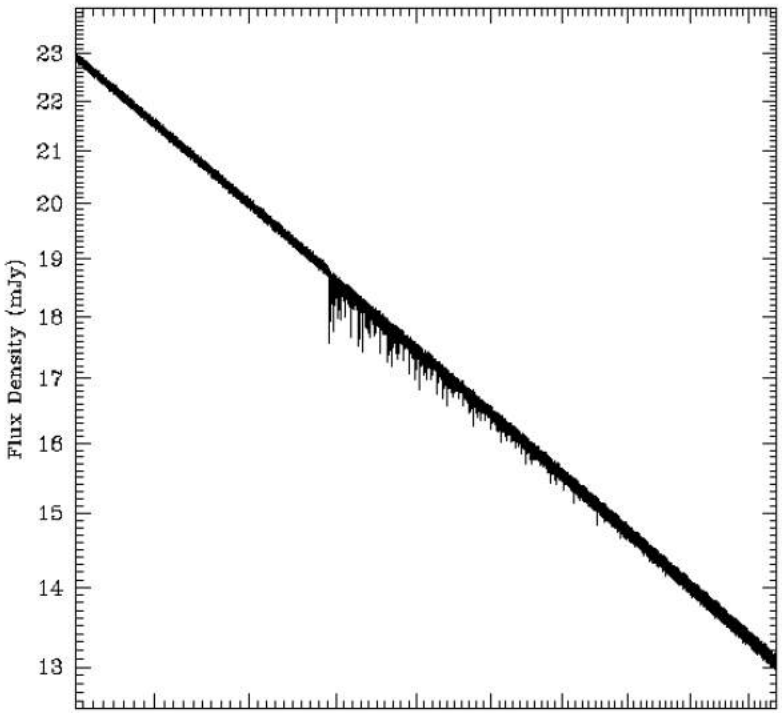

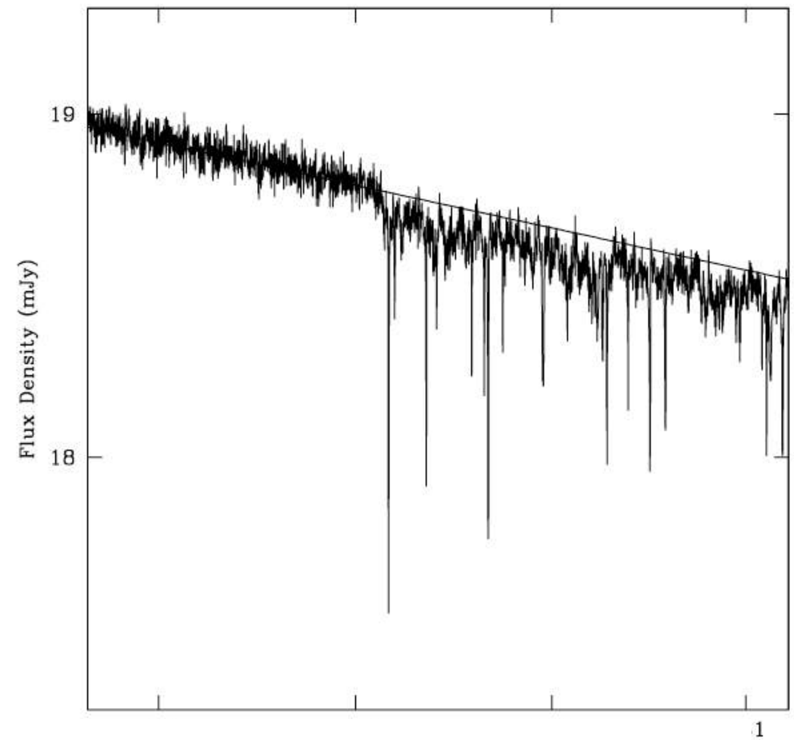

Simulated spectrum from 100 MHz to 200 MHz of a source with S_{120} = 20 mJy at z=10 using the Cygnus A spectral model and SKA noise

21 cm forest

$$\tau_{21cm} \propto x_{HI}(1+\delta)\frac{1}{T_s}$$

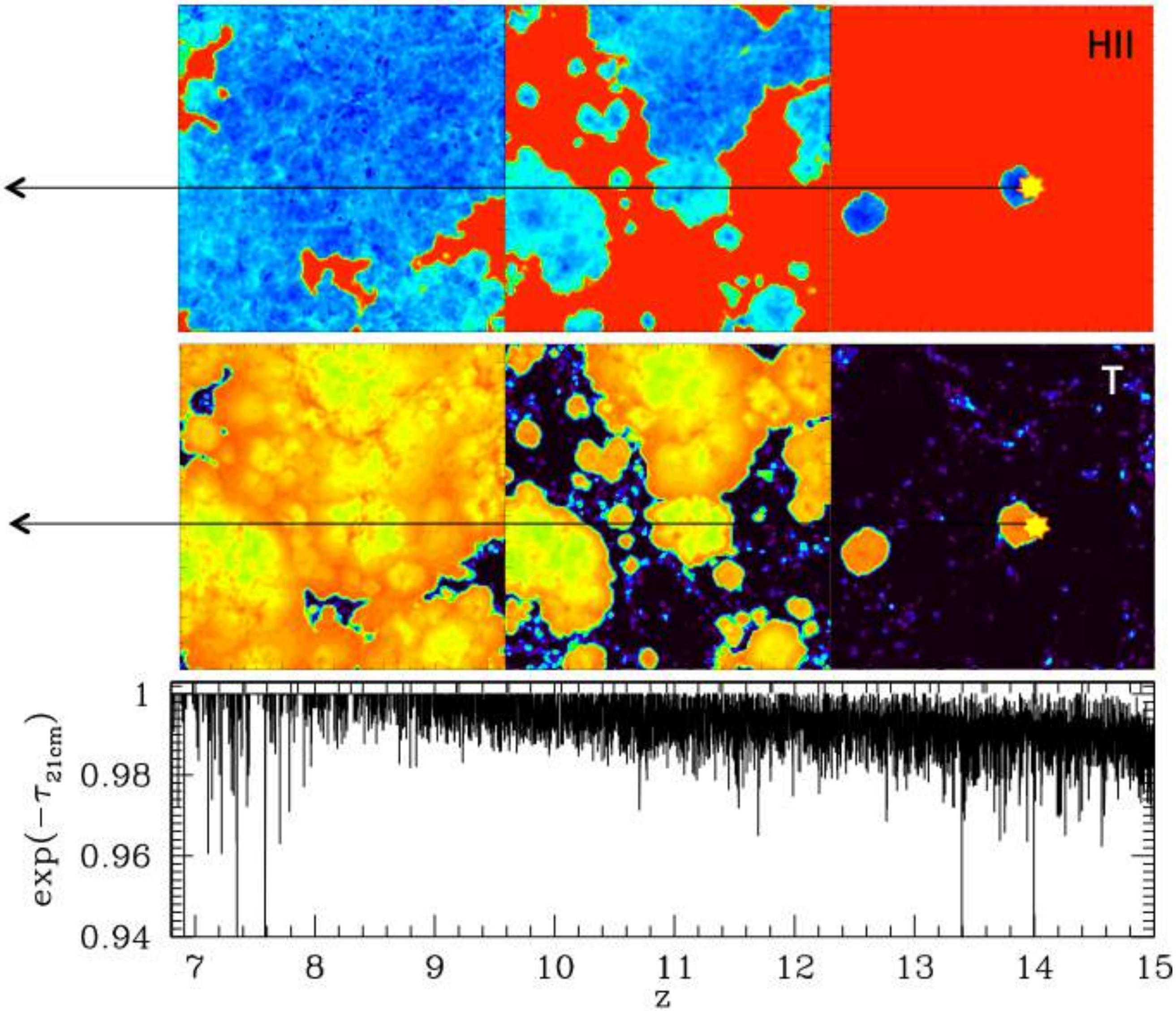

Curtsey B. Ciardi

The 21 cm forest as a result

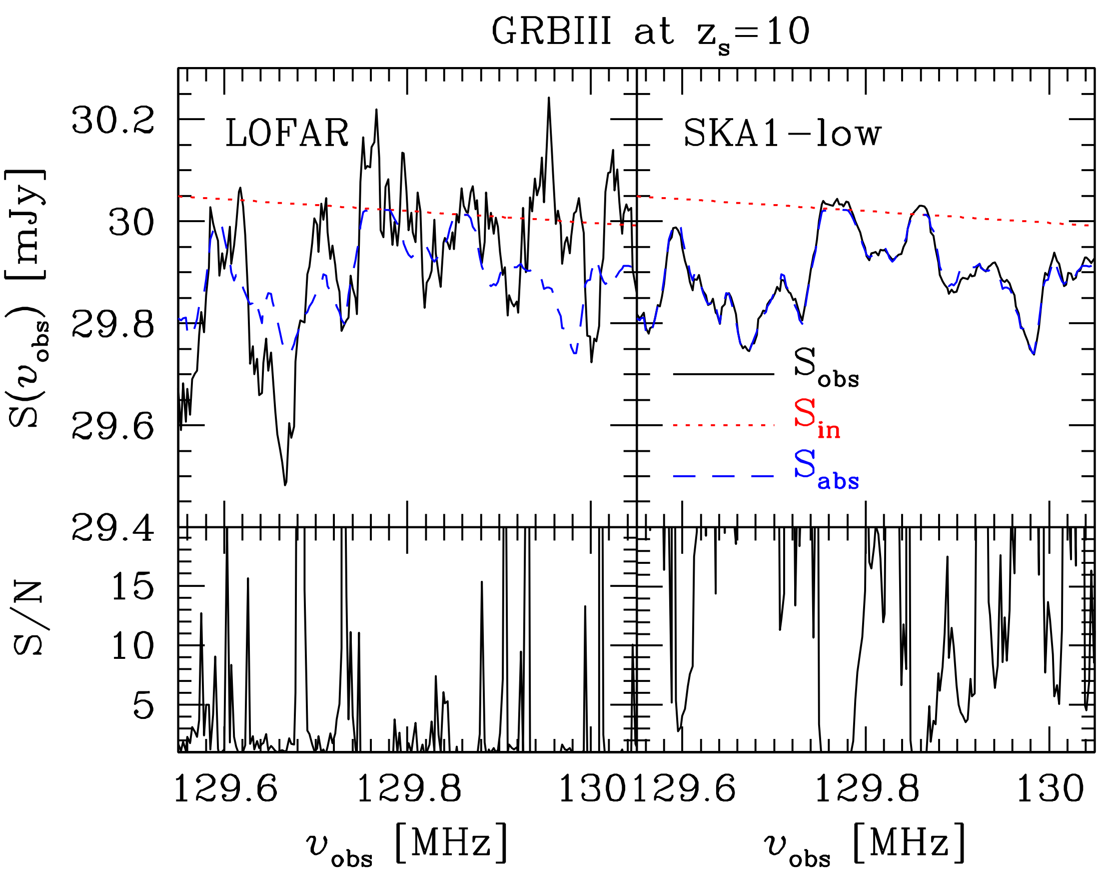

The feasibility of detecting 21 cm absorption features in the afterglow spectra of high redshift long Gamma Ray Bursts

Ciardi et al. 2015

21 cm Cosmology and HI experiments

- Current and planned experiments.
- Radio interferometry
- Key parameters in experiments.
- Observational issues: uv coverage, foregrounds, ionosphere, instrument, noise.
- Extraction issues.
- Calibration.
- Current & future experiments.
- Polarization.

Observation

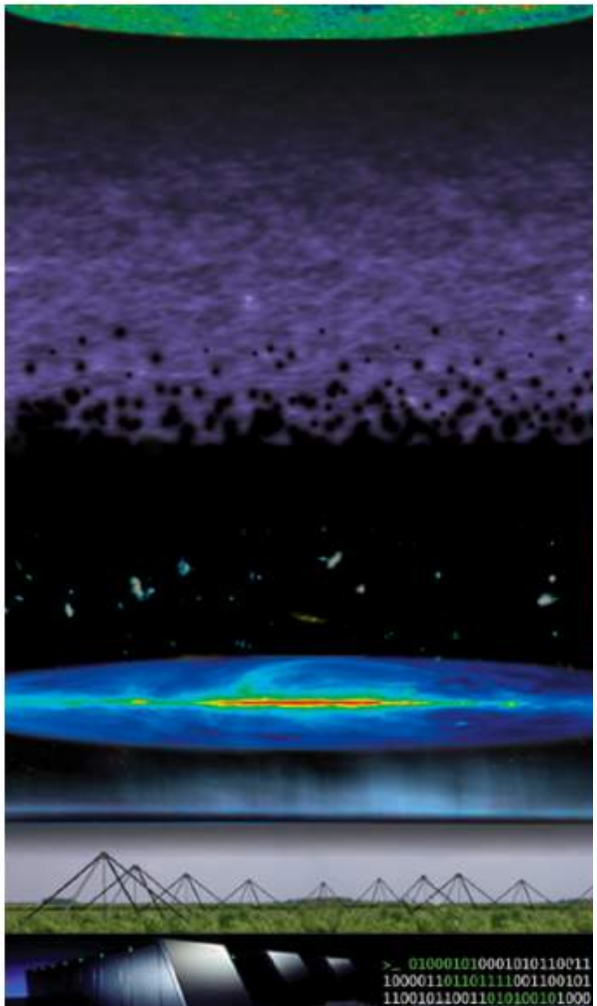

Extraction/
detection

Interpretation

The Global evolution of T_s

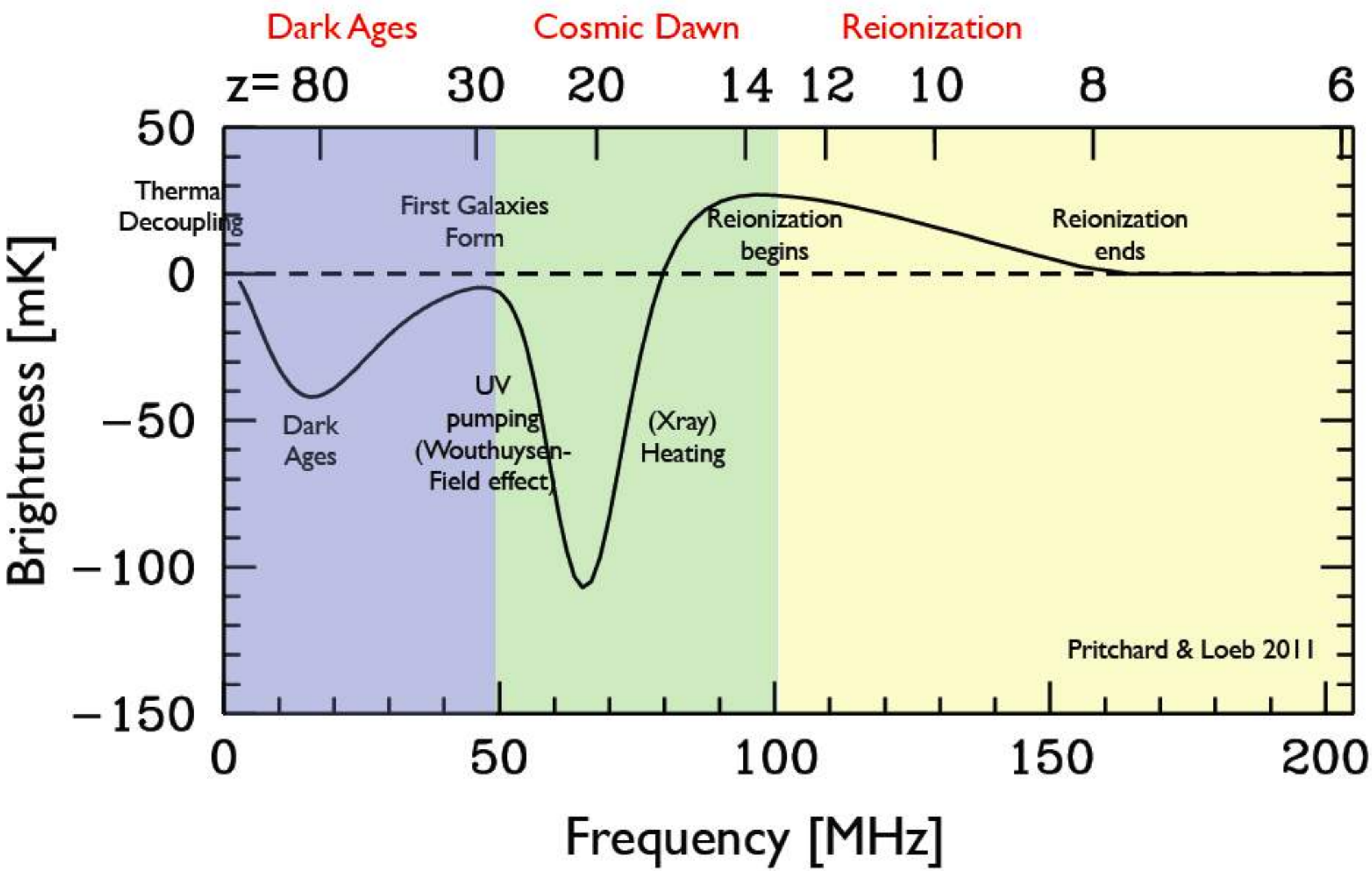

The EDGES result

Bowman+ 2018

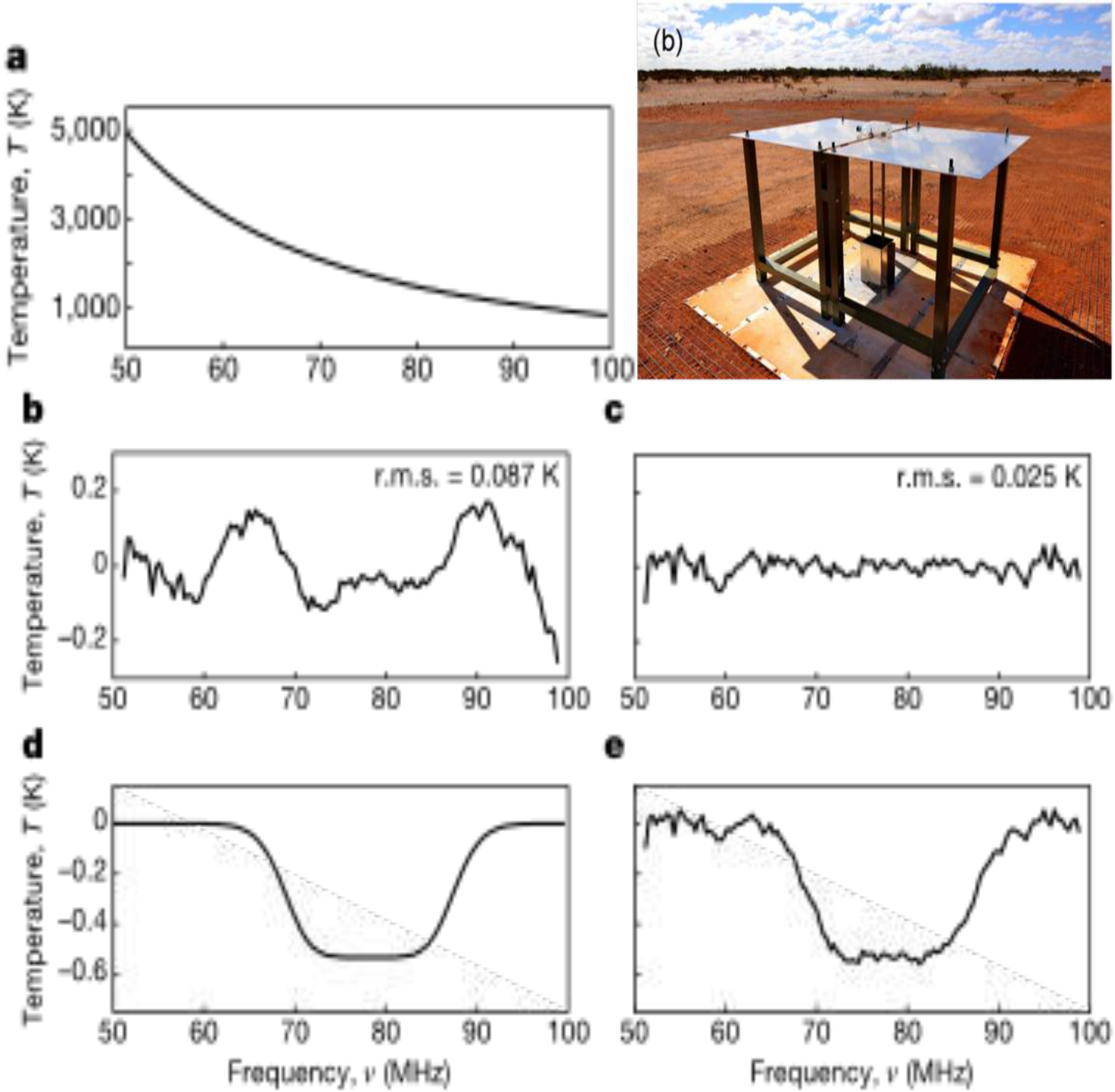

The EDGES paper

- Discussing the observations
- Proposing interpretations!!
  - Data analysis
  - Astrophysics
  - Fundamental physics
  - ETC.

Data Analysis

(Hills et al 2018)

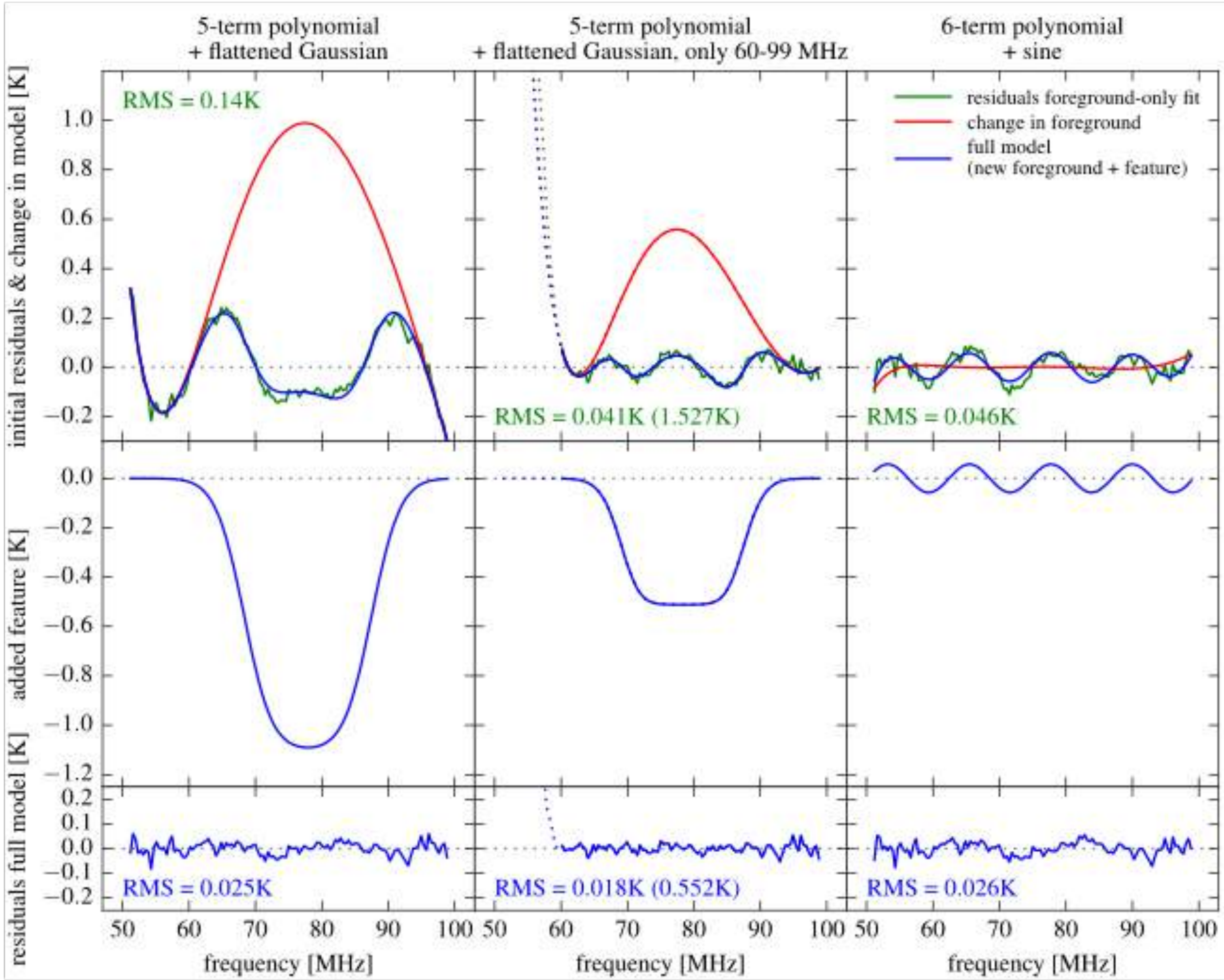

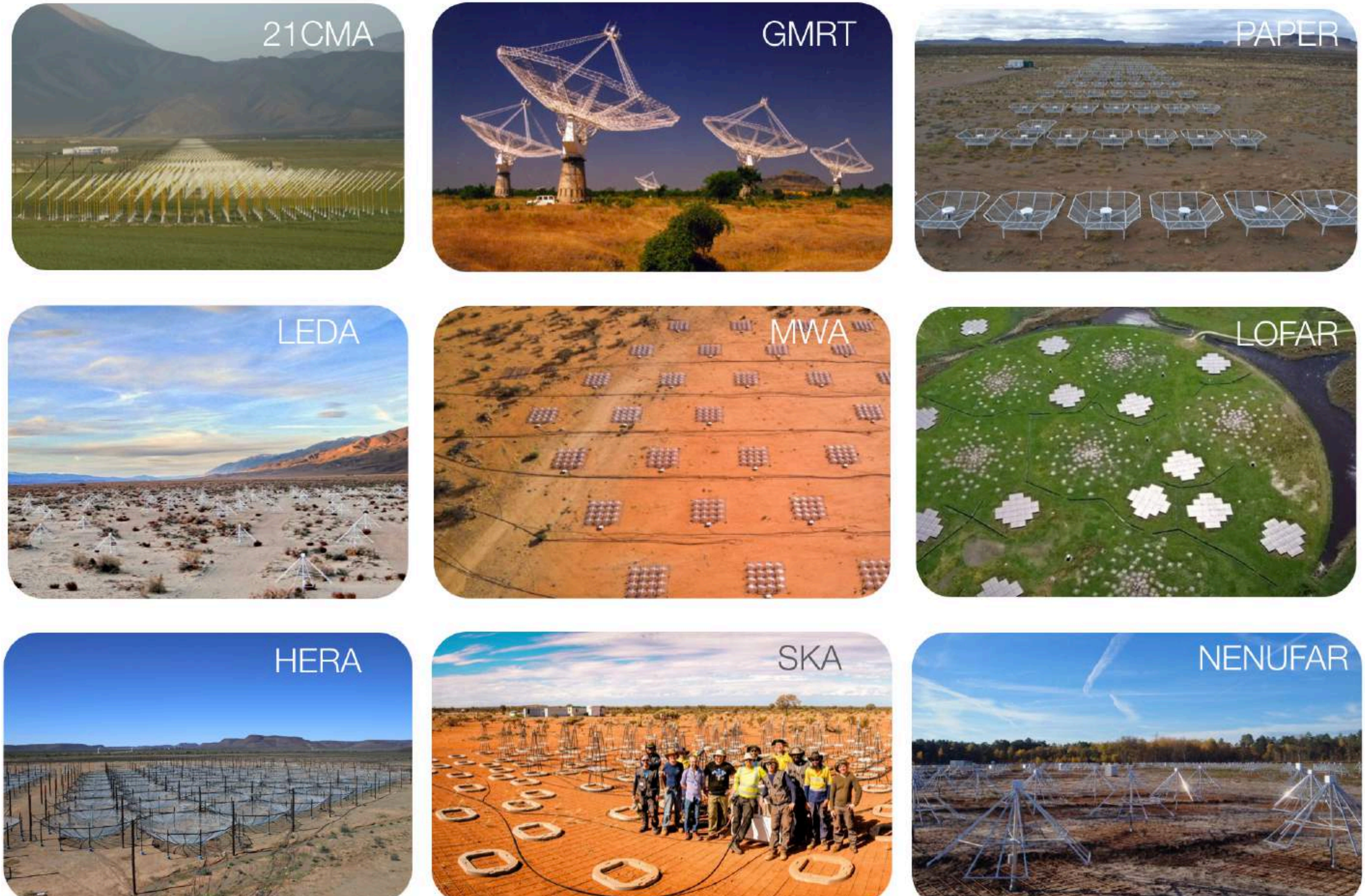
21CMA
GMRT
PAPER
LEDA
MWA
LOFAR
HERA
SKA
NENUFAR

Radio interferometry: Basic concepts

An interferometer measures coherence in the electric field between pairs of points (baselines).

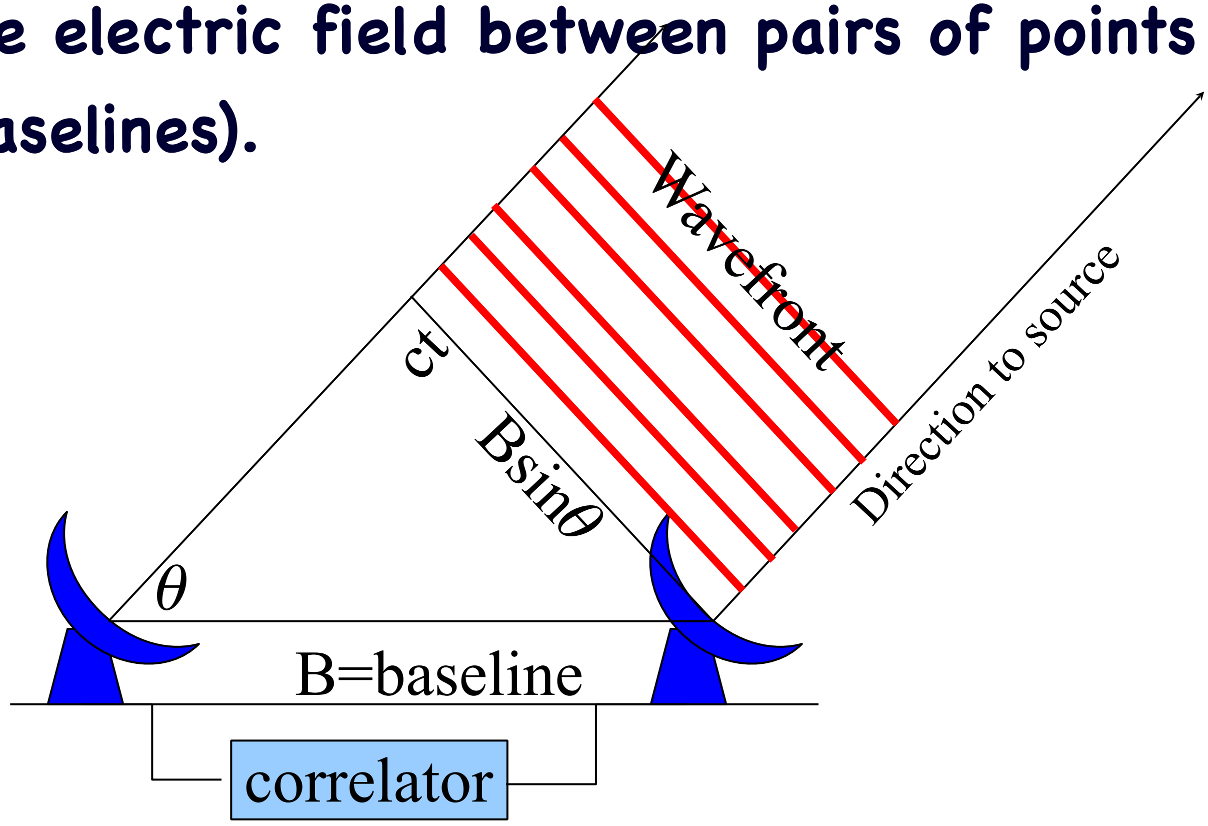

Time delay is essential to measure the same phase of the wavefront

The calibration problem

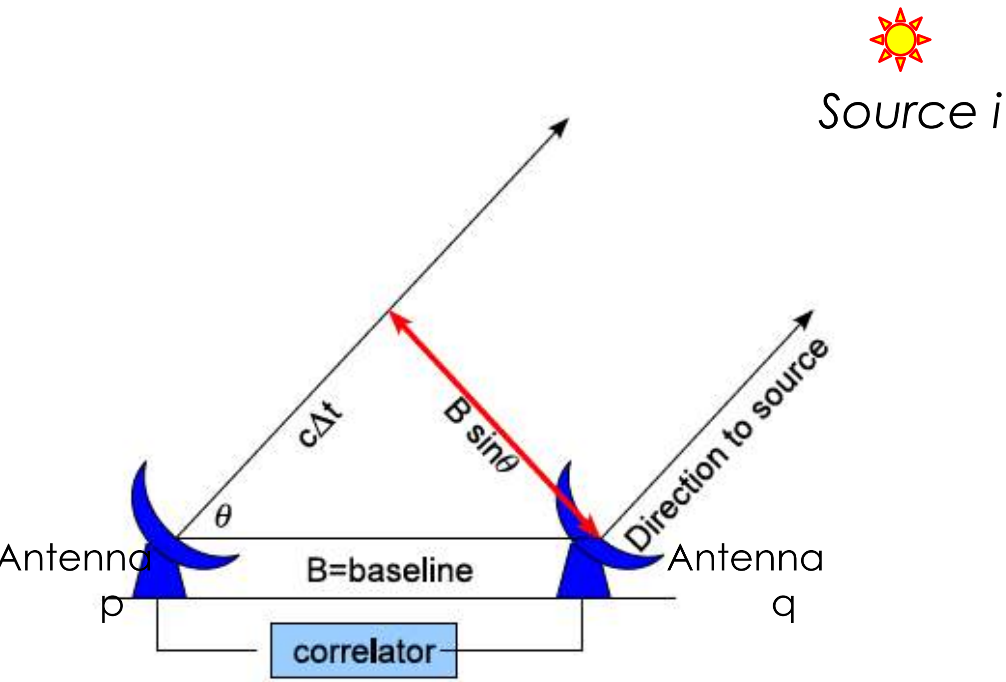

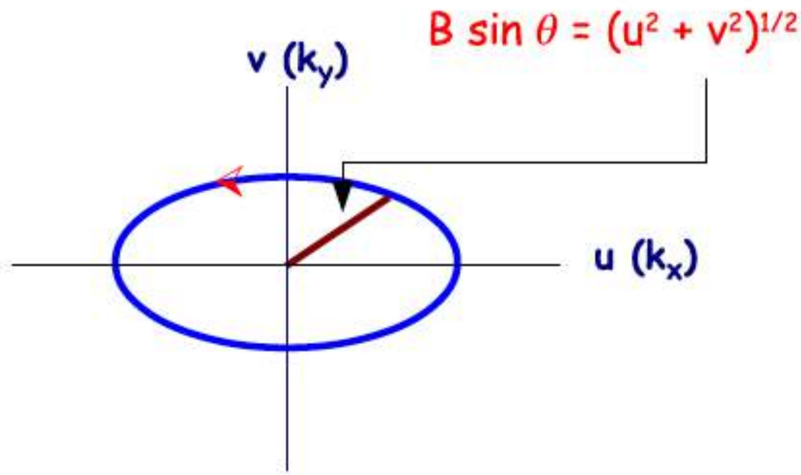

$$\mathbf{V}_{pq} = \sum_{i=1} \mathbf{J}_{pi}(\boldsymbol{\theta})\mathbf{C}_i\mathbf{J}_{qi}^H(\boldsymbol{\theta}) + \mathbf{N}_{pq}, \quad p, q \in \{1, 2, \ldots, N\}$$

Measuring Redshifted HI: Challenges

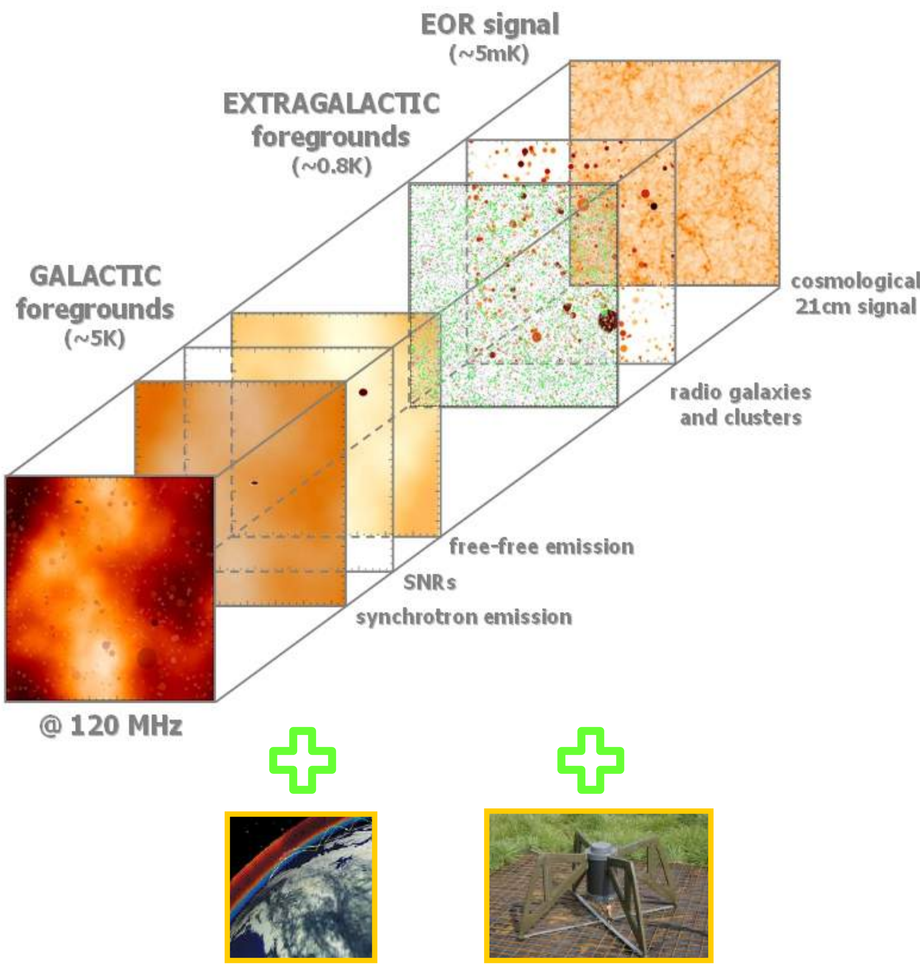

1. Astrophysical Challenges
   1. Weak unpolarized signal
   2. Foregrounds: total intensity
   3. Foregrounds: polarized
   4. Ionosphere
2. Instrumental challenges
   1. Beam stability
   2. Calibration
   3. Resolution
   4. uv coverage
3. Computational challenges
   1. Multi petabyte data set
   2. Calibration
   3. inversion

The LOFAR EoR members

Ger de Bruyn

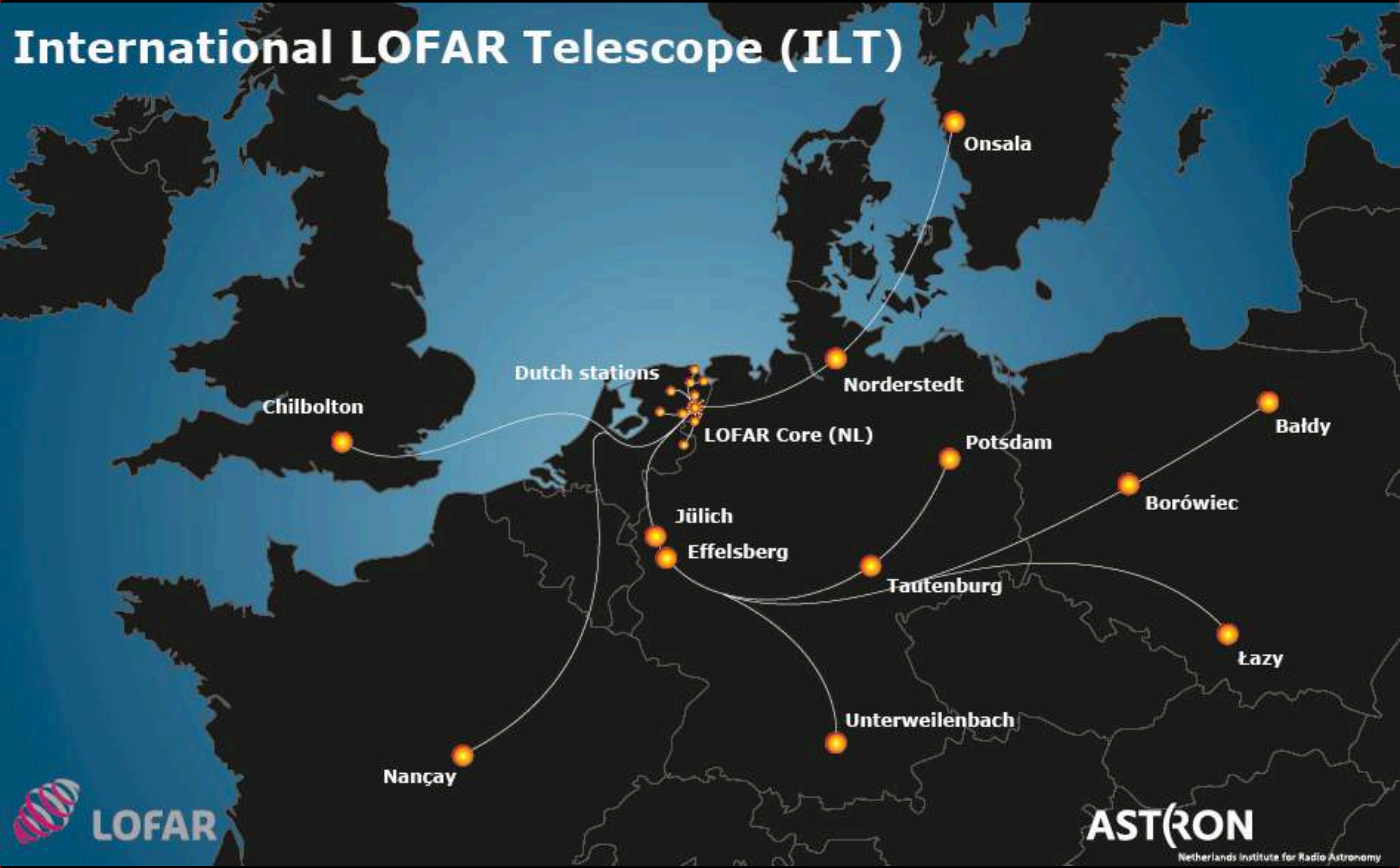
International LOFAR Telescope (ILT)
Onsala
Dutch stations
Norderstedt
Chilbolton
LOFAR Core (NL)
Potsdam
Bałdy
Borówiec
Jülich
Effelsberg
Tautenburg
Łazy
Unterweilenbach
Nançay
LOFAR
ASTRON
Netherlands Institute for Radio Astronomy

Autumn weather and muddy soil cause delays….

Nov 2008

field flattening activities

The superterp, river and ‘wetlands-to-be’

‘Field flattening’ for non-astronomers

Finally: the 1st LOFAR station (May ’09)

The ‘superterp’ a 350 m diameter raised ‘island’

Main science goals of the LOFAR EoR project

- — Statistical detection of global signal; z-evolution
- — Constrain the sources: stars, QSOs or ...
- — The environment of high z QSOs / SMBH
- — Measure underlying dark matter density spectrum
- — Statistical characterization of ionization bubbles
- — Study 21cm forest to high z radio sources (if any)
- — Cross correlation with other probes: Ly-α, NIRB, CMB,..

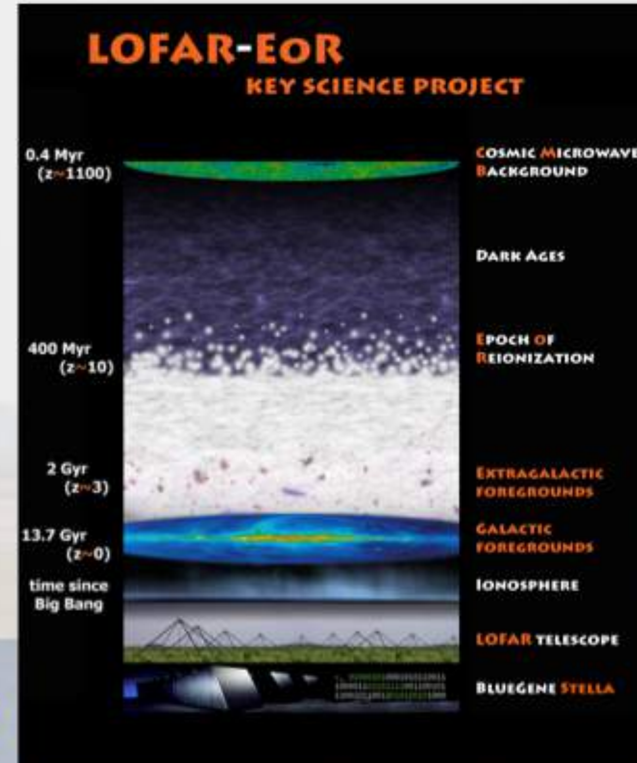

Vibor Jelic (2010)

115 - 177 MHz
z = 11.4 – 7.0

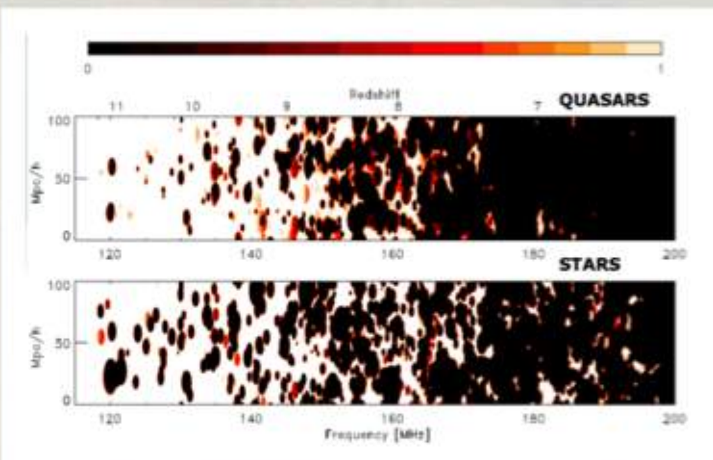

Rajat Thomas (2009)

This will take 600 - 3000h of LOFAR HBA observing (2-3 windows)

Ger de Bruyn 2015

LOFAR EoR Deep Fields

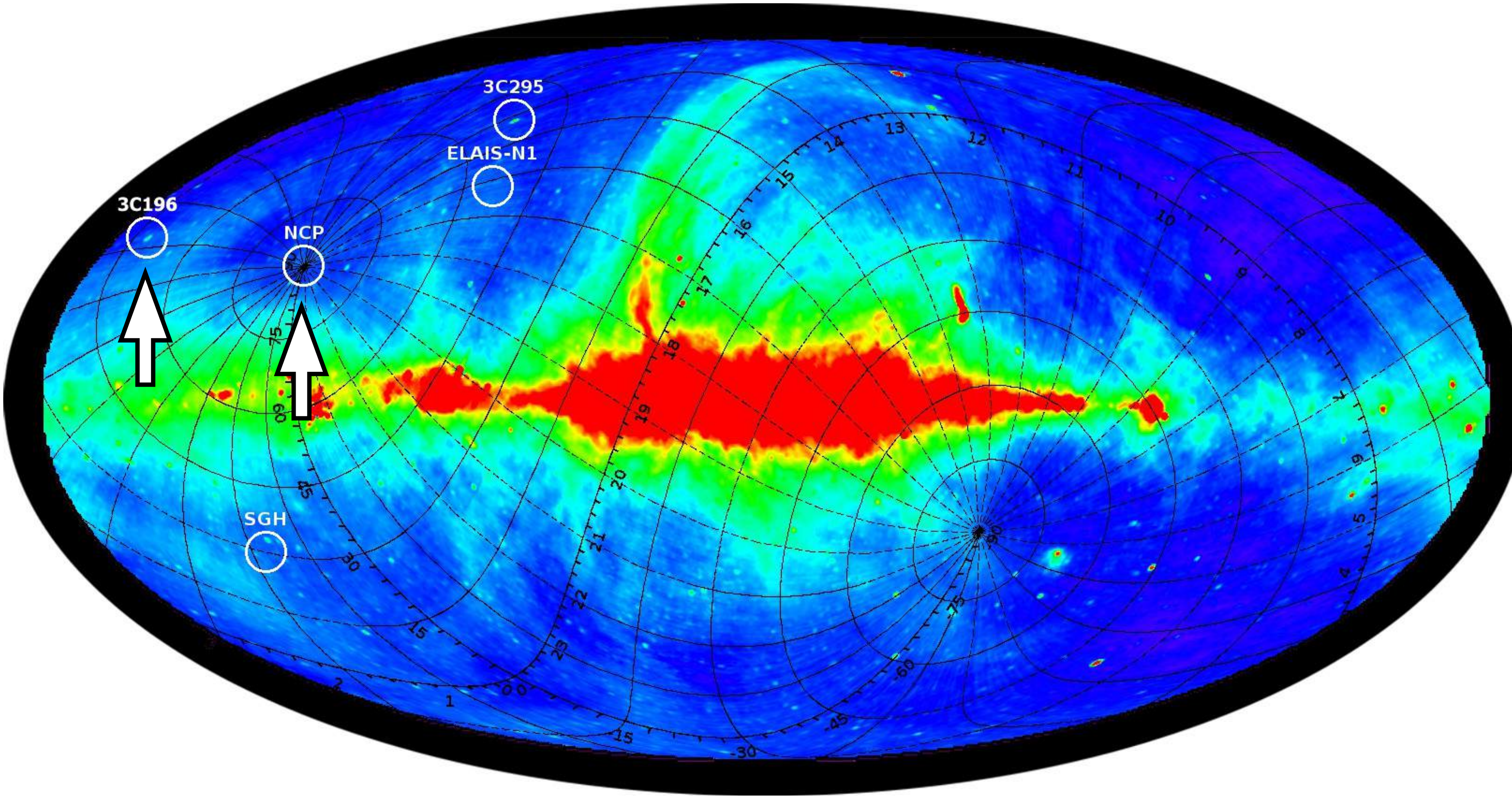

We currently focus on two deep windows: NCP and 3C196

Foregrounds

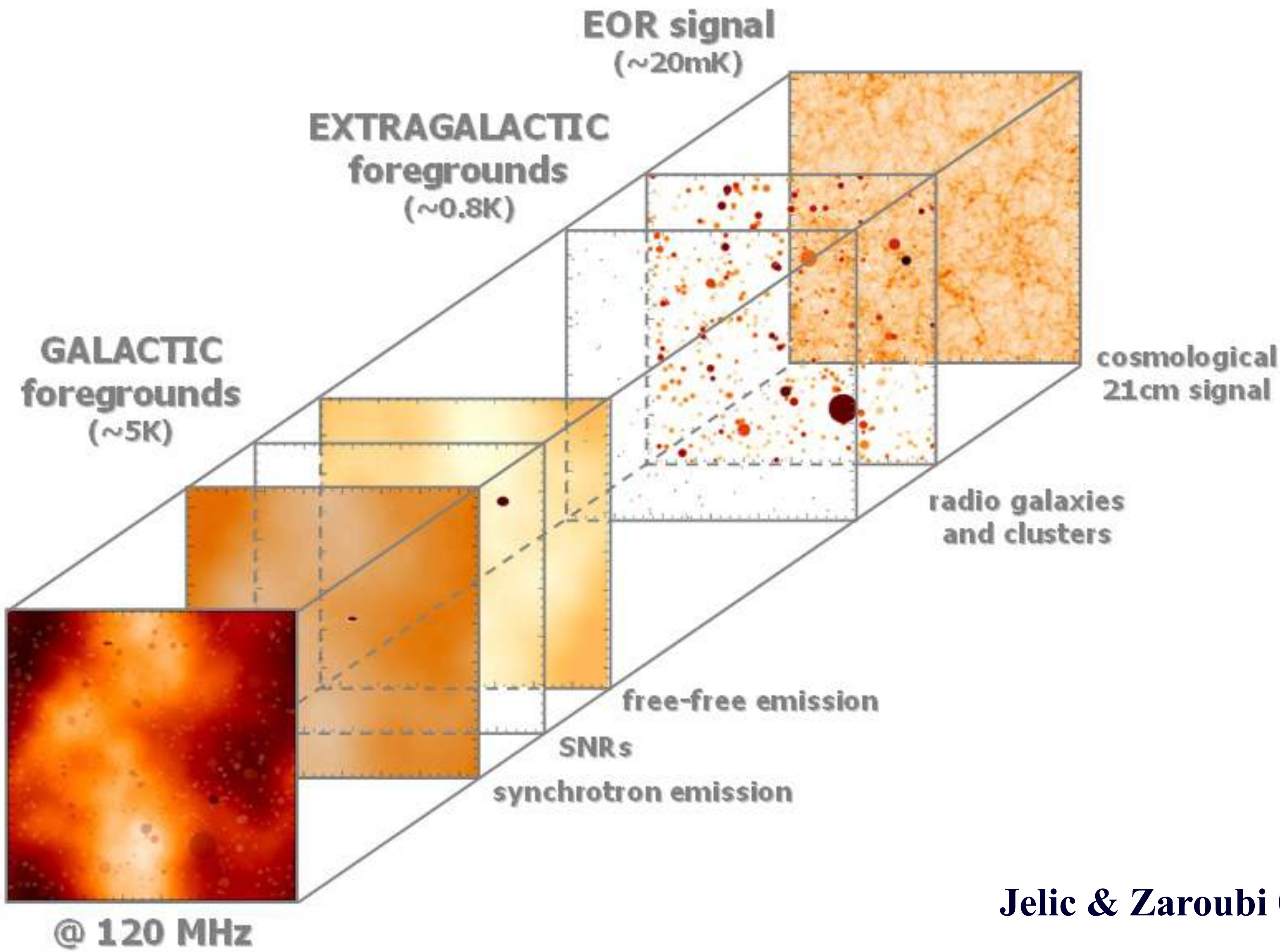

Jelic & Zaroubi 07

The FAN region: Power spectrum of the Diffuse Foregrounds

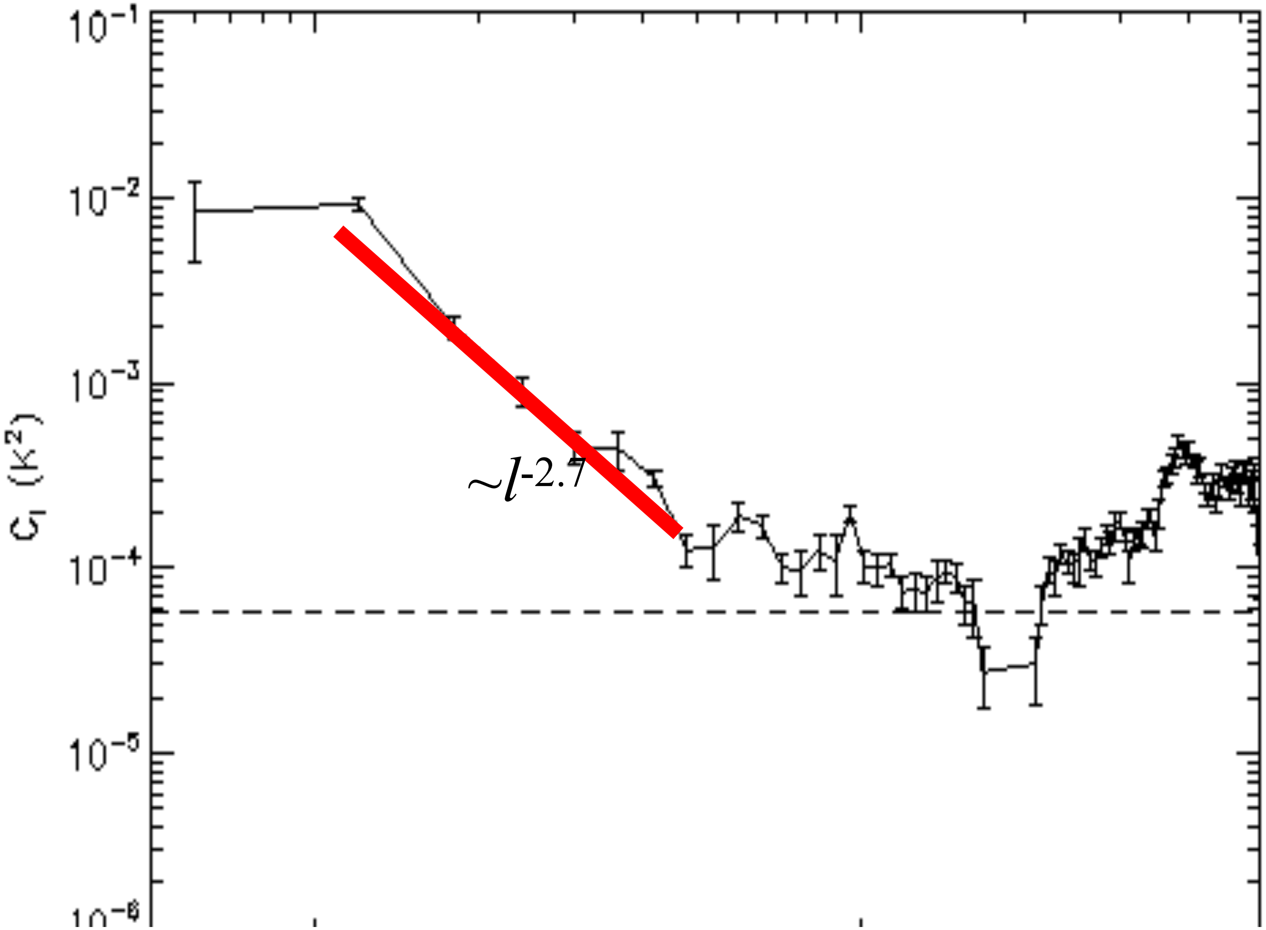

Bernardi et al, 2009

The leakage problem

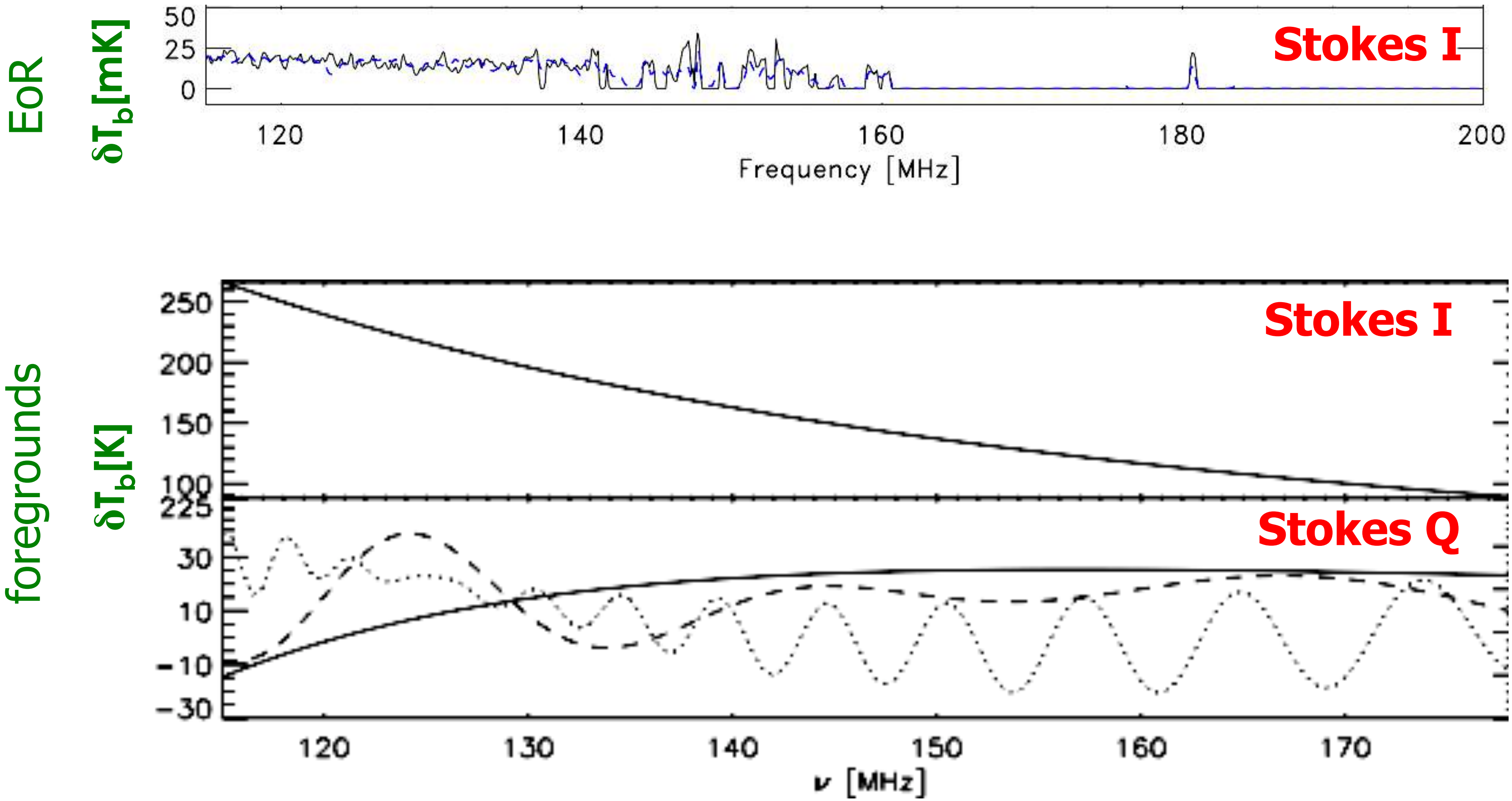

➢ **extraction is based on smoothness of the foregrounds in total intensity**

Ionospheric effects: the good and the ugly

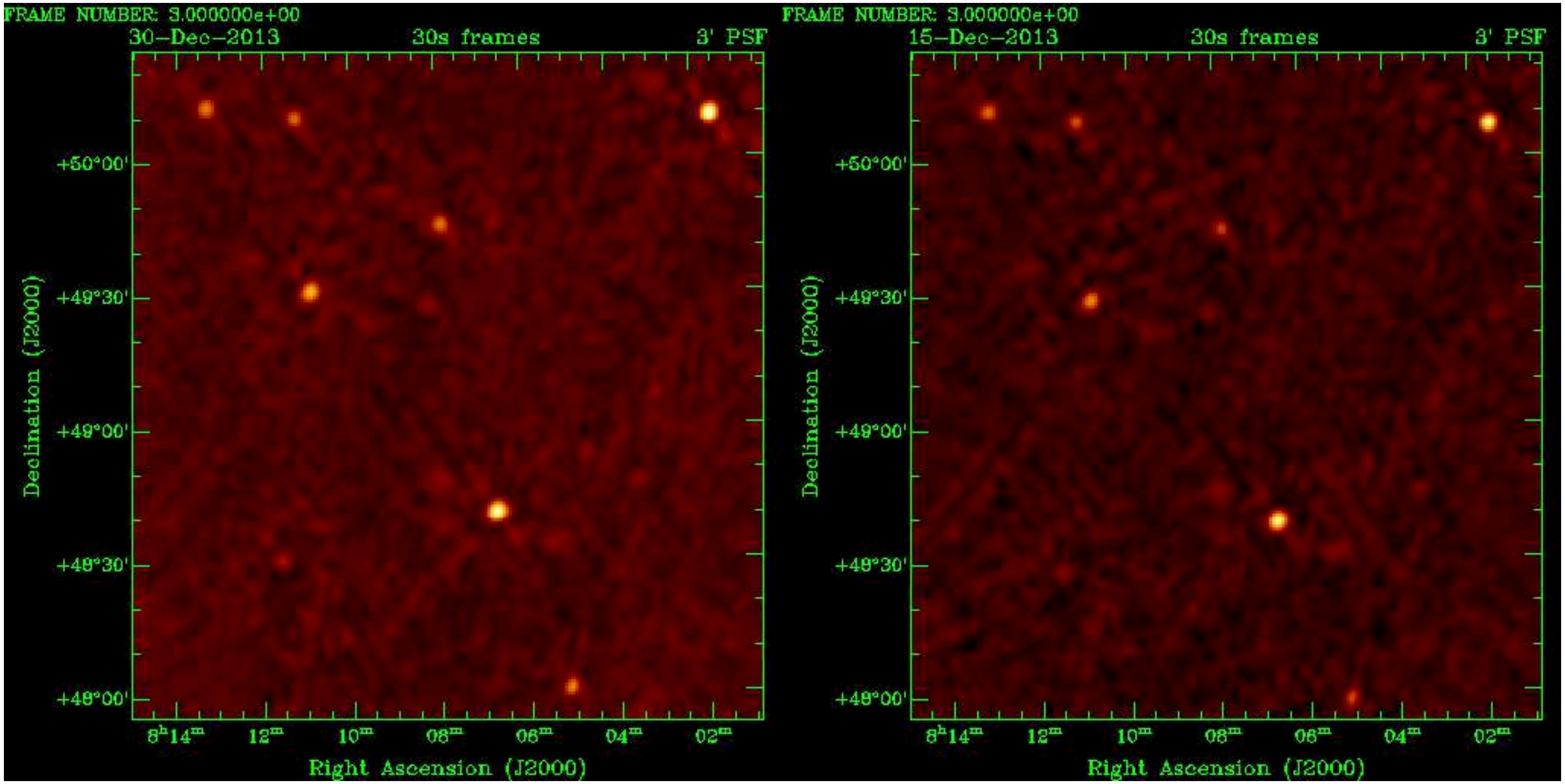

Removing the foregrounds

Step 1:
Point-sources subtraction

- ➔ Need accurate sky-model
- ➔ Solve for instruments gains in direction of sources

Direction Dependent (DD) calibration using Sagecal-CO (Yattawatta et al. 2013, 1015, ...)

Step 2:
Residual spectrally-smooth foregrounds subtraction

Using e.g. Gaussian Process Regression (GPR) (Mertens et al. 2018)

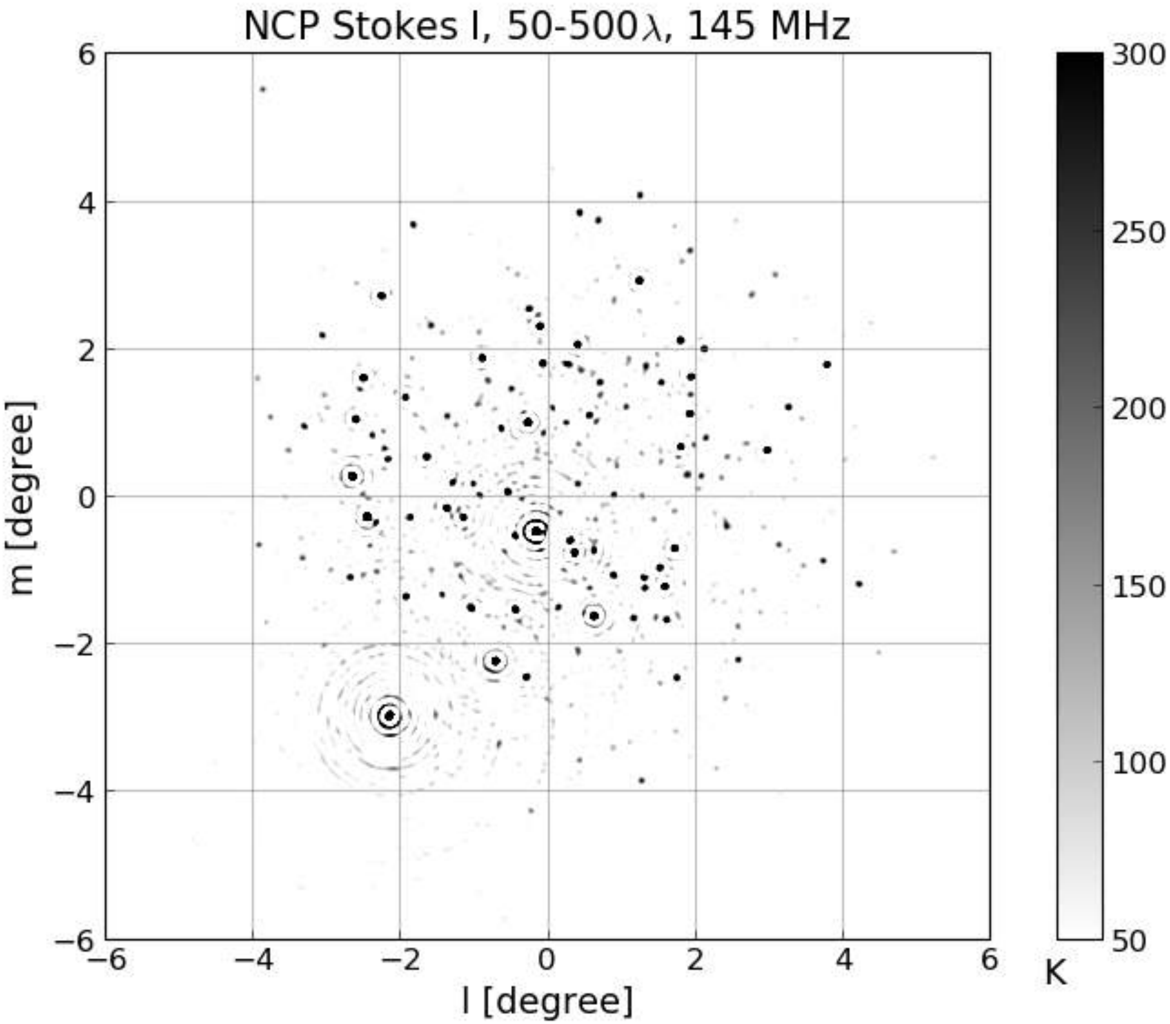

Direction Dependent calibration

Need to reduce the number of degree of freedom:

➔ Clustering (NCP ~ 120 clusters)

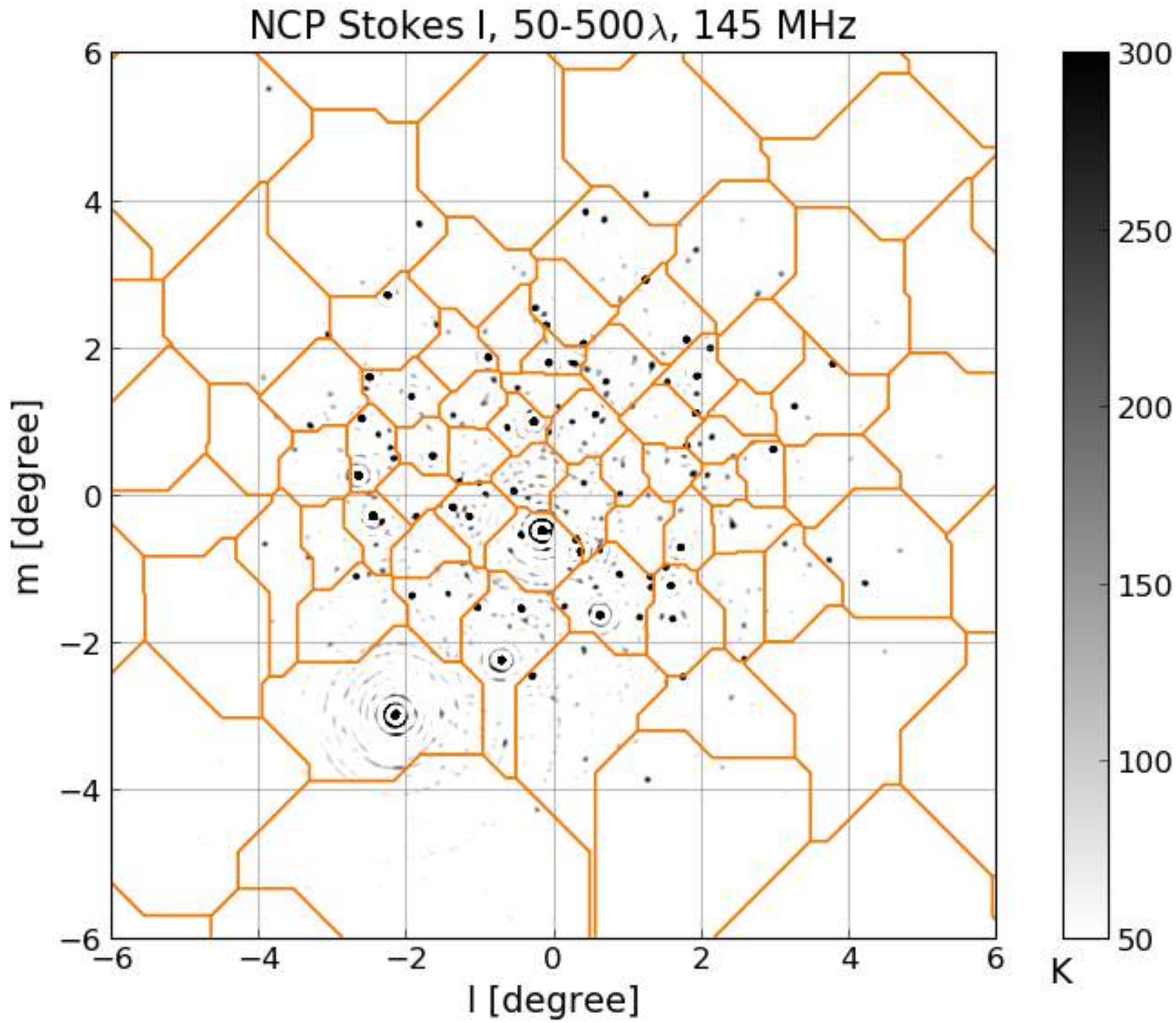

(Yatawatta et al. 2013, 2015)

Direction Dependent calibration

Need to reduce the number of degree of freedom:

- ➔ Clustering (NCP ~ 120 clusters)
- ➔ Force spectrally-smooth instrumental response

Sagecal-CO: distributed calibration, solve augmented Lagrangian:

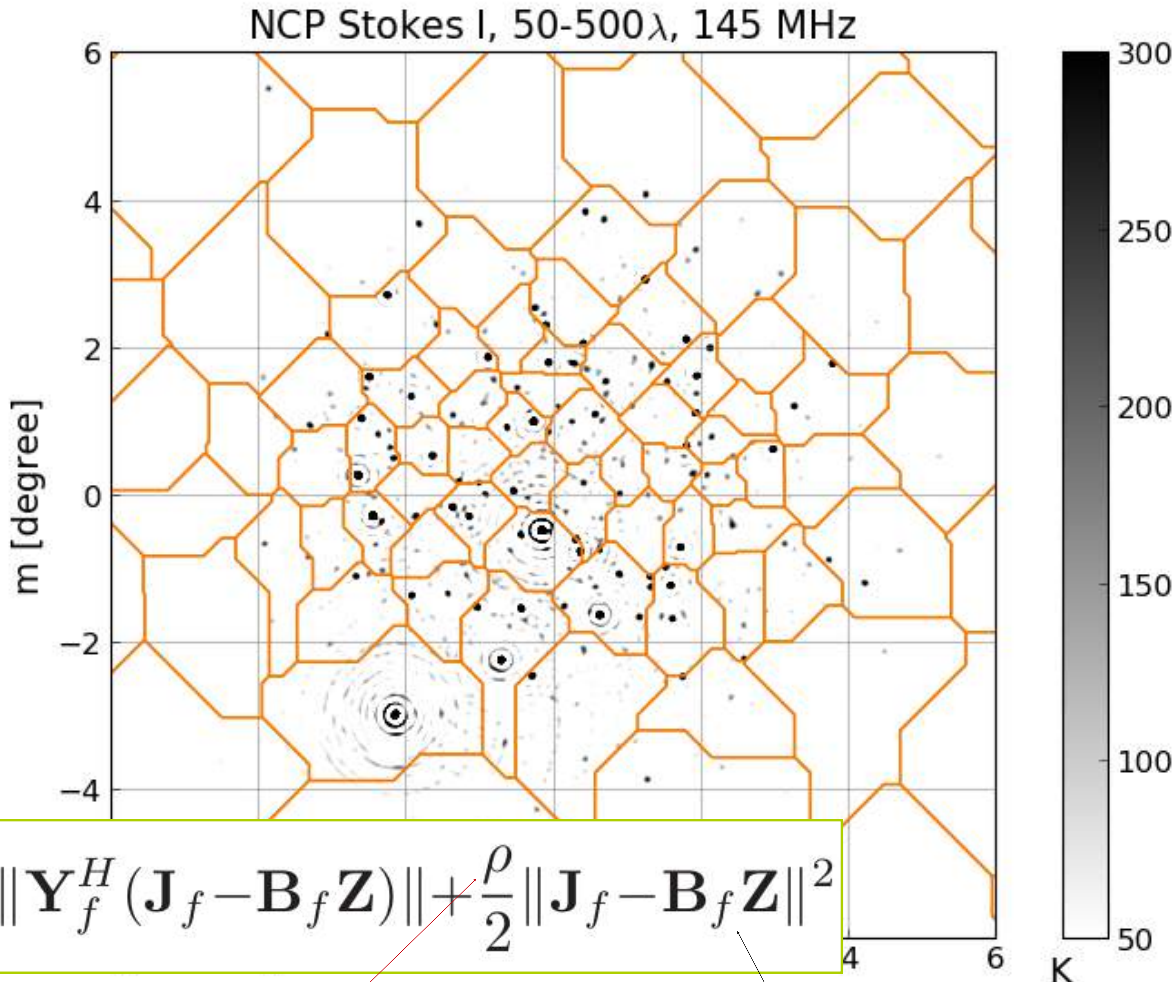

$$L_f(\mathbf{J}_f, \mathbf{Z}, \mathbf{Y}_f) = g_f(\mathbf{J}_f) + \|\mathbf{Y}_f^H(\mathbf{J}_f - \mathbf{B}_f\mathbf{Z})\| + \frac{\rho}{2}\|\mathbf{J}_f - \mathbf{B}_f\mathbf{Z}\|^2$$

Gains

Original cost function

Regularization parameter

Spectrally-smooth constraint

(Yatawatta et al. 2013, 2015)

SAGEcal: robust and broad-band processing

Yatawatta, 2015

Calibration solves for a very large number of unknowns → dangerous
Adopted approach: exclude short baselines (< 250λ) in SAGEcal and only image those !

Diffuse polarization then preserved in calibration → EoR signal will be preserved too !

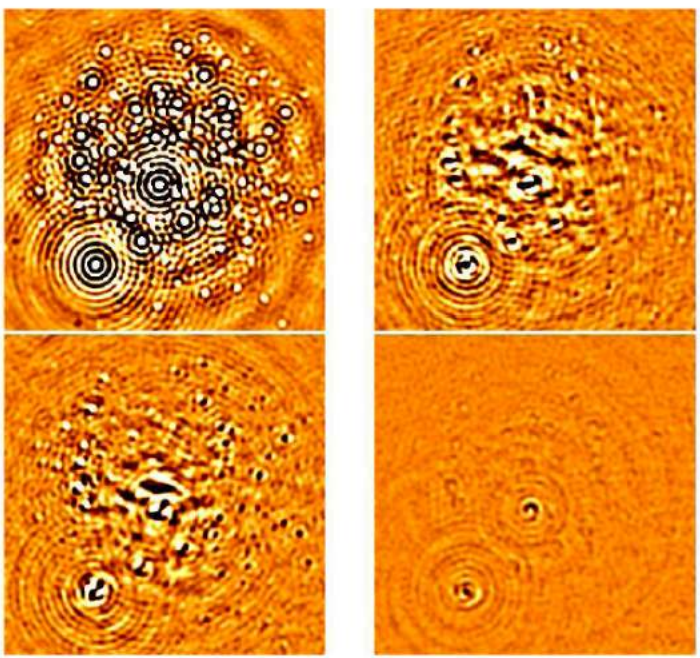

I,Q,U,V images baselines <= 250 wavelengths

One
night
60 MHz

10' PSF

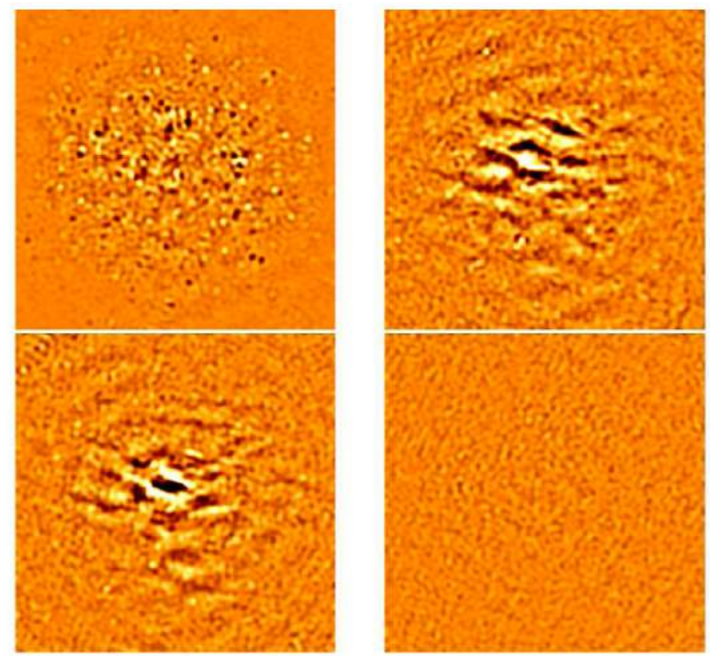

I,Q,U,V calibration using baselines > 250 wavelengths

LOFAR-EoR observations

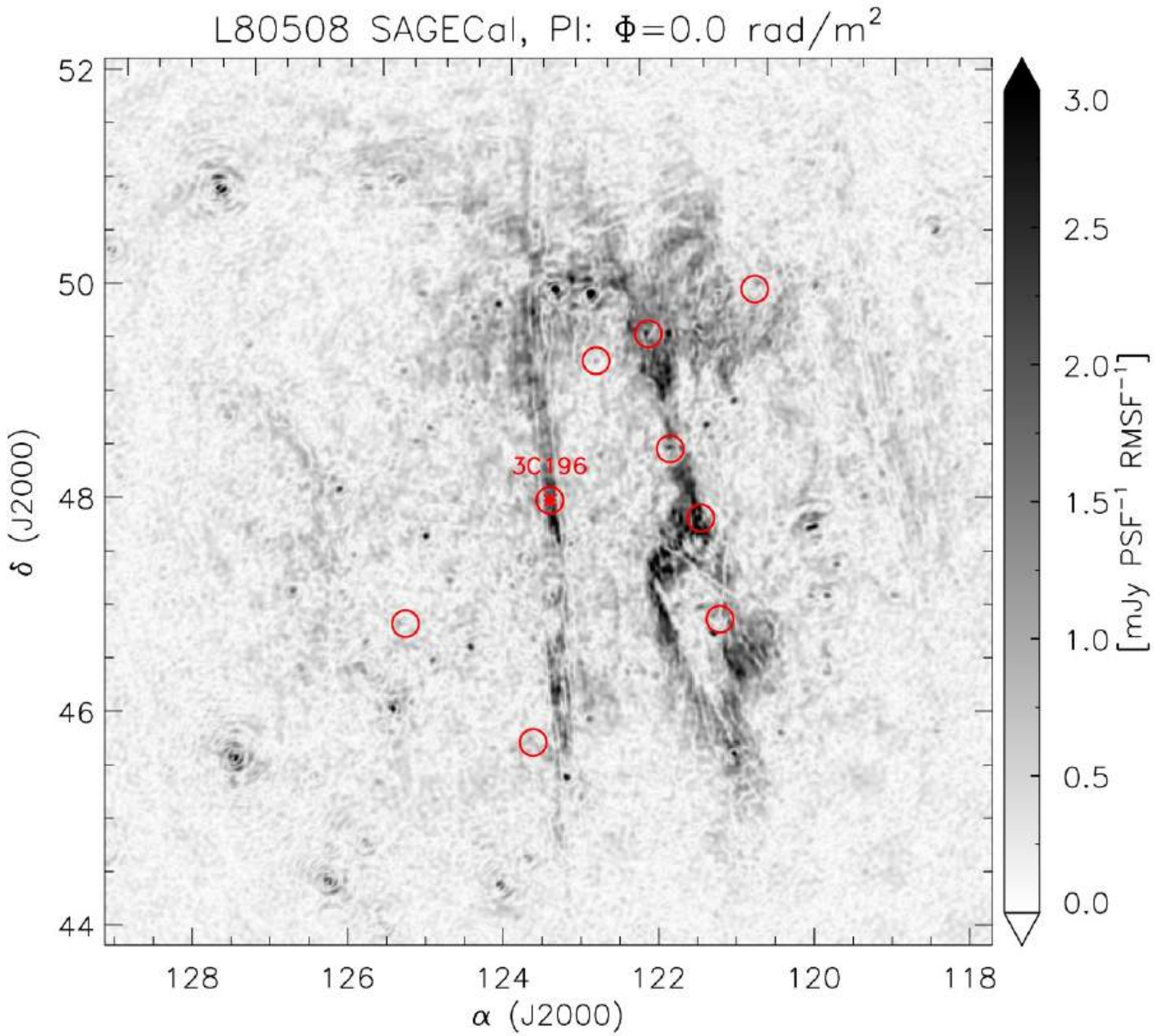

Jelic et al 2015

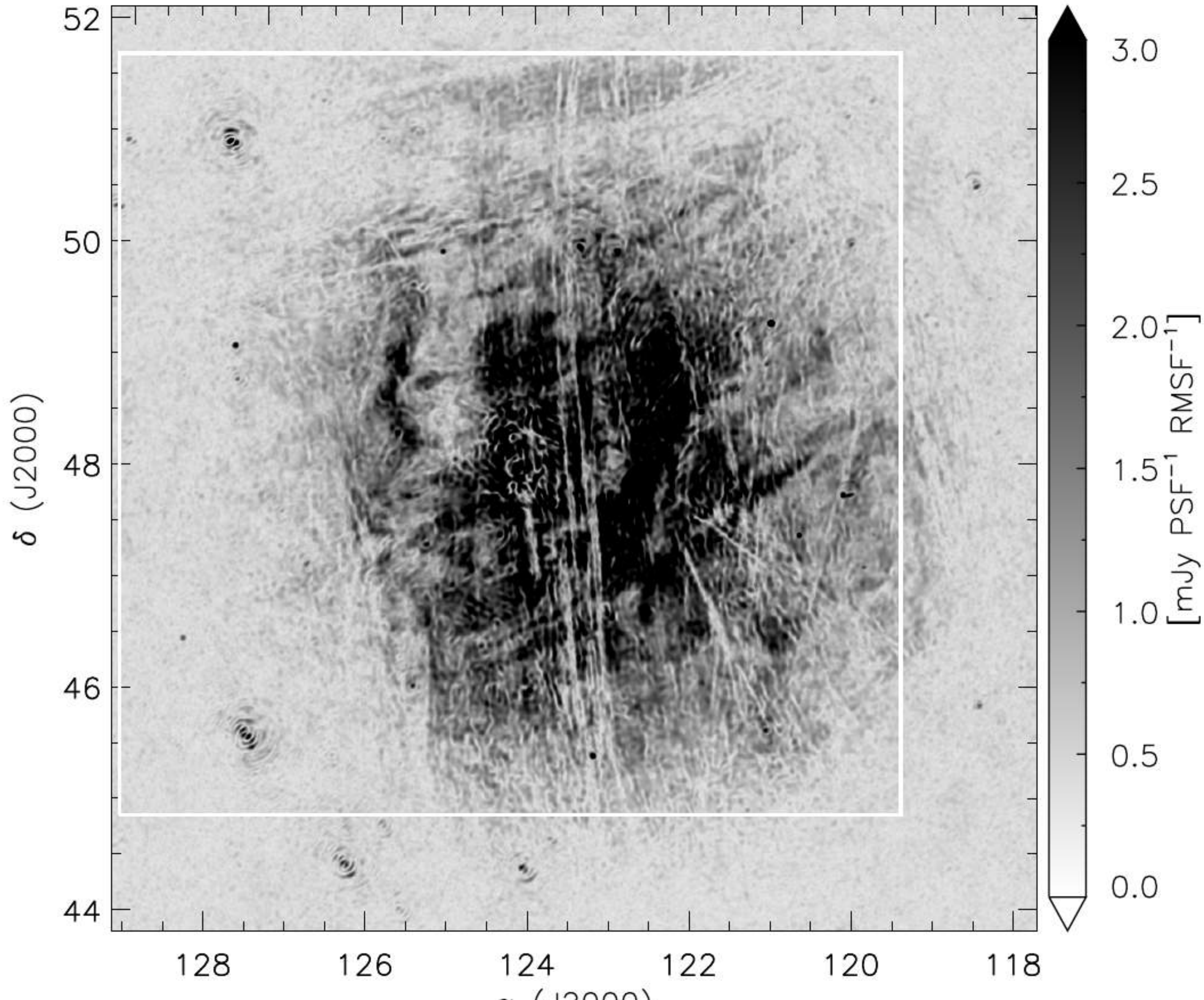

Jelic et al 2015

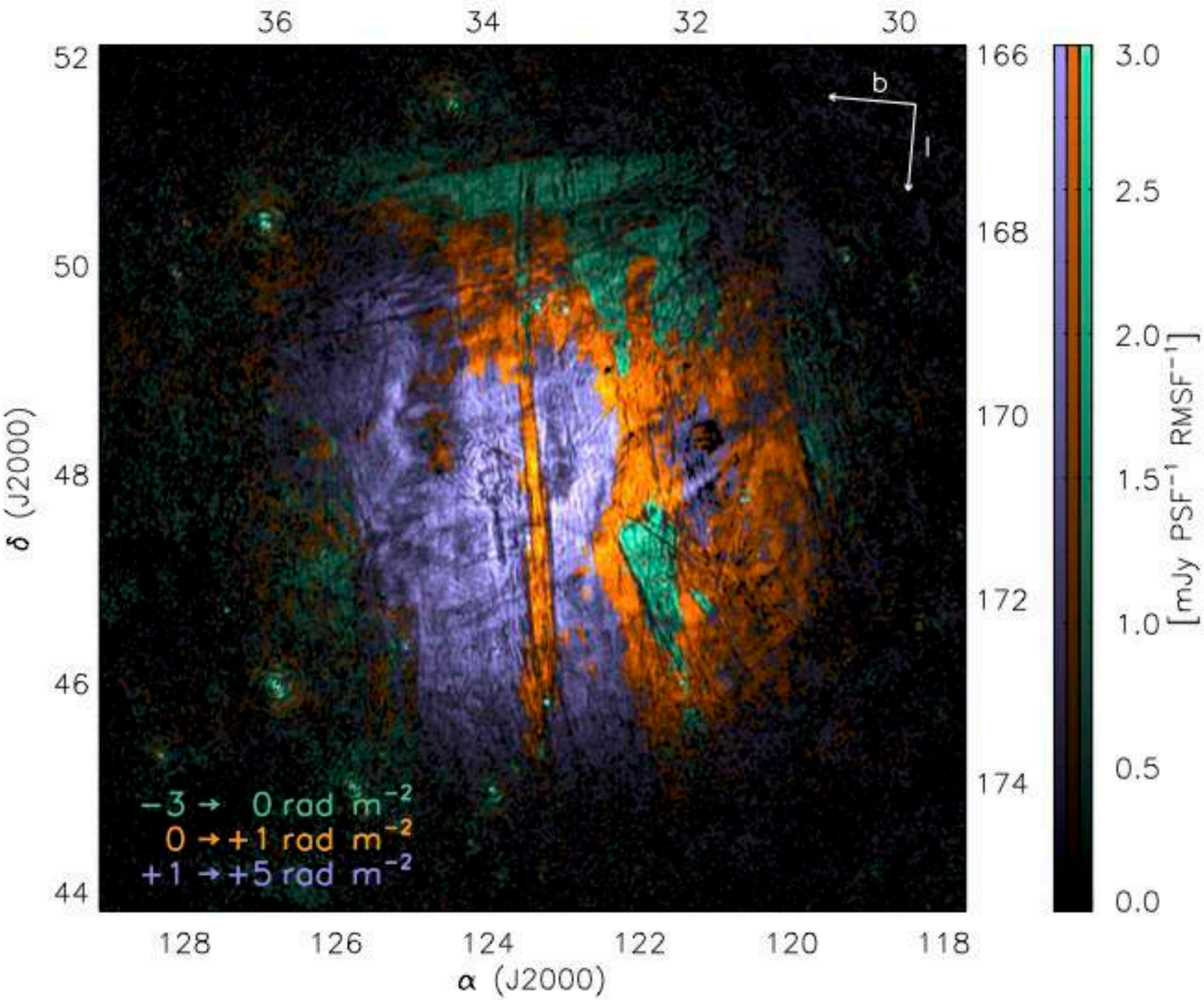

Jelic et al, 2015

ISM magnetic/Faraday depth correlation (LOFAR vs. Planck)

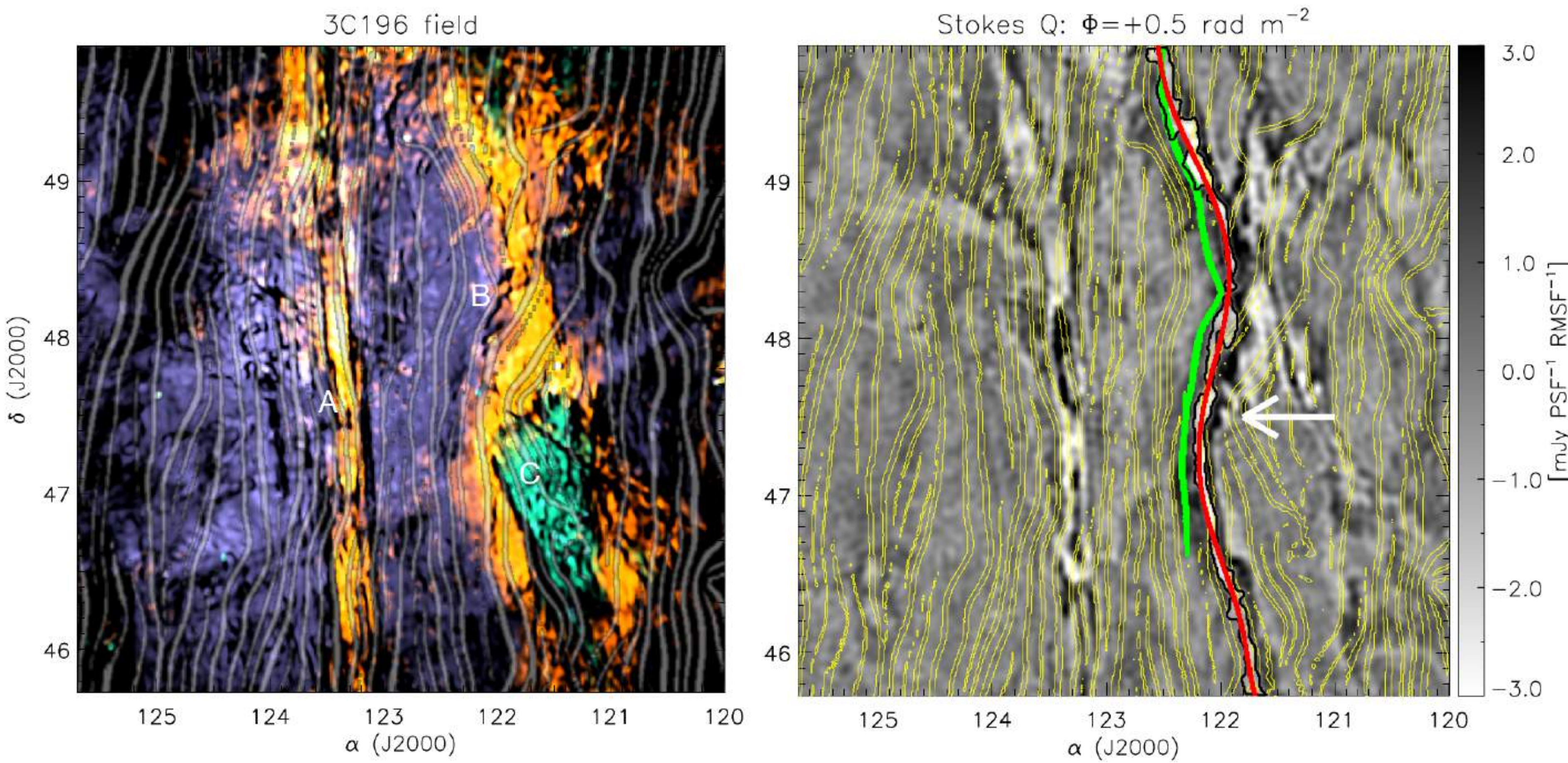

Zaroubi et al 2015, MNRAS

Example of extraction @ 150MHz
5' (σ) smoothed

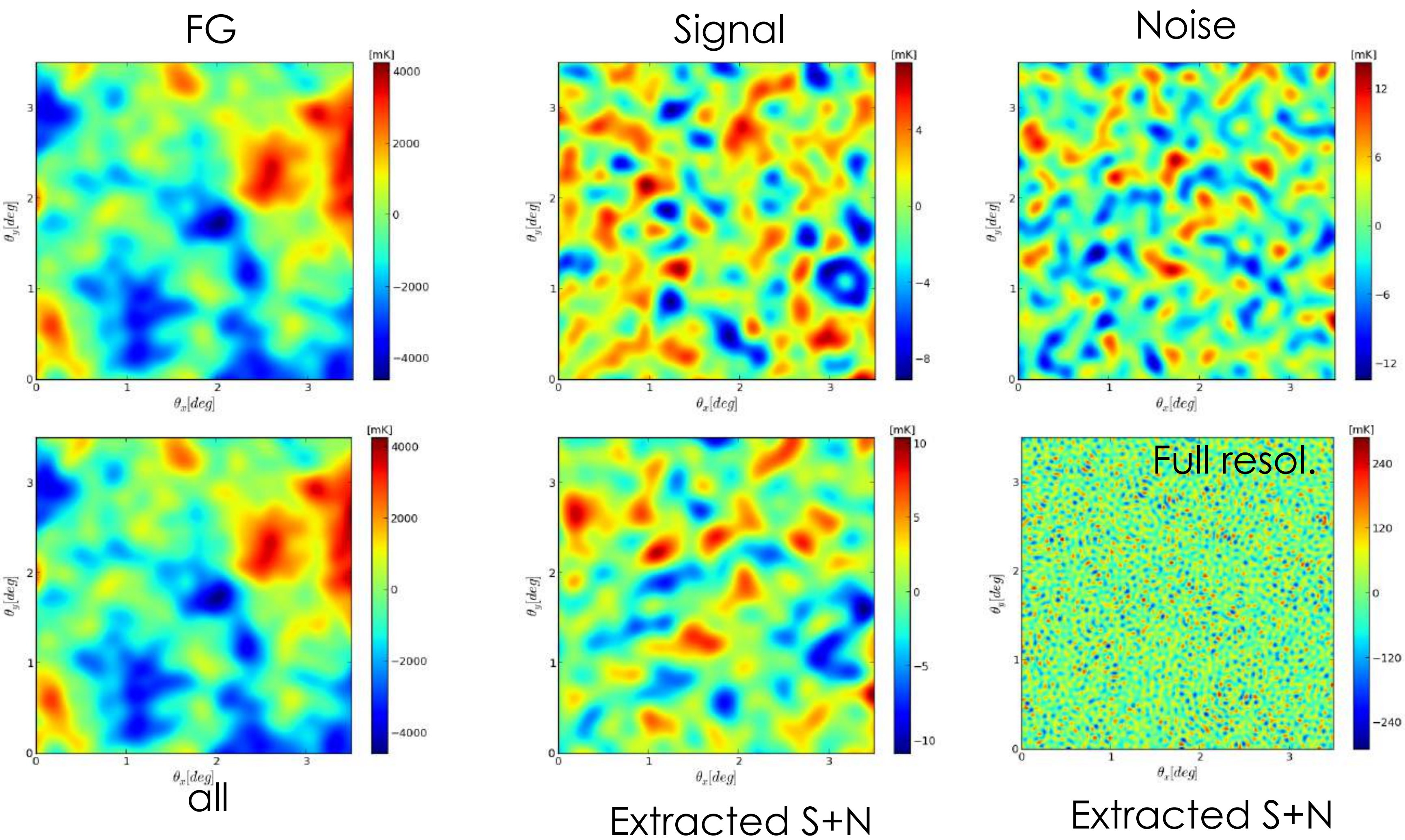

GMRT results

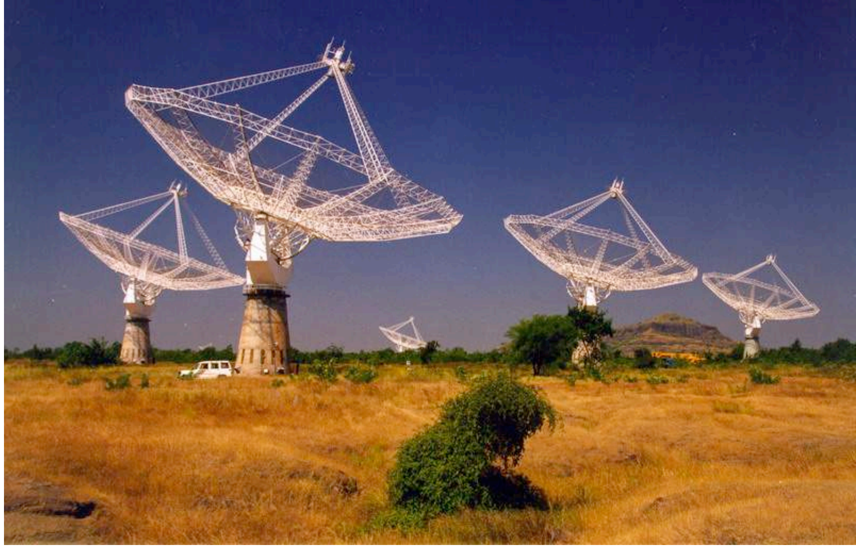

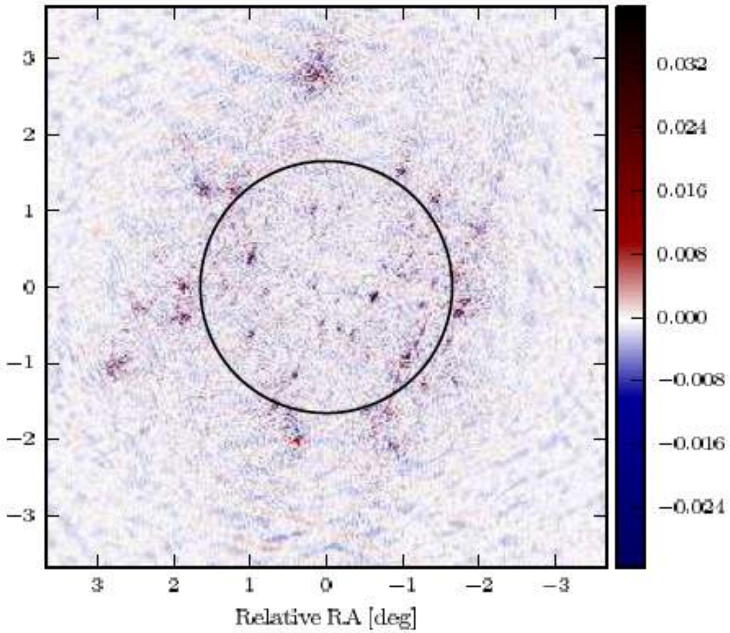

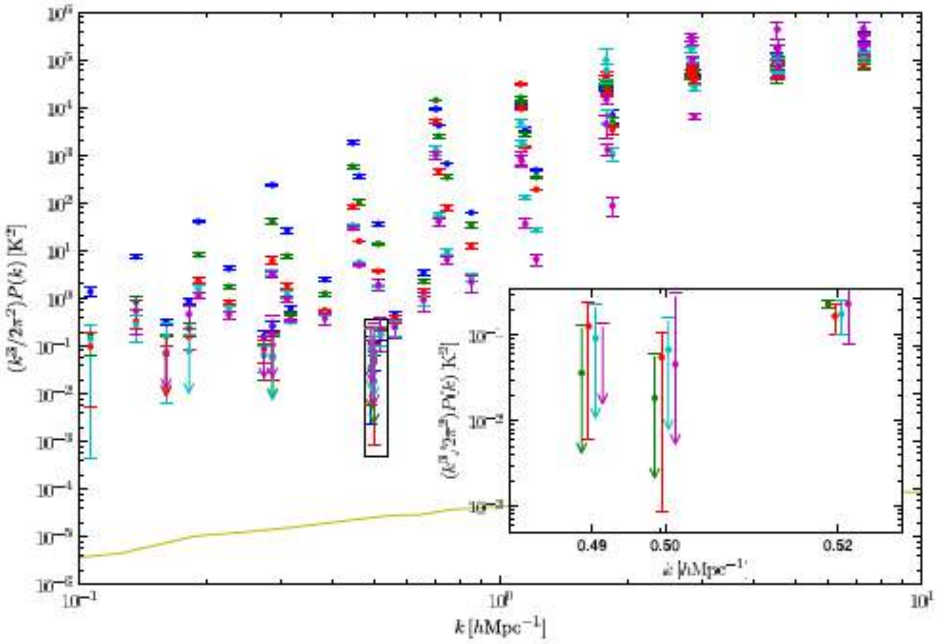

MWA current results

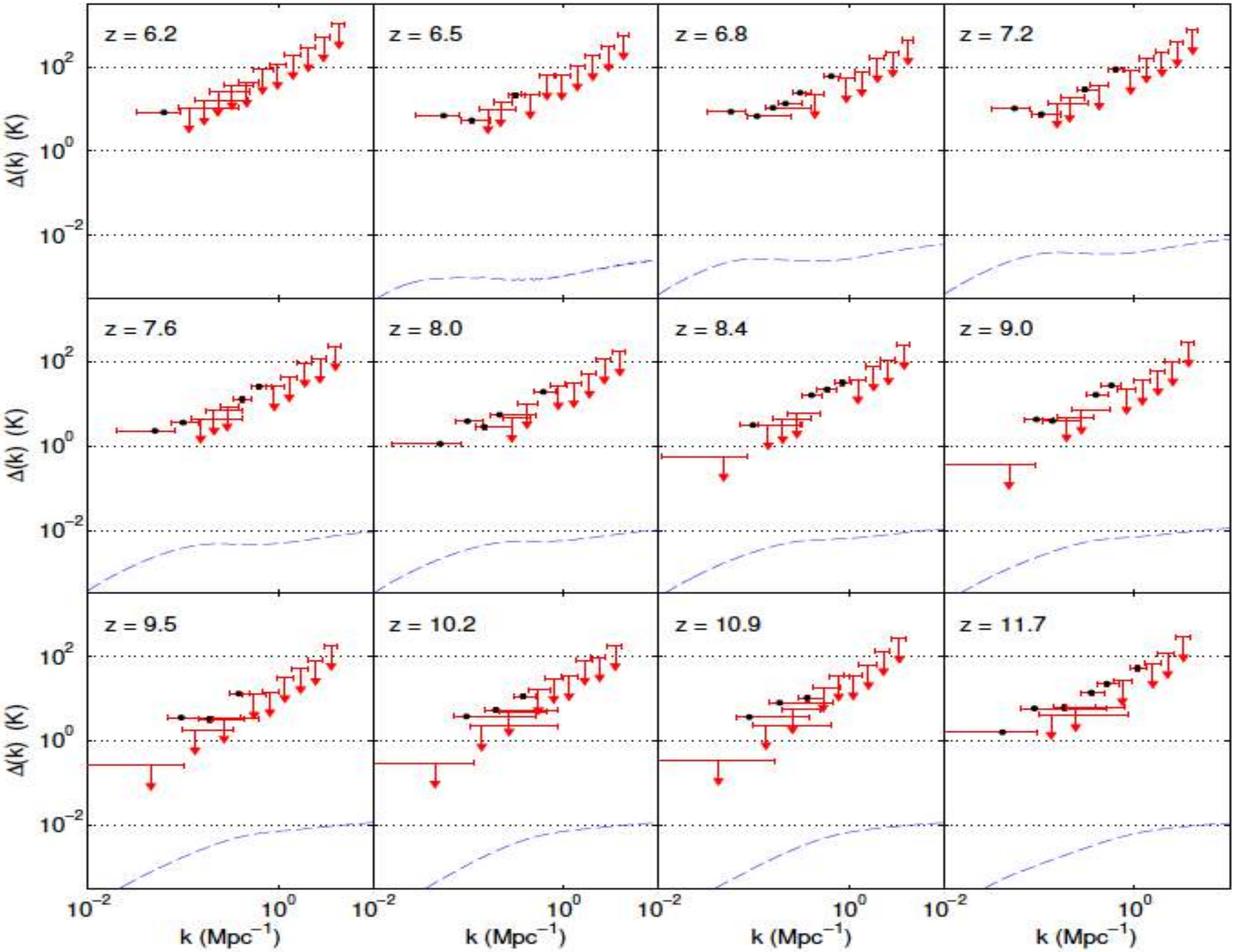

Dillon et al 2014

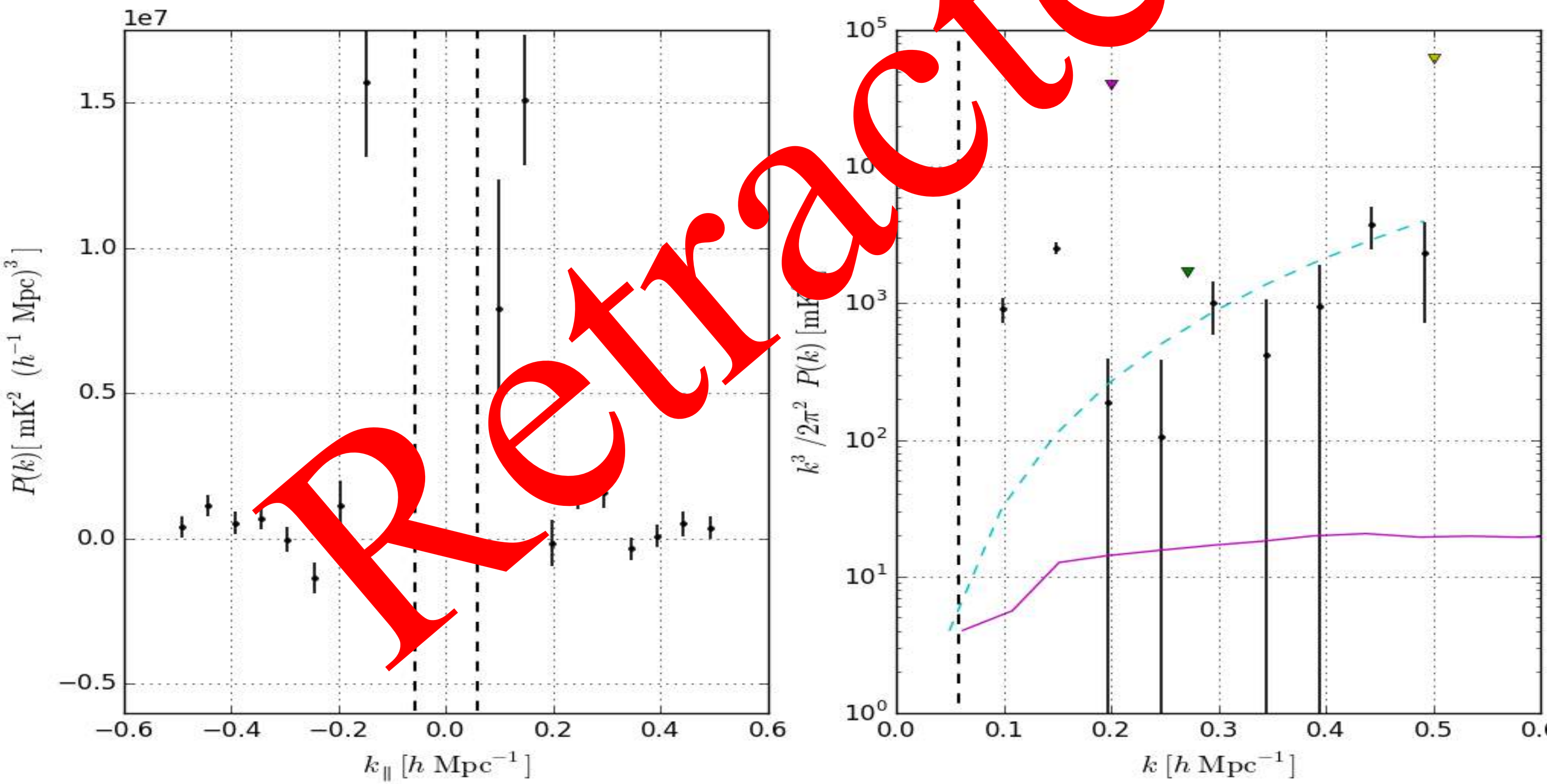

Ali et al 2015

NCP field

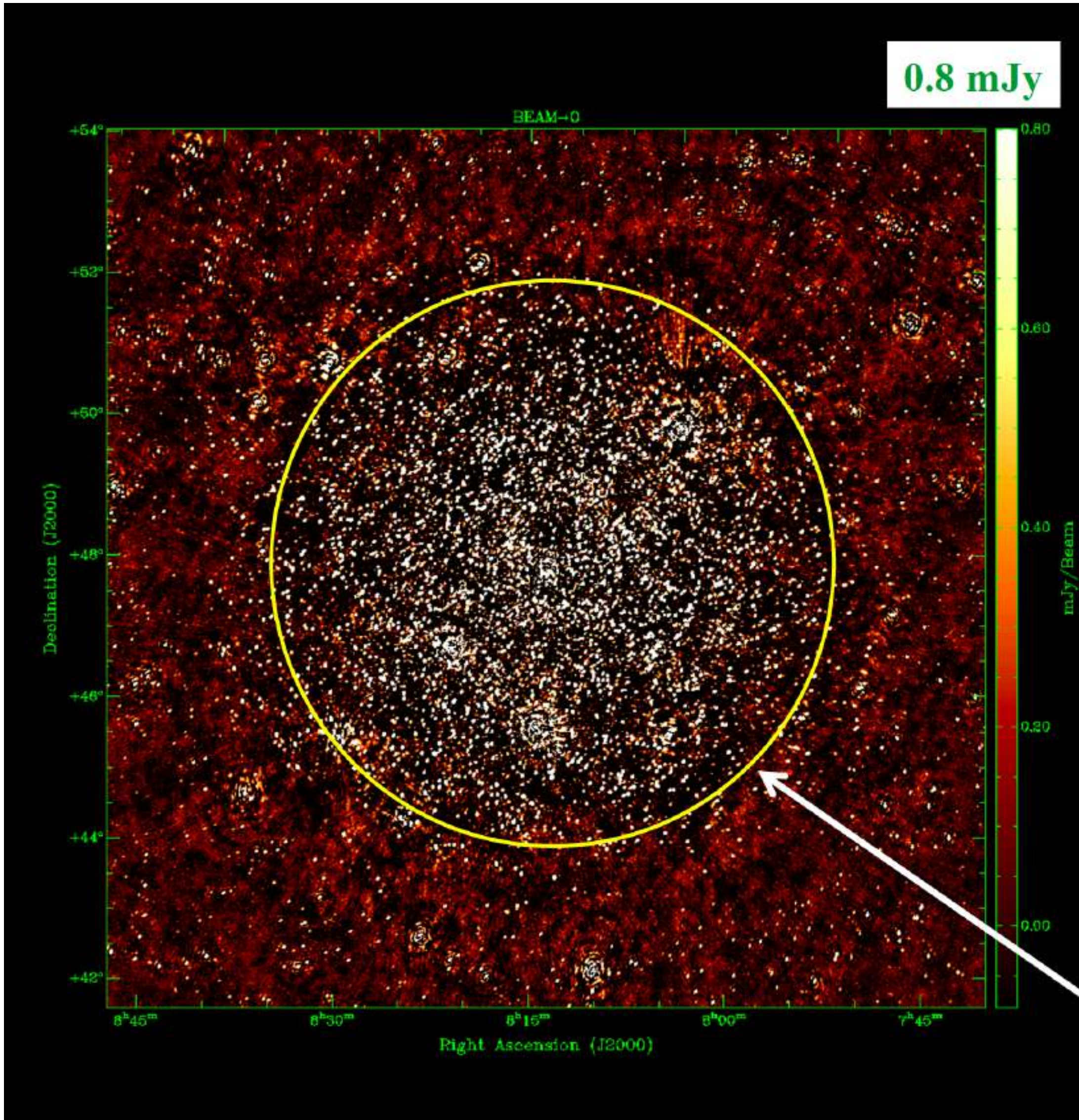

L90490

13-hr integration over ~74 MHz with all LOFAR HBA stations (Feb 11/12, 2013)

Phase Centre ($\alpha, \delta; J2000$)	$0^h, +90°$	
Minimum frequency	115.039	MHz
Maximum frequency	189.062	MHz
Target bandwidth	74.249	MHz
Stations (core/remote)	48 / 13	
Raw data volume L90490	61	Tbyte
Sub-band (SB) width	195.3125	kHz
Correlator channels per SB	64	
Correlator integration time	2	s
Channels per SB after averaging	15, 3, 3, 1	
Integration time after averaging	2, 2, 10, 10	s
Data size (488 sub-bands)	50	Tbyte

Table 1. Observational and correlator set up of LOFAR-HBA observations of the North Celestial Pole (NCP).

near the NCP is indicated by an arrow. The intensity units are mJy/PSF (see text). Right Ascension increases clockwise; RA=00h is towards the bottom.

Spherical Power Spectra

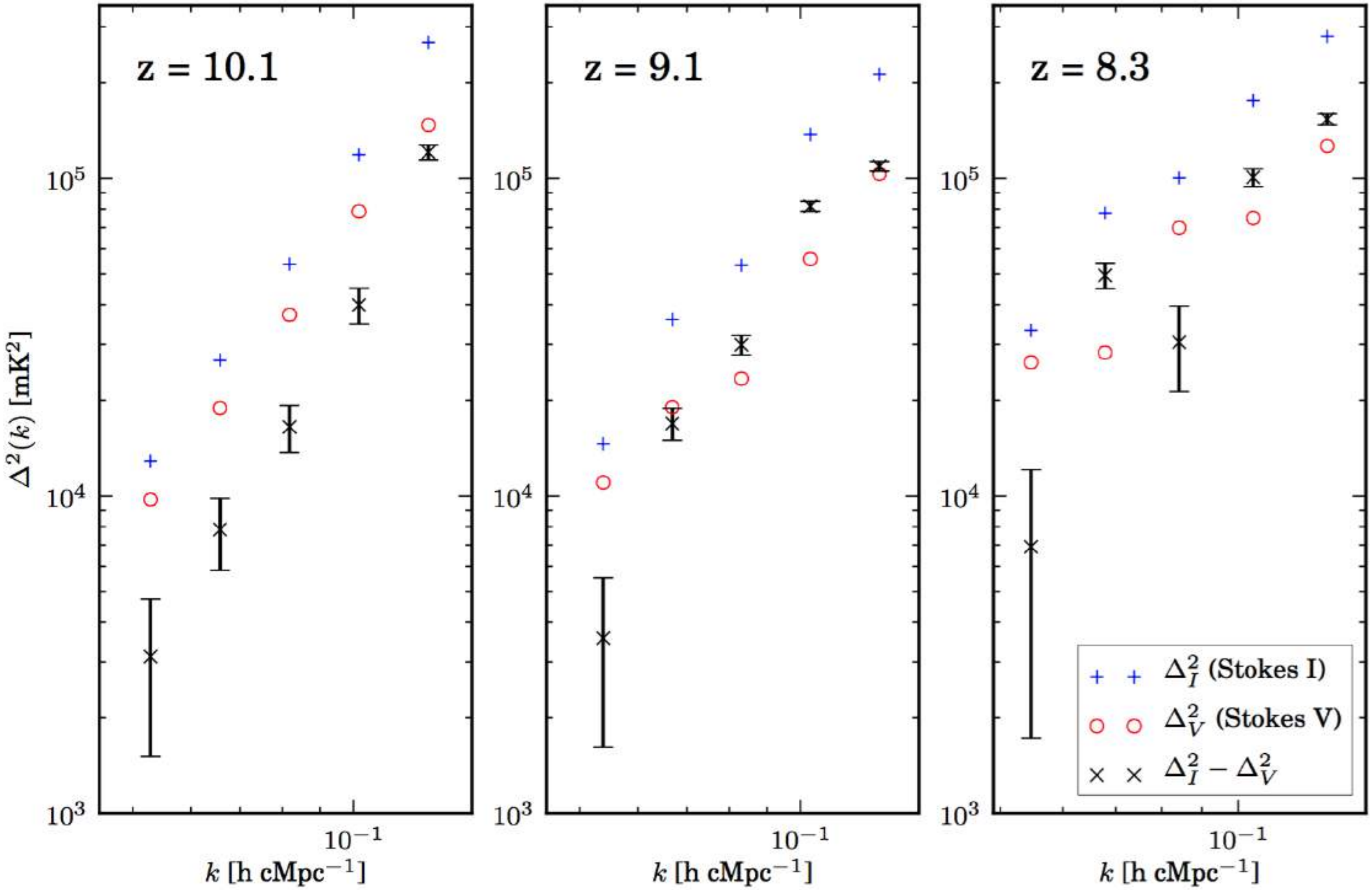

Figure 8. The spherically averaged Stokes I and V power spectra after GMCA for L90490; From left to right are shown the redshift ranges $z = 9.6 - 10.6$, $z = 8.7 - 9.6$ and $z = 7.9 - 8.7$ from left to right, respectively. The mean redshifts are indicated in the panels.

Patil et al. (2017, ApJ)

Spherical Power Spectra

- Although we have excess variance, we only give 2-sigma upper limits (incl. excess)
- Without excess variance we would have reached ~(57mK)^2 at z~10 and k~0.05
- We go less deep at higher-frequencies (issues with FG removal ?).

k h cMpc^{-1}	$z = 7.9 - 8.7$ mK^2	$z = 8.7 - 9.6$ mK^2	$z = 9.6 - 10.6$ mK^2
0.053	$(131.5)^2$	$(86.4)^2$	$(79.6)^2$
0.067	$(242.1)^2$	$(144.2)^2$	$(108.8)^2$
0.083	$(220.9)^2$	$(184.7)^2$	$(148.6)^2$
0.103	$(337.4)^2$	$(296.1)^2$	$(224.0)^2$
0.128	$(407.7)^2$	$(342.0)^2$	$(366.1)^2$

Table 3. Δ^2_{21} upper limits at the 2-σ level.

Patil et al. (2017, ApJ)

Where do we stand ?

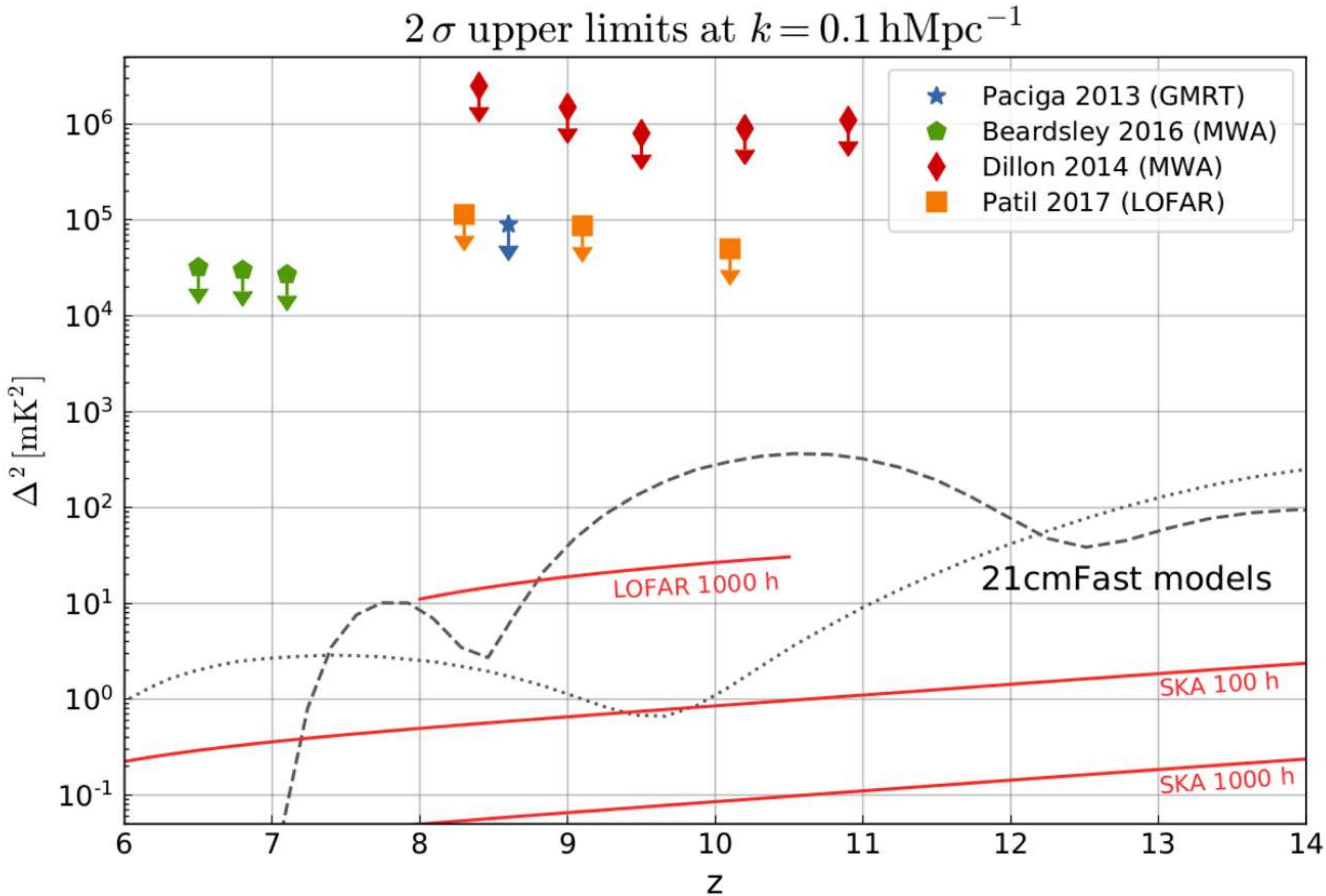

Current power-spectrum results
As of March 2019

Going ~30-40x deeper…

Image of the NCP field

From top-left to bottom-right

1- the sky-model restored with 6.8 arcmin gaussian beam, the mean over frequencies residual
2- Stokes I after DD
3- the Stokes I frequency-rms after DD
4-the Stokes I frequency-rms after GPR.

All units are Kelvin

The three circles have diameter of 2, 4 and 8 time the primary beam FWHM (~4 deg)

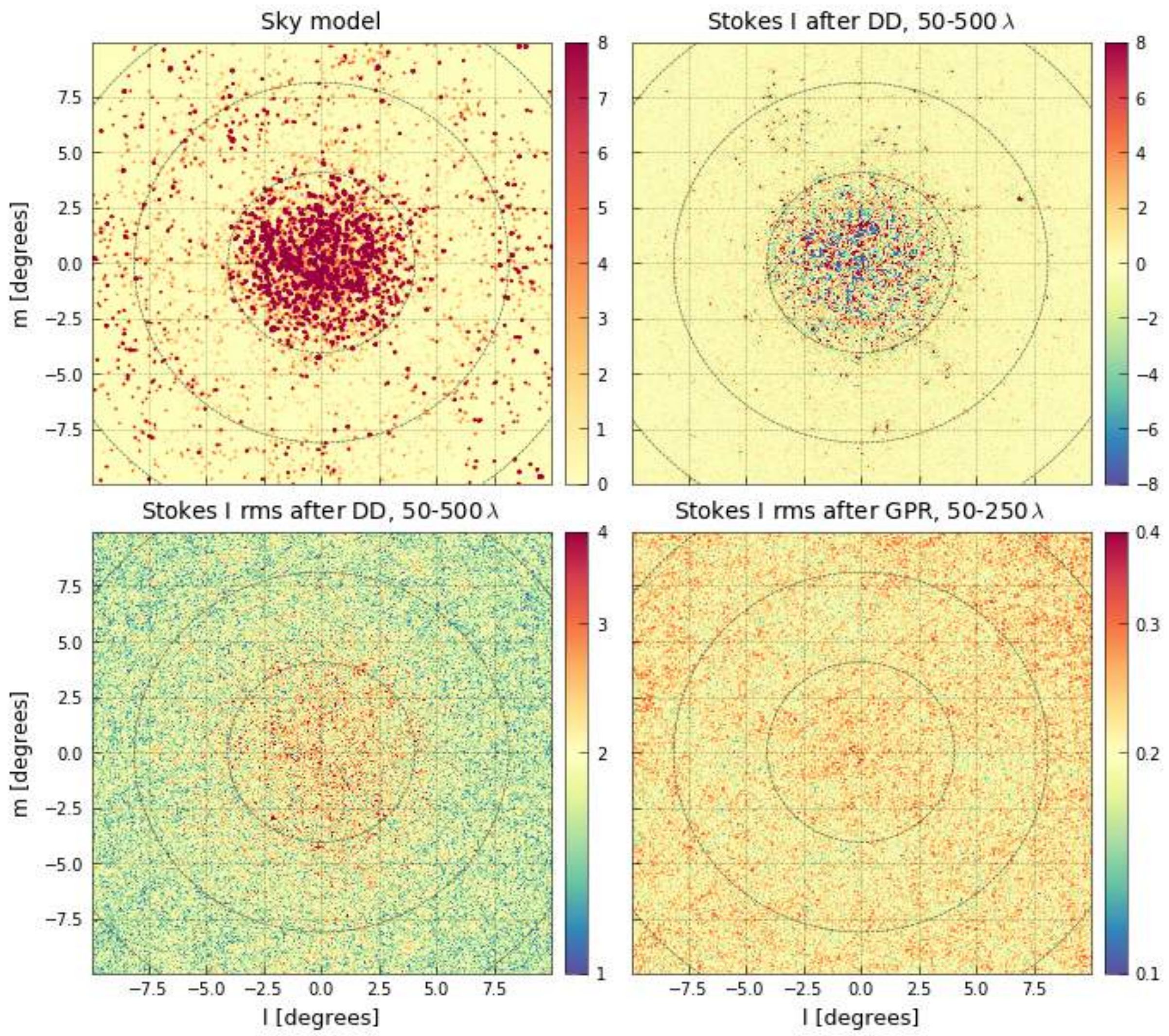

GPR on LOFAR data

NCP field, 140 hours, 134-146 MHz, z ~ 9.1

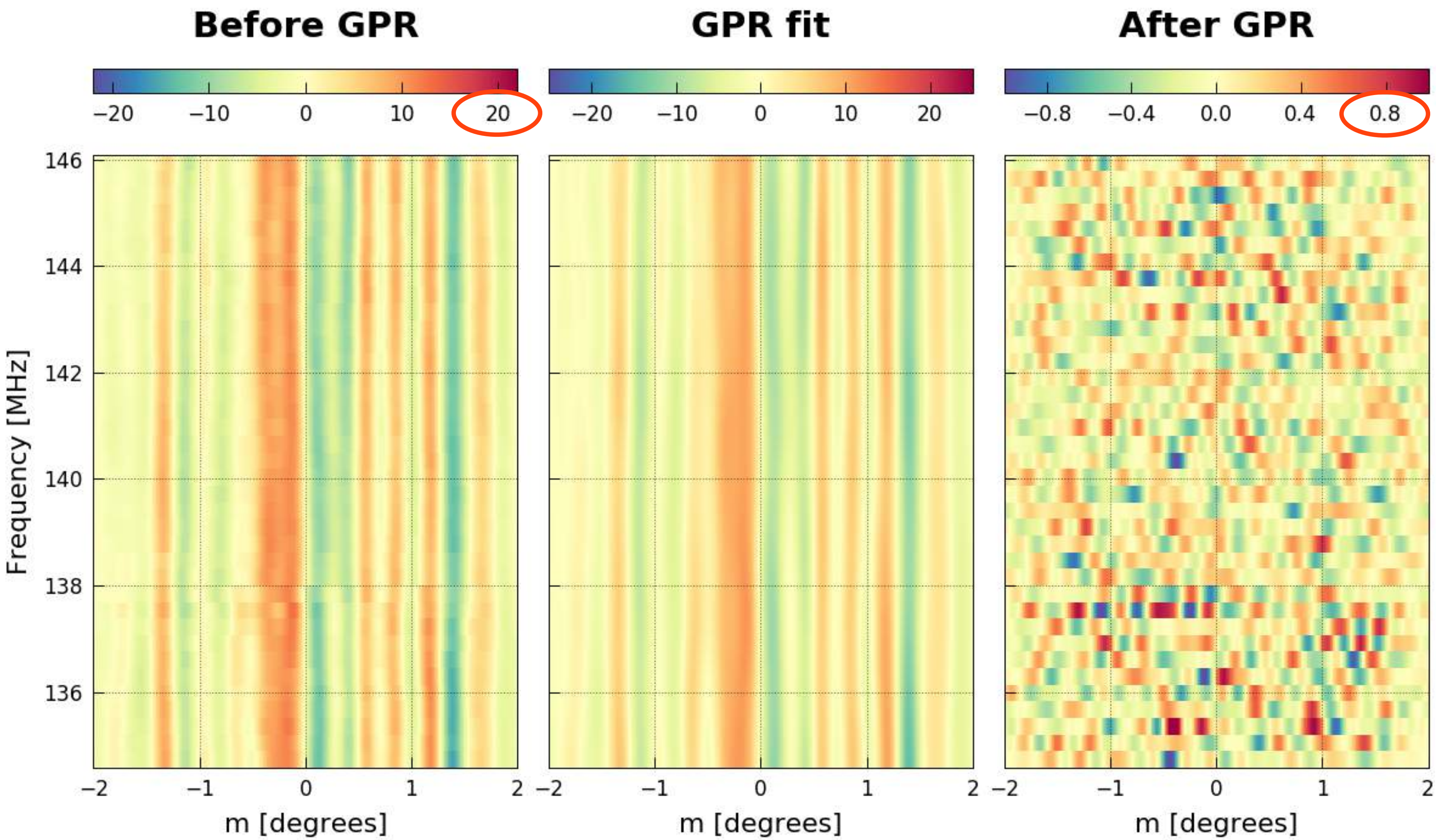

GPR remove frequency-coherent structure
Residual power level close to thermal noise

GPR on LOFAR data

NCP field, 140 hours, 134-146 MHz, z ~ 9.1

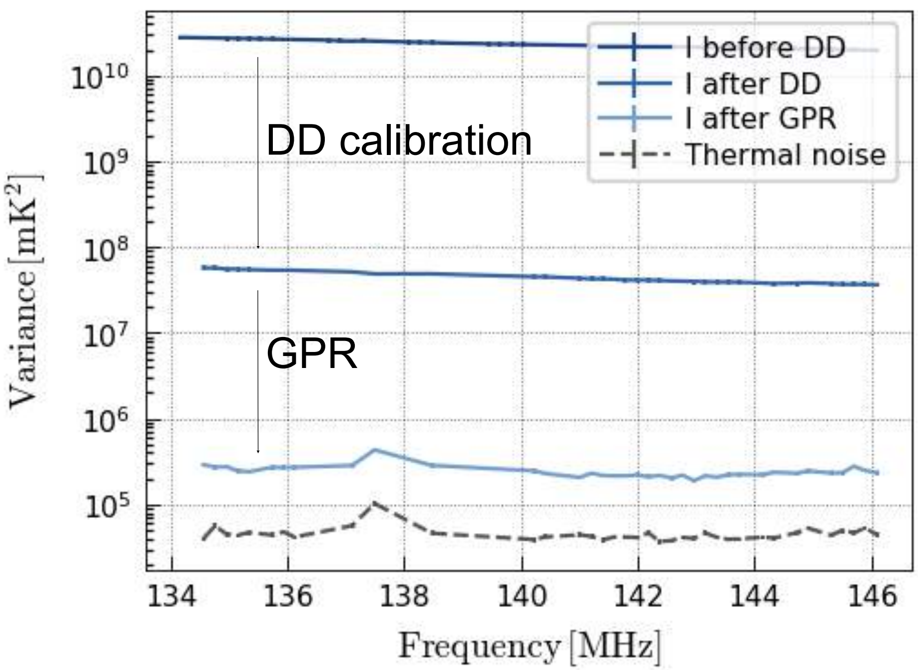

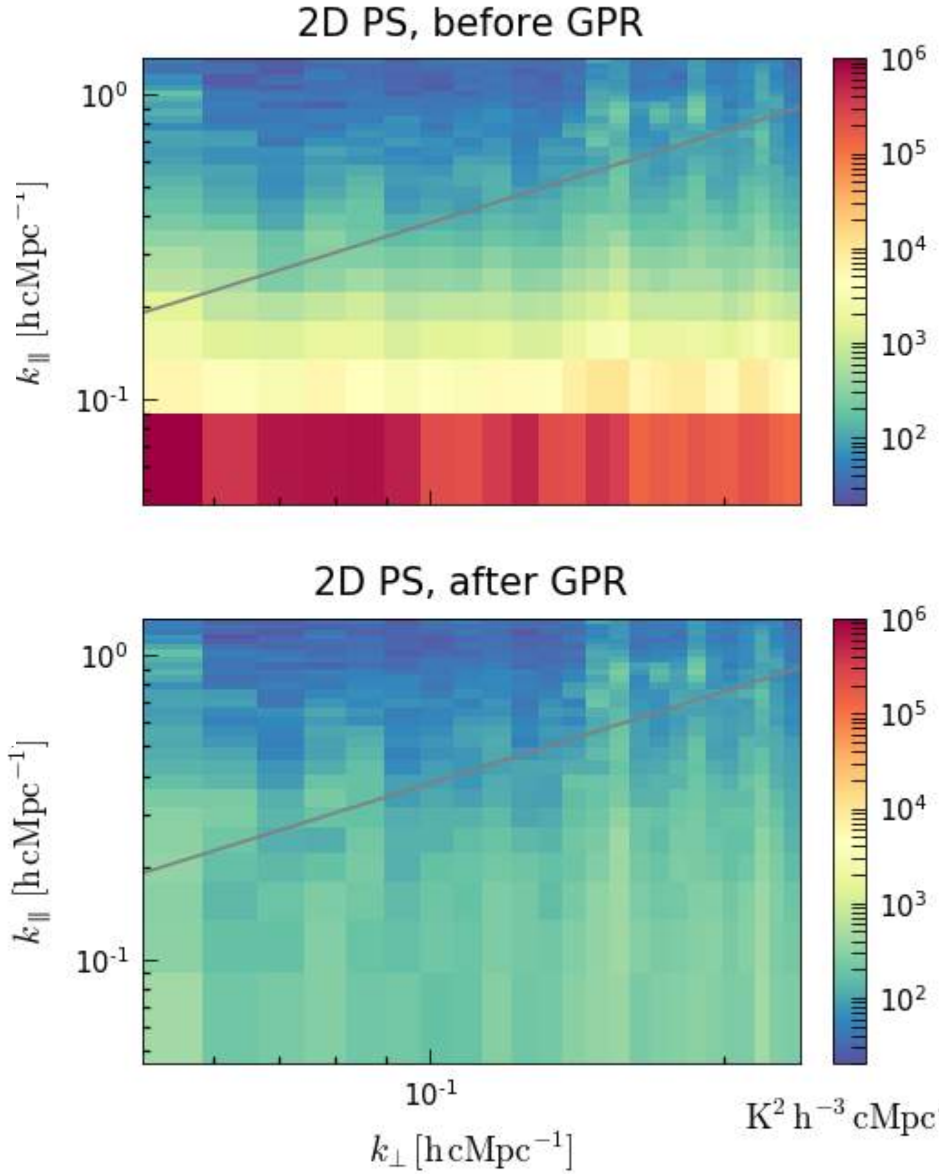

- ➔ DD calibration reduce foregrounds power by an order of magnitude down to confusion limit
- ➔ GPR remove residual foregrounds down to (very close to) noise level
- ➔ Residual power mostly incoherent between nights

New upper limit !

NCP field, 140 hours, 134-146 MHz, z ~ 9.1

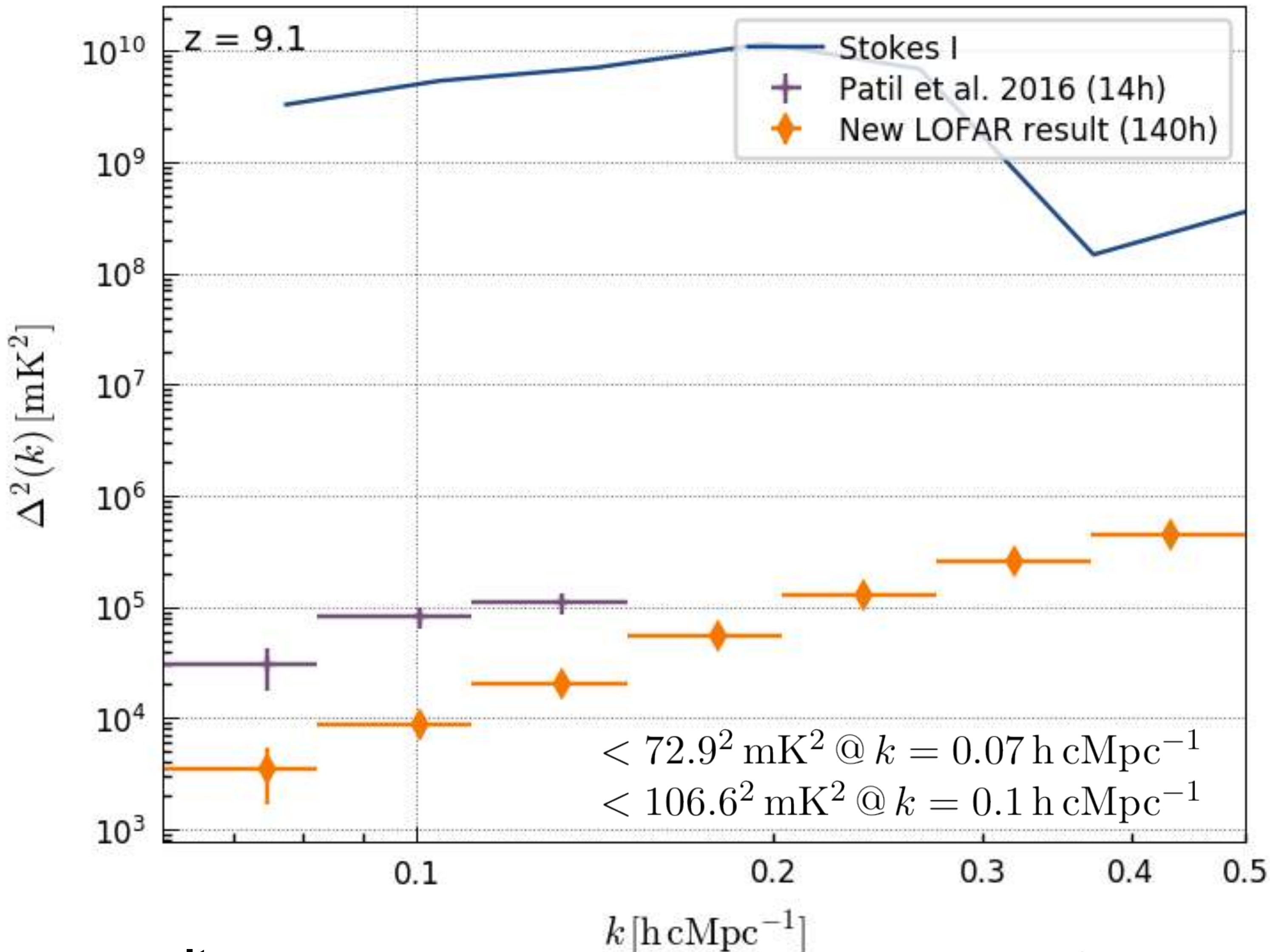

Preliminary results

(Mertens et al. In prep.)

Spherical power spectra for 10 nights

Upper limits (2 sigma) are:
At k ~ 0.075: $\Delta^2 < 72.4^2$ mK^2
At k ~ 0.1: $\Delta^2 < 105.4^2$ mK^2

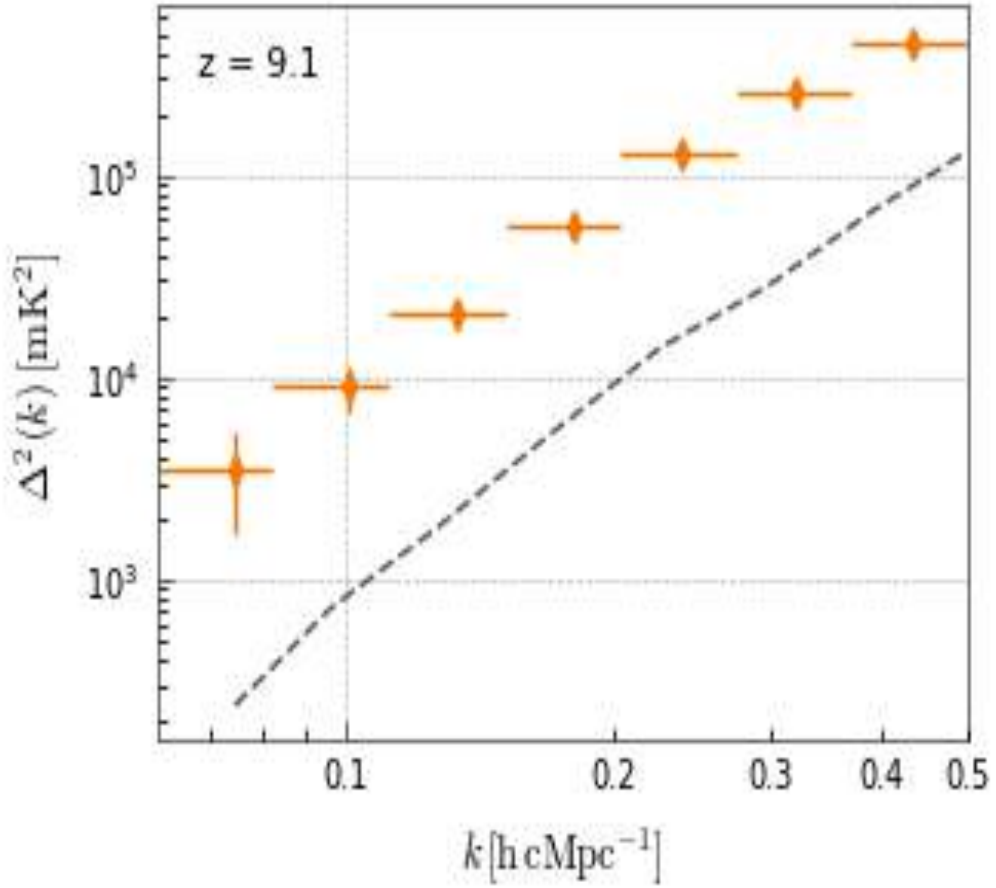

The 1-sigma uncertainty is 2 time the sampling variance of the noise-power + 1 time sampling variance of the noise-unbiased residual power (cosmic variance).

Where do we stand ? (updated)

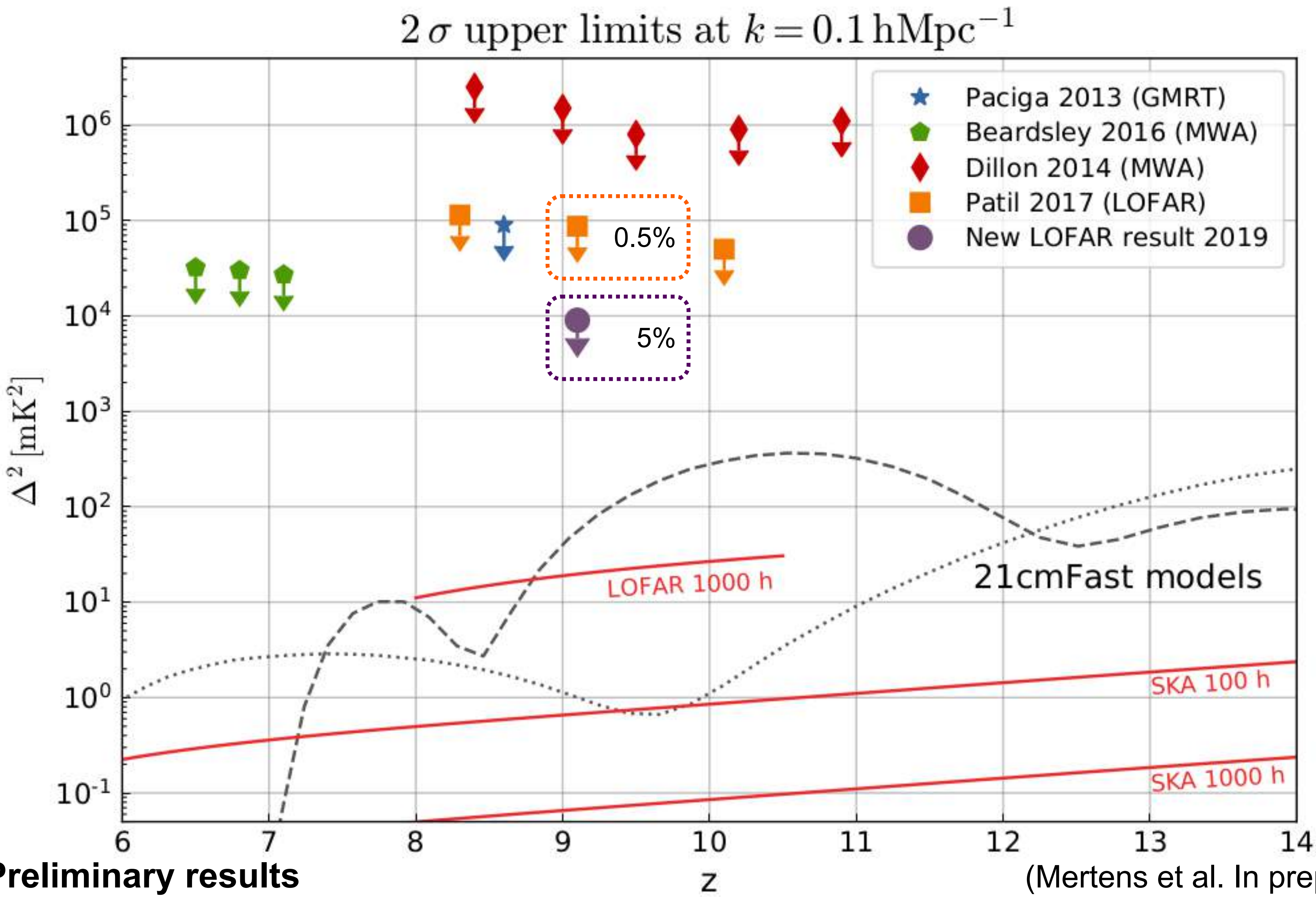

Preliminary results

(Mertens et al. In prep.)

Perspective: ACE, NenuFAR, SKA

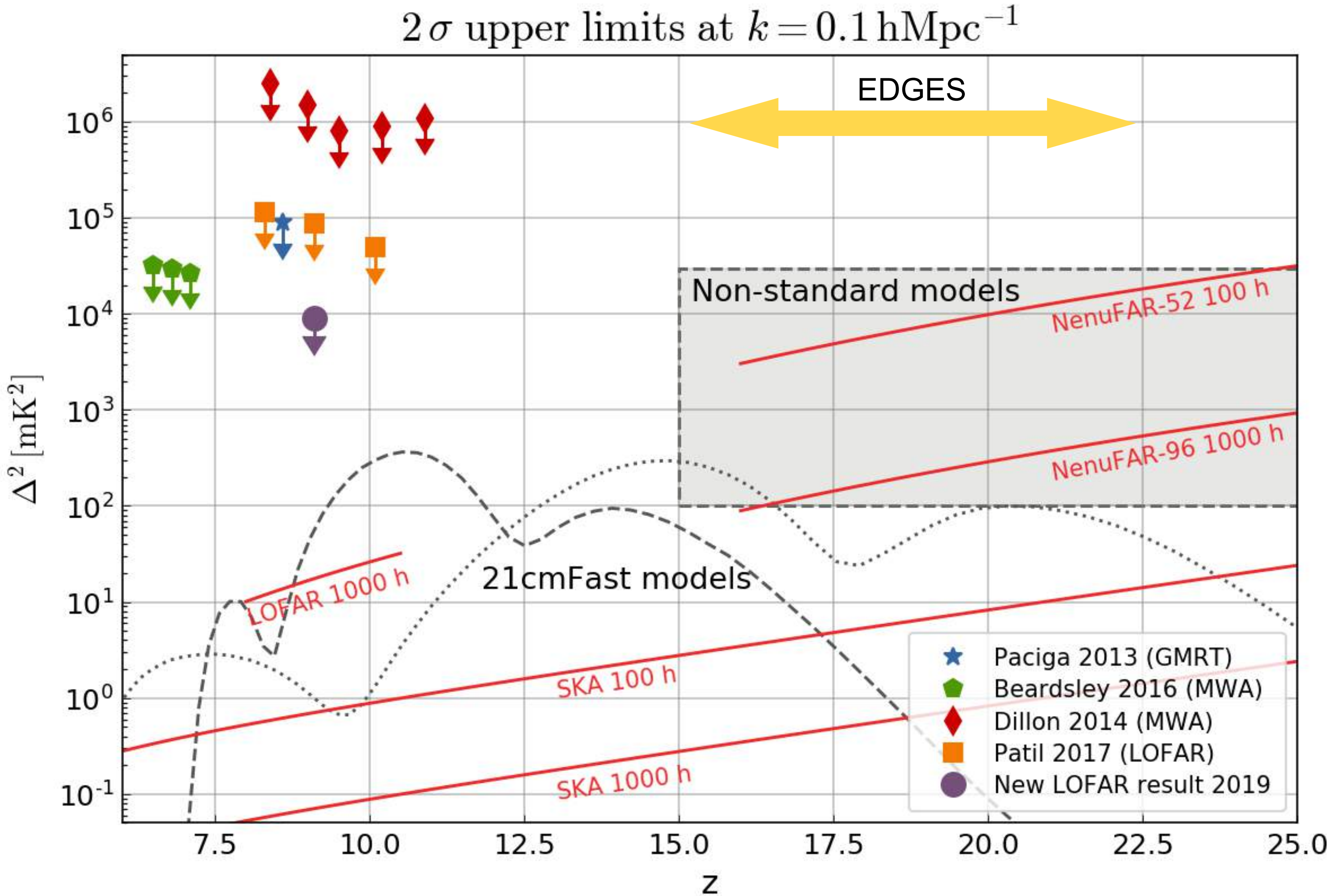

Credit: Science magazine

The History

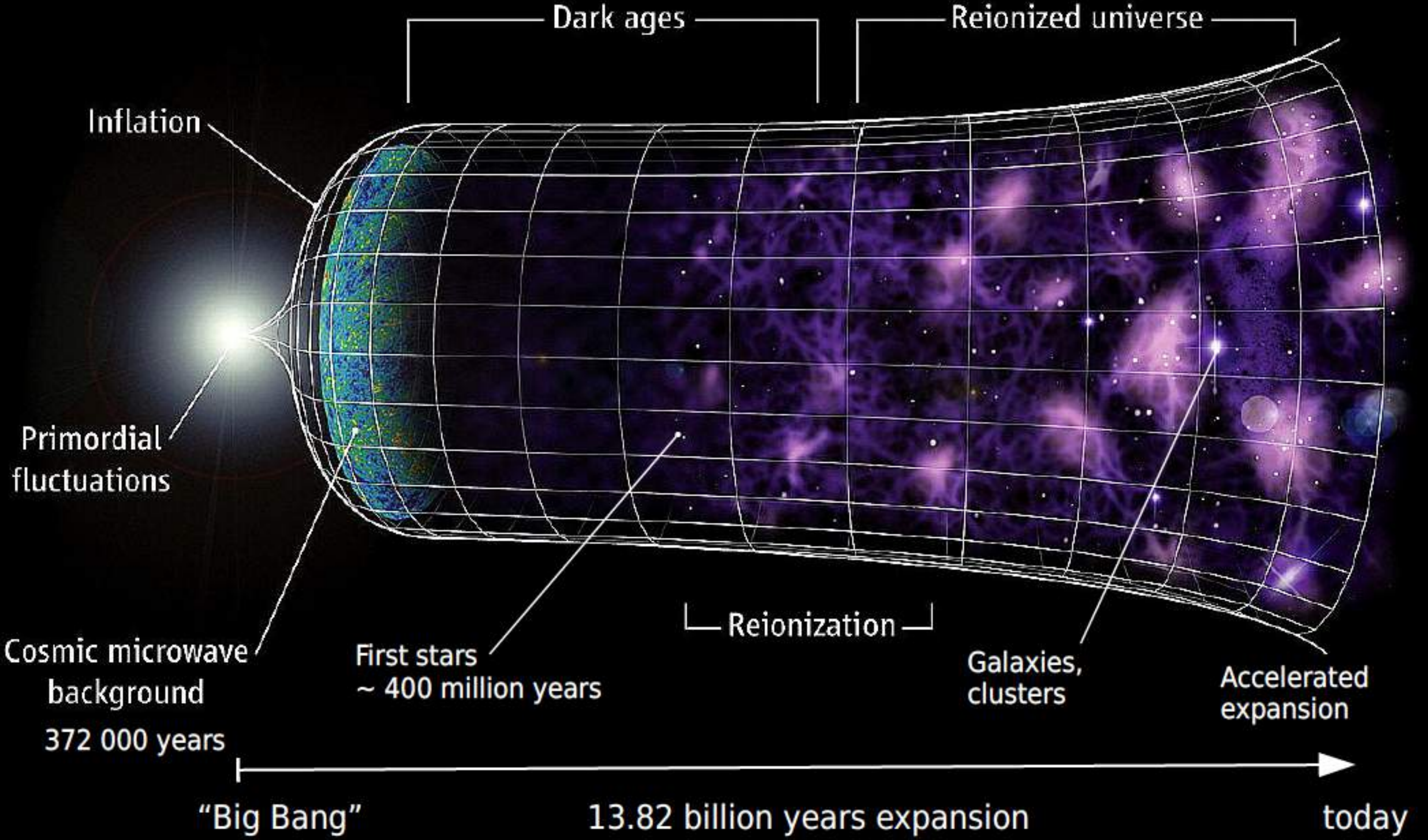

The End of Darkness

The Egyptian God Osiris

I am the only being in an abyss of Darkness. From an abyss of Darkness came I forth ere my birth, from the silence of a primal sleep. And the voice of ages said unto my soul, 'I am he who formulates in Darkness, the Light that shineth in the Darkness, yet the Darkness comprehendeth it not.' **Let the mystical circumambulation take place onto the Path of Darkness that leadeth unto Light with the Lamp of Hidden Knowledge to guide the way.**

We are amongst the first generations to have a comprehensive scientific narrative of the story of the Universe across space and time, and our place in it, from the beginning of time until now.

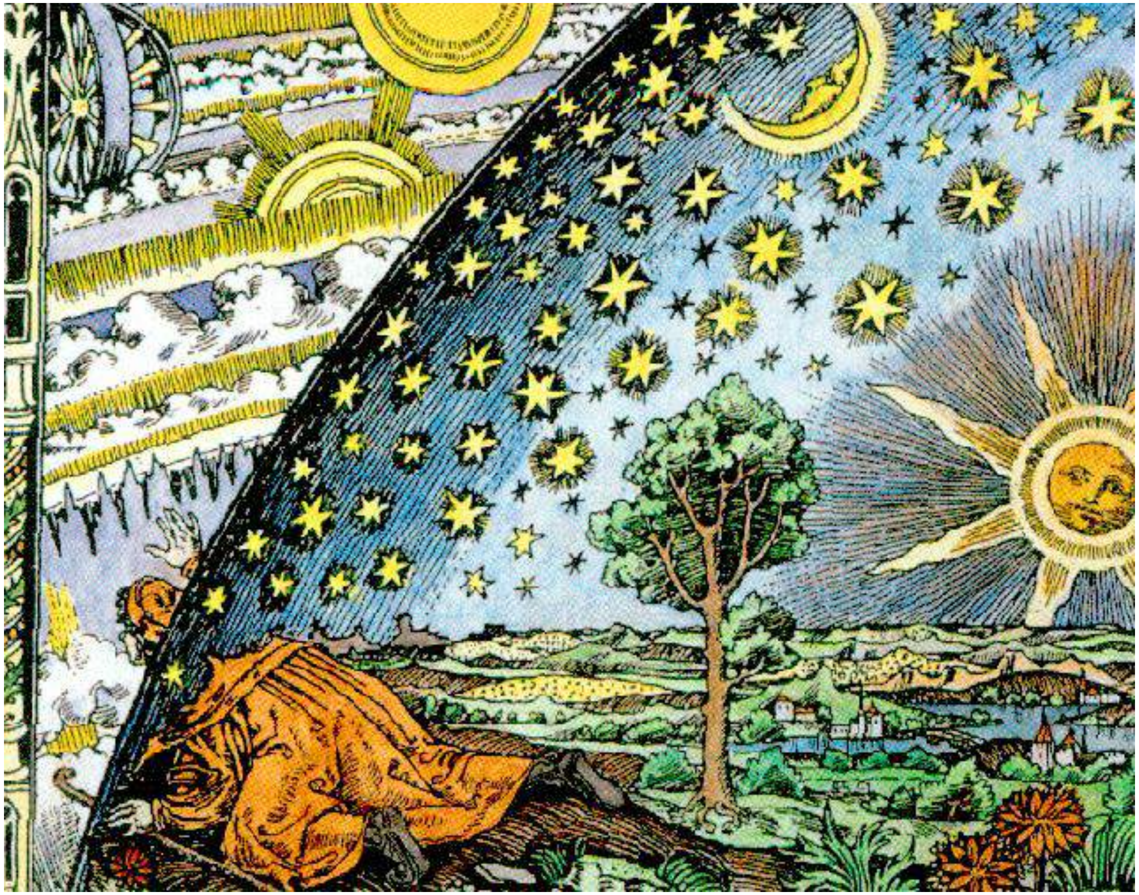

Illusion is the first of all pleasures.
(Voltaire)

Illusion is the first of all pleasures.
(Voltaire)

Discovery is the greatest of all pleasures.